

Georgia State University

ScholarWorks @ Georgia State University

Biology Dissertations

Department of Biology

8-8-2023

SUMOylation as a modulator of ion channel function and expression

Leslie-Anne R. Jansen

Follow this and additional works at: https://scholarworks.gsu.edu/biology_diss

Recommended Citation

Jansen, Leslie-Anne R., "SUMOylation as a modulator of ion channel function and expression." Dissertation, Georgia State University, 2023.
doi: <https://doi.org/10.57709/35862583>

This Dissertation is brought to you for free and open access by the Department of Biology at ScholarWorks @ Georgia State University. It has been accepted for inclusion in Biology Dissertations by an authorized administrator of ScholarWorks @ Georgia State University. For more information, please contact scholarworks@gsu.edu.

SUMOylation as a modulator of ion channel function and expression

by

Leslie-Anne Jansen

Under the Direction of Deborah Baro

A Dissertation Submitted in Partial Fulfillment of the Requirements for the Degree of

Doctor of Philosophy

in the College of Arts and Sciences

Georgia State University

2023

ABSTRACT

The small ubiquitin-like modifier protein (SUMO) is a 12kD peptide that is post-translationally added to target lysine residues. SUMOylation can dynamically regulate a target's function and expression by promoting or preventing protein-protein interactions. The nuclear targets of SUMOylation are well studied, while ion channel SUMOylation is still a growing field. SUMO modulates HCN2 and Kv4 currents by regulating their surface expression. HCN2 channels regulate the resting membrane potential in neurons and Kv4 channels regulate action potential repolarization in the myocardium. Altered HCN2 expression is reported in neuronal pathologies, while altered Kv4 expression is reported in cardiac diseases. This work investigated the contribution of ion channel SUMOylation to diseased states, by examining changes in HCN2 SUMOylation during pathological pain. Secondly, this work examined the regulatory mechanisms of ion channel SUMOylation by identifying the Protein Inhibitor of Activated STAT3 (PIAS3) as an E3 SUMO ligase for Kv4 channels.

This work shows that HCN2 expression is bilaterally increased in putative nociceptors following injection of Complete Freud's Adjuvant. HCN2 SUMOylation exhibited a unilateral increase in putative nociceptors. As HCN2 channels mediate unilateral mechanical hyperalgesia during persistent inflammation, this work indicates that ion channel SUMOylation may underpin pain behaviors during persistent inflammation.

Target SUMOylation is regulated by E3 SUMO ligases; however, none have been identified for ion channels. This work shows that PIAS3 is an E3 SUMO ligase for Kv4 channels. PIAS3 augmented Kv4 SUMOylation in HEK cells and in cultured cardiomyocytes by enhancing SUMOylation at K579. The net effect was an increase in Kv4 currents due to enhanced Rab11a-dependent slow recycling of the channel. PIAS3 required its canonical E3

SUMO ligase properties to mediate these effects. Further, the effects of PIAS3 could be blocked by PKA-mediated phosphorylation of Kv4 channels in HEK cells and in cardiomyocytes, suggesting that the targets of PIAS3 are shaped by their phosphorylation status.

SUMOylation is enhanced in many pathological conditions due to upregulation of the SUMOylation machinery. This work provides insights into the consequences of enhanced SUMOylation of ion channels in diseased states, and importantly, is the first to identify PIAS3 as a regulator for ion channel SUMOylation.

INDEX WORDS: SUMO, PIAS3, E3 SUMO Ligase, Voltage-gated ion channels, Kv4.2, HCN2

Copyright by
Leslie-Anne Jansen
2023

SUMOylation as a modulator of ion channel function and expression

by

Leslie-Anne Jansen

Committee Chair: Deborah Baro

Committee: Taras Nazarko

Bingzhong Xue

Electronic Version Approved:

Office of Graduate Services

College of Arts and Sciences

Georgia State University

August 2023

DEDICATION

This work is dedicated to my family. Without you, I would not have made it this far.

ACKNOWLEDGEMENTS

I would like to thank my Ph.D. advisor, Dr. Deborah Baro for her help, support, and advice. You have helped me become a confident researcher. I would also like to thank my dissertation committee members, Dr. Bingzhong Xue and Dr. Taras Nazarko, for their support and advice.

I would like to thank the past members of the lab for being great friends and indispensable resources to me. I would also like to thank Dr. Vitaly Ryu for his technical support when I first began this journey, and Dr. Ruth Harris for providing access to indispensable equipment.

Finally, I would like to thank the Brains and Behavior Fellowship program for their support during my Ph.D.

TABLE OF CONTENTS

ACKNOWLEDGEMENTS	V
LIST OF TABLES	XI
LIST OF FIGURES	XII
INTRODUCTION	1
1.1 Kv4 channels as regulators of cardiac excitability.....	1
<i>1.1.1 Kv4 channels.....</i>	<i>1</i>
<i>1.1.2 Functional role of I_{tof} in the heart.....</i>	<i>1</i>
<i>1.1.3 Kv4 macromolecular complex.....</i>	<i>3</i>
1.2 HCN2 channels as modulators of peripheral neuronal excitability during persistent inflammation.....	5
<i>1.2.1 HCN channels</i>	<i>5</i>
<i>1.2.2 Functional role of I_f in cardiac cells</i>	<i>6</i>
<i>1.2.3 Functional role of I_h in neurons.....</i>	<i>7</i>
<i>1.2.4 I_h in chronic inflammatory pain</i>	<i>7</i>
1.3 SUMOylation	8
<i>1.3.1 SUMO peptides.....</i>	<i>8</i>
<i>1.3.2 The SUMOylation conjugation cascade.....</i>	<i>9</i>
<i>1.3.3 E3 SUMO ligases.....</i>	<i>9</i>
<i>1.3.4 Consequences of SUMOylation</i>	<i>11</i>

1.4	Hypothesis.....	14
2	ALTERATIONS IN SUMOYLATION OF THE HYPERPOLARIZATION- ACTIVATED CYCLIC NUCLEOTIDE-GATED ION CHANNEL 2 DURING PERSISTENT INFLAMMATION	15
2.1	Abstract.....	16
2.2	Significance	17
2.3	Introduction	17
2.4	Materials and Methods	20
2.4.1	<i>Animal Ethics</i>	<i>20</i>
2.4.2	<i>CFA model and tissue preparation</i>	<i>20</i>
2.4.3	<i>Antibodies and Reagents</i>	<i>21</i>
2.4.4	<i>Immunohistochemistry.....</i>	<i>21</i>
2.4.5	<i>Immunohistochemistry analysis</i>	<i>22</i>
2.4.6	<i>Proximity Ligation Assay</i>	<i>23</i>
2.4.7	<i>PLA analysis</i>	<i>24</i>
2.4.8	<i>Rat DRG membrane preparation and denaturing immunoprecipitation.....</i>	<i>24</i>
2.4.9	<i>Western Blot</i>	<i>25</i>
2.4.10	<i>Statistics</i>	<i>26</i>
2.5	Results	26

2.5.1	<i>Inflammation increases the level of HCN2 expression and the number of cells expressing HCN2.....</i>	26
2.5.2	<i>HCN2 is SUMOylated in the rat DRG.....</i>	28
2.5.3	<i>Significantly more HCN2 SUMO2/3 conjugation is observed in small diameter neurons from ipsilateral DRG on day 1 but not day 3 post-CFA.....</i>	30
2.5.4	<i>Conjugation of SUMO1 to HCN2 channels was reduced in medium and large diameter neurons on 1 day post CFA and increased in small neurons on day 3 post-CFA.....</i>	32
2.6	Discussion.....	33
2.6.1	<i>HCN2 protein expression and SUMOylation of HCN2 channel complexes are increased in small diameter neurons during CFA-induced inflammation.....</i>	33
2.6.2	<i>SUMOylation of HCN2 channel complexes is decreased in medium and large diameter neurons during CFA-induced inflammation.....</i>	38
3	CHANGES IN PERIPHERAL HCN2 CHANNELS DURING PERSISTENT INFLAMMATION	55
3.1	Abstract.....	56
3.2	Introduction	57
3.3	Materials and Methods	64
3.3.1	<i>Animal Ethics</i>	64
3.3.2	<i>CFA Model and Tissue Preparation.....</i>	64
3.3.3	<i>Antibodies and Reagents.....</i>	65

3.3.4	<i>Immunohistochemistry and Analysis</i>	65
3.3.5	<i>Proximity Ligation Assay</i>	65
3.3.6	<i>Statistics</i>	66
3.4	Results	67
3.4.1	<i>HCN2 expression and SUMOylation in L4 DRG neuron on days 1 and days 3 post-CFA</i>	67
3.4.2	<i>HCN2 expression and SUMOylation in L6 DRG neurons on days 1 and day 3 post-CFA</i>	68
3.5	Discussion	69
4	PIAS3 IS AN E3 SUMO LIGASE FOR KV4 CHANNELS	84
4.1	Introduction	85
4.2	Materials and Methods	87
4.2.1	<i>Antibodies</i>	87
4.2.2	<i>Cell Culture</i>	88
4.2.3	<i>Plasmids</i>	88
4.2.4	<i>Calcium Phosphate Transfections</i>	89
4.2.5	<i>TAT-PIAS3 peptide synthesis</i>	89
4.2.6	<i>Electrophysiology</i>	90
4.2.7	<i>Immunoprecipitation</i>	91
4.2.8	<i>Western Blot Assays</i>	92

4.2.9	<i>Immunohistochemistry</i>	93
4.2.10	<i>Proximity Ligation Assay</i>	93
4.2.11	<i>Proximity Ligation Analysis</i>	94
4.3	Results	95
4.3.1	<i>PIAS3 increases Kv4.2 I_A at K579 in the TC by increasing Rab11a-dependent slow recycling.</i>	95
4.3.2	<i>PIAS3 requires its E3 SUMO ligase properties to modulate I_A.</i>	97
4.3.3	<i>PIAS3 increases Kv4.2-K579 SUMOylation but not HA-KChIP2a or HA-DPP10 SUMOylation in the TC.</i>	98
4.3.4	<i>PIAS3 augments HCN2-mediated I_h.</i>	99
4.3.5	<i>PKA-mediated phosphorylation at S552 blocks PIAS3-mediated SUMOylation of Kv4.2g in the TC.</i>	100
4.3.6	<i>PIAS3 augments Kv4 SUMOylation in cardiomyocytes.</i>	101
4.4	Discussion	103
5	CONCLUSION	126
5.1	Summary	126
5.2	SUMOylation as a modulator of pain behaviors	127
5.3	Target SUMOylation can be altered by disrupting PIAS3-Ubc9 interactions or PIAS3-target interactions.	129
5.4	Target SUMOylation is gated by a target's phosphorylation status.	130

LIST OF TABLES

Table 1 Fold Change in Mean HCN2 Expression in L4-L6 DRG.....	82
Table 2 Fold Change in Mean HCN2 SUMOylation in L4-L6 DRG.....	83
Table 3 Primer Sequences.....	87
Table 4-Whole-patch clamp data for the Kv4.2g TC +/- PIAS3.....	125
Table 5-Whole-patch clamp data for the Kv4.2g-K579R TC +/- PIAS3.....	125

LIST OF FIGURES

Figure 2-1 Validation of anti-HCN2 and quantification of HCN2 positive cells.	39
Figure 2-2 CFA-induced inflammation alters HCN2 protein expression on 1 day post-CFA.	40
Figure 2-3 HCN2 protein expression is altered on day 3 post-CFA.....	42
Figure 2-4 HCN2 is SUMOylated in rat DRG.....	44
Figure 2-5 Measuring HCN2 channel SUMOylation.	45
Figure 2-6 SUMO2/3 conjugation to HCN2 channels is increased in small diameter neurons from ipsilateral relative to contralateral DRG at 1 day post-CFA.....	47
Figure 2-7 SUMOylation of HCN2 channels by SUMO2/3 does not change 3 days post-CFA..	49
Figure 2-8 HCN2 channel SUMOylation by SUMO1 is diminished in medium and large diameter neurons from ipsilateral relative to contralateral DRG at 1 day post-CFA.	51
Figure 2-9 HCN2 channel SUMOylation by SUMO1 is increased in small neurons from ipsilateral relative to contralateral DRG at 3 days post-CFA	53
Figure 3-1 HCN2 protein expression but not SUMOylation is altered in the L4 DRG 1 day post- CFA.....	73
Figure 3-2 HCN2 protein expression and HCN2 SUMOylation are unaltered in the L4 DRG 3 days post CFA.....	76
Figure 3-3 HCN2 protein expression and HCN2 SUMOylation are enhanced in the L6 DRG 1 day post-CFA.....	78
Figure 3-4 HCN2 SUMOylation but not protein expression is altered in the L6 DRG 3 days post-CFA.....	80
Figure 4-1 : PIAS3 increases IA Gmax at K579.....	105
Figure 4-2 PIAS3 acts via slow recycling.....	106

Figure 4-3 PIAS3 acts via SIM1 and requires Ubc9.....	108
Figure 4-4 PIAS3 increases Kv4.2 SUMOylation.....	109
Figure 4-5 PIAS3 does not alter HA-KChIP2a and HA-DPP10 SUMOylation in the ternary complex.....	112
Figure 4-6 PIAS3 increases I_h at K669 of HCN2	113
Figure 4-7 PKA-mediated phosphorylation of Kv4.2 at S552 blocks its PIAS3-mediated SUMOylation at K579.	116
Figure 4-8 PKA-mediated phosphorylation of Kv4.2 at S552 blocks the PIAS3-mediated increase in Kv4.2 SUMOylation.....	117
Figure 4-9 Kv4 channels are SUMOylated in the mouse heart and interact with PIAS3.....	119
Figure 4-10 TAT-PIAS3 increases Kv4 SUMOylation in cardiomyocytes.	121
Figure 4-11- PKA Activation blocks the TAT-PIAS3-mediated increase in Kv4 SUMOylation	123

INTRODUCTION

1.1 Kv4 channels as regulators of cardiac excitability

1.1.1 Kv4 channels

The *Shal* family of voltage-gated K⁺ channels include Kv4.1-Kv4.3. Each Kv4 gene encodes a six transmembrane domain (α subunit) that contains a canonical S4 voltage sensor and S5-S6 pore loop and selectivity filter (Birnbaum et al., 2004). All Kv4 α subunits are homologous in their transmembrane region but are highly divergent at their N and C termini (Birnbaum et al., 2004). A functional channel consists of 4 α subunits that multimerize using an N-terminal T1 tetramerization domain and can either be homotetrameric or heterotetrameric (Birnbaum et al., 2004). Kv4 channels are calcium-independent and are rapidly activated and inactivated in response to subthreshold potentials, producing a transient, outward K⁺ current that is often called A-type. As other Kv channels produce A-type currents with the same features, Kv4 currents can be identified by their pharmacological sensitivity to heteropodatoxins, phrixotoxins, and lower sensitivity to 4-aminopyridine, as well as their rapid recovery from inactivation, which is $\sim 10^3$ ms faster than other Kv's (Birnbaum et al., 2004; Jerng, Pfaffinger, & Covarrubias, 2004).

1.1.2 Functional role of I_{to} in the heart

Kv4 channels contribute to both neuronal I_A and cardiac I_{to} (Jerng, Pfaffinger, et al., 2004; Niwa & Nerbonne, 2010). In the heart, the cardiac action potential (AP) initiates and coordinates the contraction of the myocardium. Cardiac repolarization occurs over several phases in higher order mammals; here, I_{to} shapes phase 1 of AP repolarization and sets the plateau potential during phase 2 (Niwa & Nerbonne, 2010). I_{to} predominates AP repolarization in rodents who lack distinct phases (Niwa & Nerbonne, 2010). Reductions in I_{to} have been shown to extend

the AP duration (H. Xu, Li, & Nerbonne, 1999) and increase intracellular Ca^{2+} through L-type voltage gated Ca^{2+} channels which peak during phase 2 (Kaprielian et al., 1999), thus alterations in I_{to} greatly effect excitation-contraction coupling.

I_{to} can be separated into two currents, I_{tof} and I_{tos} , which are mediated by Kv4 and Kv1.4 channels, respectively (Niwa & Nerbonne, 2010). The molecular correlates of I_{tof} vary by species. Kv4.2-Kv4.3 heterotetrameric channels are reported in rodents and ferrets, Kv4.3 homomeric subunits in humans and canines, and in some species, there is complete absence of I_{to} (Q. He, Feng, & Wang, 2015). In cardiomyocytes, Kv4 channels are localized to the sarcolemma (El-Haou et al., 2009), where they associate in caveolae and non-caveolae fractions (Alday, Urrutia, Gallego, & Casis, 2010; Rudakova, Wagner, Frank, & Volk, 2015).

Adrenergic signaling is used as a mechanism to fine-tune I_{to} . Acute treatment of cardiomyocytes with phenylephrine, an $\alpha 1$ agonist, decreased I_{tof} by increasing phosphorylation and subsequent internalization of Kv4 channels through a cAMP/PKA dependent axis (Gallego et al., 2005). Acute β -adrenergic stimulation is required to maintains I_{to} at physiological levels in diabetic rats (Gallego, Casis, Izquierdo, & Casis, 2000). I_{to} is reduced during myocardial infarction (B. Huang, Qin, & El-Sherif, 2001; Kaprielian et al., 1999; Rose et al., 2005). This is due to elevated levels of norepinephrine which sustain adrenergic signaling, resulting in the transcriptional repression of Kv4.2, Kv4.3 and KCHIP2 genes through activation of the calcenurin-NFATc3 pathway (Lameris et al., 2000; Rossow, Dilly, & Santana, 2006; Rossow et al., 2009; Rossow, Minami, Chase, Murry, & Santana, 2004). Similar reductions in I_{to} are reported in humans with failing hearts (E. K. Johnson et al., 2018).

1.1.3 Kv4 macromolecular complex

Kv4 channels are often tethered to other proteins in supramolecular complexes. Tandem affinity purification followed by mass spectrometry has identified ~120 endogenous proteins in HEK cells (Hu et al., 2020) and even more in hippocampal neurons (Hu, Liu, & Hoffman, 2022) that interact with Kv4.2 channels. The two most associated proteins are the Kv Channel Interacting Proteins 1-4 (KChIPs1-4) and the dipeptidyl peptidase-like proteins 6 and 10 (DPP6 and DPP10).

KChIPs are a class of cytosolic, Ca²⁺ binding EF-hand containing proteins that belong to the neuronal calcium sensor family. KChIP1-4 are encoded by individual genes and each gene gives rise to several isoforms (Pruunsild & Timmusk, 2005). KChIP proteins bind to the N-terminus of Kv4 channels in a preferred 4:4 stoichiometry in the ER and promote forward trafficking of the channel by 1) masking an ER retention sequence in Kv4 (An et al., 2000; Pioletti, Findeisen, Hura, & Minor, 2006; Shibata et al., 2003; H. Wang et al., 2007) and by 2) trafficking Kv4-KChIP complexes in non-conventional post Golgi pathway using non-COP II coated vesicles (Hasdemir, Fitzgerald, Prior, Tepikin, & Burgoyne, 2005) and a SNARE complex containing VAMP7 and Vti1a (Flowerdew & Burgoyne, 2009). At the surface, KChIP proteins stabilize surface expression (Foeger, Wang, Mellor, & Nerbonne, 2013), increase Kv4 currents densities (Amarillo et al., 2008; An et al., 2000; Bähring et al., 2001; Jerng, Kunjilwar, & Pfaffinger, 2005; Jerng & Pfaffinger, 2008; Shibata et al., 2003; Zhou, Qian, Kunjilwar, Pfaffinger, & Choe, 2004), induce a leftward shift in the voltage of half inactivation and accelerate the rate of recovery from inactivation (Murphy & Hoffman, 2019). KChIP expression profiles vary by tissue and species (Jerng & Pfaffinger, 2014). KChIP2 is essential for Kv4

expression in rodent Dorsal Root Ganglion (DRG) neurons, and in human and canine cardiomyocytes (H. C. Kuo et al., 2001; Y. L. Kuo et al., 2017; Rosati et al., 2001).

In native tissue, DPP6 and DPP10 are expressed in ternary complexes with Kv4 and KChIP proteins (Jerng et al., 2005; Nadal et al., 2003; W. C. Wang, Cheng, & Tsaur, 2015; Zaghera et al., 2005). DPP6 and DPP10 proteins are single pass type II transmembrane proteins that belong to the serine family of proteases, however both proteins contain a single point mutation in their catalytic triad rendering their protease activity inactive (S. Y. Qi, Riviere, Trojnar, Junien, & Akinsanya, 2003). These proteins bind to the S1-S2 loop of Kv4 channels, with DPP6 binding in a preferred 4:4 stoichiometry and DPP10 in a 4:2 configuration (Kitazawa, Kubo, & Nakajo, 2015; S. Y. Qi et al., 2003; X. Ren, Hayashi, Yoshimura, & Takimoto, 2005; Soh & Goldstein, 2008). DPP6 and DPP10 proteins promote the forward trafficking of Kv4 channels from the ER, stabilize Kv4 surface expression, increase Kv4 current density, induce a hyperpolarizing shift in the voltage-dependence of inactivation, reduce the time constants of decay, and increase the rate of recovery (Foeger, Norris, Wren, & Nerbonne, 2012; Jerng, Qian, & Pfaffinger, 2004; Lin, Long, Hatch, & Hoffman, 2014; Nadal, Amarillo, Vega-Saenz de Miera, & Rudy, 2006; Nadal et al., 2003; Zaghera et al., 2005). There are multiple variants of DPP6 and DPP10 (Jerng & Pfaffinger, 2014), with DPP6 and DPP10 proteins overlapping in central regions of the brain (Clark et al., 2008; Jerng, Lauver, & Pfaffinger, 2007) and in cardiac ventricles (Belau et al., 2019; Xiao et al., 2013), while segregating in peripheral neurons (C. F. Cheng et al., 2016).

Kv4 interacting partners influence the subcellular localization of Kv4 complexes and therefore modulate their function and/or expression. SAP97, a membrane-associated guanylate kinase, directs Kv4.2 channels to hippocampal spines through interaction with its PDZ domain

(Gardoni et al., 2007). The uneven distribution of Kv4.2 channels in the somatodendritic compartments of CA1 neurons contribute, in part, to its regulation of dendritic excitability (Hoffman, Magee, Colbert, & Johnston, 1997; Jung, Kim, & Hoffman, 2008; J. Kim, Wei, & Hoffman, 2005). SAP97 interacts with Kv4.3 channels through a C-terminal SAL on Kv4.3 (El-Haou et al., 2009). These proteins colocalize in the sarcolemma of cardiomyocytes where SAP97 acts to anchor Kv4.3 to the calmodulin binding sites on CaMKII, forming a tripartite complex (El-Haou et al., 2009; Keskanokwong et al., 2011). Uncoupling of Kv4.3 at these sites, increases CaMKII dissociation from the complex, CaMKII autophosphorylation and L-type calcium currents (Keskanokwong et al., 2011). In hippocampal neurons, the scaffold protein AKAP79/150 colocalizes with Kv4 channels and anchors PKA in proximity to the channel (Lin, Sun, Kung, Dell'Acqua, & Hoffman, 2011). Activity dependent or chemically induced PKA-mediated phosphorylation of Kv4.2 at S552 induces internalization of the channel (R. S. Hammond, Lin, Sidorov, Wikenheiser, & Hoffman, 2008; J. Kim, Jung, Clemens, Petralia, & Hoffman, 2007) and causes dynamic cycling of Kv4.2 channels in CA1 apical dendrites (Nestor & Hoffman, 2012). In Kv4.2-KChIP complexes, PKA-induced S552 phosphorylation reduces surface expression (Schrader, Anderson, Mayne, Pfaffinger, & Sweatt, 2002) by causing the dissociation of the two proteins in lipid rafts in heterologous systems (Y. Li et al., 2022).

1.2 HCN2 channels as modulators of peripheral neuronal excitability during persistent inflammation

1.2.1 HCN channels

The hyperpolarization-activated cyclic nucleotide gated (HCN) family of voltage-gated ion channels comprises 4 members, HCN1-4. Each HCN gene encodes a six transmembrane domain (α subunit) with a canonical S4 voltage-sensor and S5-S6 pore conducting and selectivity filter

(Rivolta, Binda, Masi, & DiFrancesco, 2020). Functional homotetrameric or heterotetrameric channels are formed by multimerization of 4 α subunits using a conserved N-terminal domain and N-glycosylation of at least 3 α subunits (Kaku, Matsuoka, & Yang, 2019; M. Li, Tonggu, Tang, & Wang, 2015; Much et al., 2003; Proenza et al., 2002; Tran et al., 2002). The defining features of HCN channels include activation by membrane potentials below -50 mV, conduction of a mixed Na^+/K^+ inward current, and a lack of voltage-dependent inactivation (Biel, Wahl-Schott, Michalakakis, & Zong, 2009; Peters, Singh, Bankston, & Proenza, 2022). HCN isoforms can be distinguished by their selective modulation of cAMP which binds to a conserved cyclic nucleotide binding domain (CNBD) at the C-terminus (Combe & Gasparini, 2021). Binding of the auxiliary protein TRIP8b to the CNBD can block cAMP modulation and regulate HCN trafficking (Santoro et al., 2011; Santoro et al., 2009; Santoro, Wainger, & Siegelbaum, 2004)

1.2.2 Functional role of I_f in cardiac cells

HCN channels mediate I_f in the heart. HCN4 is the most abundant in Sinoatrial node (SAN) and Purkinje fibers where it is targeted to caveolin-3 domains (Barbuti et al., 2012; Rivolta et al., 2020; Sartiani, Mannaioni, Masi, Novella Romanelli, & Cerbai, 2017; Ye et al., 2008). I_f confers a pacemaker activity to the SAN by providing a steady-state inward current to bring the membrane potential closer to the threshold potential (Sartiani et al., 2017). HCN channel expression in the myocardium is much lower than in the conduction system (Herrmann, Layh, & Ludwig, 2011). HCN2 and HCN4 channels are expressed in the ventricles (Whitaker, Angoli, Nazzari, Shigemoto, & Accili, 2007; Ye & Nerbonne, 2009; Zhang, Huang, Lin, & Yu, 2009), and are postulated to prolong late repolarization (Fenske, Krause, Biel, & Wahl-Schott, 2011) and have a proarrhythmic effect in cardiac diseases (Hofmann et al., 2012).

1.2.3 Functional role of I_h in neurons

HCN channels mediate I_h in neurons. HCN2 channels are found in most brain regions while other HCN channels display region specific distributions (Robinson & Siegelbaum, 2003). In neurons, I_h stabilizes the resting membrane potential near subthreshold levels through a small fraction of HCN channels that are tonically open at the resting membrane potential (C. He, Chen, Li, & Hu, 2014). Tonic I_h decreases the membrane input resistance and membrane time constant and length constant (Shah, 2014). In neurons, I_h has also been shown to control synaptic transmission, dendritic integration, and rhythmic oscillations (Biel et al., 2009; Combe & Gasparini, 2021). HCN2 channels are implicated in several neurological disorders (DiFrancesco & DiFrancesco, 2015; Rivolta et al., 2020) including epilepsy where HCN2 knockout mice exhibit spontaneous absence seizures (Ludwig et al., 2003), and Parkinson disease, where progressive downregulation of HCN activity is reported in animal models of Parkinson disease (Good et al., 2011).

1.2.4 I_h in chronic inflammatory pain

The DRG is heterogenous population of cells that transduce various somatosensations including nociception. The canonical nociceptor is defined by a small or medium diameter somata. HCN1 and HCN2 are the primary channels in the DRG, with HCN1 channels predominating in large diameter DRG neurons and HCN2 in small diameter DRG neurons (Herrmann, Schnorr, & Ludwig, 2015). HCN channels have a minimal role in nociceptor transmission during normal conditions (Herrmann et al., 2015). However, in pathological conditions such as persistent inflammation, these channels accrue new roles as mediators of mechanical pain. Complete Freund's Adjuvant (CFA) is a common model of persistent inflammation that induces allodynia (pain response to innocuous stimulus) and hyperalgesia

(exaggerated pain response to noxious stimulus) for 1-2 weeks post-injection (K. Ren & Dubner, 1999). Sensory specific knockout of HCN2 prevented mechanical, but not thermal hyperalgesia in CFA-induced inflammation (Schnorr, Eberhardt, Kistner, Rajab, Kaer, et al., 2014). Administration of the non-selective I_h blocker ZD7288 significantly reduced mechanical allodynia post-CFA injection (Weng, Smith, Sathish, & Djouhri, 2012). At the molecular level, nociceptors show increased electrical excitability and increased I_h currents in small diameter neurons during CFA-induced inflammation (Weng et al., 2012). This is concurrent with increases in HCN2 channel expression in small and medium diameter DRG neurons at day 1 and day 7 post-injection, but not at day 3 when HCN2 expression was reported to return to normal (Acosta et al., 2012; Weng et al., 2012). Dynamic changes in HCN2 during long-standing inflammation suggests that multiple mechanisms may regulate channel expression. Similar increases in HCN2 expression were reported in a neuropathic pain model, where nerve injury is used as the chronic stimulus (Smith, Al Otaibi, Sathish, & Djouhri, 2015).

1.3 SUMOylation

1.3.1 *SUMO peptides*

The small ubiquitin-like modifier (SUMO) is a 12 kD peptide post-translationally added to lysine residues on target proteins. SUMO peptides contain a classic $\beta\beta\alpha\beta\beta\alpha\beta$ ubiquitin fold and are named for their structural similarity to ubiquitin (Cappadocia & Lima, 2018). There are four identified SUMO peptides (SUMO1-4) in mammals, with emerging evidence for a novel 5th isoform (SUMO5) (Liang et al., 2016). SUMO1 shares ~40% sequence homology with SUMO2 and SUMO3, which are 97% identical, and are collectively referred to as SUMO2/3 (Flotho & Melchior, 2013). The physiological relevance of SUMO4 and SUMO5 are unknown (Pichler, Fatouros, Lee, & Eisenhardt, 2017). 65% of SUMOylation preferentially occurs within a SUMO

consensus motif V/L-K-X-E, where X is any residue. SUMO2/3 has an internal SUMO motif allowing for poly-SUMO chain formation, while SUMO1 peptides lack this sequence and cannot form chains (Flotho & Melchior, 2013). Both SUMO1 and SUMO2/3 peptides are conjugated to proteins under physiological conditions. During stress response, SUMO2/3 conjugation is upregulated during pathological conditions due, in part, to a large reserve pool of unconjugated peptides (Saitoh & Hinchev, 2000; Su & Li, 2002).

1.3.2 The SUMOylation conjugation cascade

In comparison to the ubiquitin system, target SUMOylation is facilitated by a limited repertoire of enzymes. The SUMOylation cascade begins with maturation of the SUMO peptide by SUMO specific isopeptidases called SENPs. These enzymes cleave residues at the C-terminus of immature SUMOs to reveal a terminal diglycine motif that is used in the formation of thioester bonds during the enzymatic cascade. First, SUMO forms a thioester bond with the E1 enzyme, SAE1/SAE2, in an ATP consuming step. Next, SUMO forms a covalent bond with a catalytic cysteine on Ubc9, the only E2 conjugating enzyme. Finally, Ubc9 transfers the donor SUMO to the ϵ -group of the target lysine with the aid of E3 SUMO ligases. Target SUMOylation is antagonized by SENPs. There are 7 identified SENPs and each display a preference in subcellular localization and SUMO moieties (Cappadocia & Lima, 2018; Flotho & Melchior, 2013).

1.3.3 E3 SUMO ligases

E3 SUMO ligases aid in target SUMOylation by 1) interacting with the target, 2) stabilizing the Ubc9-SUMO bond through SUMO Interacting Motifs (SIMs) and 3) positioning the SUMO in an optimal position for discharge (Lascorz, Codina-Fabra, Reverter, & Torres-Rosell, 2022). A SIM motif is a 3-4 stretch of hydrophobic residues generally valine, isoleucine

or leucine intermixed by a single acidic amino acid. SIMs enable non-covalent SUMO interactions by binding to the second β strand of SUMO moieties in a parallel or antiparallel fashion (Lascorz et al., 2022). Some classes of SIMs display preference for the SUMO moieties they bind (Namanja et al., 2012). The 3 families of E3 SUMO ligases, SP-RING, RanBP2, and ZN451, have little structural similarity, with the exception that each possesses at least one SIM (Pichler et al., 2017).

In the early 2000's, the SP-RING family member Protein Inhibitor of Activated Stat 3 (PIAS3) was identified as an E3 SUMO ligase for transcription factors (E. S. Johnson & Gupta, 2001; Kahyo, Nishida, & Yasuda, 2001; Kotaja, Karvonen, Janne, & Palvimo, 2002; Schmidt & Muller, 2002; Takahashi, Kahyo, Toh, Yasuda, & Kikuchi, 2001). Work by Wible and colleagues during the late 1990's suggest that PIAS3 may also be an E3 SUMO ligase for ion channels. Wible and colleagues first identified PIAS3 as the K^+ Channel Associated Protein (KChAP). They showed that KChAP interacted with Kv1 and Kv2 α subunits and Kv β subunits in a yeast two hybrid assay, and co-immunoprecipitated with Kv2.1 and Kv4.3 channels in rat heart lysate (Kuryshhev, Gudz, Brown, & Wible, 2000; Wible, Yang, Kuryshhev, Accili, & Brown, 1998). Subsequently, they determined that KChAP was PIAS3, who's only known function at that time was as a transcriptional regulator for STAT3. From here on out, the protein will be called PIAS3. In heterologous systems, PIAS3 co-expression with Kv1.3, Kv2.1, and Kv4.3 increased their respective currents, co-expression with Kv1.2 and Kv1.4 decreased their respective currents and co-expression had no effect on Kv1.5 currents (Kuryshhev et al., 2000; Kuryshhev, Wible, Gudz, Ramirez, & Brown, 2001; Wible et al., 1998). It is not clear how PIAS3 exerts its effects on Kv channels. The most likely scenario is that PIAS3 acts as a SUMO ligase for Kv channels; however, PIAS3 is known to produce SUMOylation-independent effects

(Chung et al., 1997; B. Liu et al., 1998). Thus, it is important to determine if PIAS3 facilitates SUMOylation of Kv channels and the mechanism involved. PIAS3 is a multi-domain protein that includes SAP, PINIT, SP-RING, an S/T stretch and 2 SIM domains (Lussier-Price et al., 2020; Pichler et al., 2017; Rytinki, Kaikkonen, Pehkonen, Jaaskelainen, & Palvimo, 2009). Wible and colleagues determined that PIAS3's effects were mediated by an ~100 amino acid fragment (M fragment) through an unknown mechanism that was independent of transcription (Kuryshv et al., 2000). The only domain to be wholly incorporated into the M fragment is the SIM1 domain. The SIM1 domain of PIAS3 binds to the donor SUMO when it is conjugated to Ubc9 and positions it correctly for conjugation to the ϵ -group of the target lysine. The SIM1 domain is necessary for the PIAS3 SUMO ligase function (Lussier-Price et al., 2020). Thus far, no experiments have tested the hypothesis that PIAS3 acts through the SIM1 domain to facilitate SUMOylation of Kv channels.

1.3.4 Consequences of SUMOylation

Substrate SUMOylation can have a variety of effects. First, SUMOylation can facilitate protein-protein interactions, the most well studied being SUMO-SIM interactions, where the SUMO conjugated to the target protein is recognized by a SIM on an interacting partner protein. Second, SUMO can inhibit protein-protein interactions via steric hindrance. Third, SUMO can competitively inhibit post-translational modifications that occur on the same lysine residue. Finally, SUMO can localize a target protein through its interactions with phosphoinositides in the trans-Golgi [PI(3)P] or plasma membrane [PI(3,4,5)P3] (Kunadt et al., 2015).

The nuclear roles of SUMOylation on gene expression, cell division, and senescence have been well studied, as have the extra-nuclear roles of SUMO in metabolism (Vertegaal, 2022). The role of SUMOylation in regulating cell excitability is a growing field. SUMO has

been shown to modulate the function of numerous ion channels including: Kv1.5 (Benson et al., 2007), Kv2.1 (X. Q. Dai, Kolic, Marchi, Sipione, & Macdonald, 2009; Plant, Dowdell, Dementieva, Marks, & Goldstein, 2011), Kv4.2 (M. A. Welch, L. A. Forster, S. I. Atlas, & D. J. Baro, 2019; Welch, Jansen, & Baro, 2021), Kv7.1 (Xiong et al., 2017), Kv7.2/Kv7.3 (Y. Qi et al., 2014), Kv11.1 (Steffensen, Andersen, Mutsaers, Mujezinovic, & Schmitt, 2018), Nav1.2 (Plant, Marks, & Goldstein, 2016), Nav1.5 (Plant, Xiong, Romero, Dai, & Goldstein, 2020), and HCN2 (Parker et al., 2017). Ion channel SUMOylation produces different effects depending upon the ion channel involved. SUMO has also been shown to regulate HCN2 and Kv4.2 surface expression (Parker et al., 2017; M. A. Welch et al., 2019). In HEK cells, enhanced SUMOylation of HCN2 and Kv4.2 (in the ternary complex) at established SUMO sites increased maximal conductance and surface expression by enhancing Rab11a-dependent slow recycling of the channels after endocytosis (Welch et al., 2021) (L. A. Forster, Jansen L.R., Baro D.J). SUMOylation of these ion channels maybe manipulated in neurons, where the localization and function of the SUMOylation machinery is known to be regulated by activity-dependence (Feligioni, Nishimune, & Henley, 2009; Jaafari et al., 2013; Loriol, Khayachi, Poupon, Gwizdek, & Martin, 2013).

SUMO is also important for many cellular stress responses. In such cases, altered levels of SUMOylation at a group or global level facilitate a protective response. This is highlighted in the double stranded break response, where DNA damage induced by Methyl Methosulfate (MMS) enhanced the SUMOylation of multiple DNA repair proteins by the yeast E3 SUMO ligase Siz2 (Cremona et al., 2012; Psakhye & Jentsch, 2012). This “group SUMOylation” promoted genome integrity by facilitating protein complex formation through increased SUMO-SIM interactions (Psakhye & Jentsch, 2012). Importantly, mutating SUMO sites on these

proteins impaired the DNA repair response (Cremona et al., 2012; Psakhye & Jentsch, 2012). A similar effect was seen in mammalian cells where enhanced SUMO2 conjugation to chromatin modifier proteins resulted in coordinated transcriptional repression in response to MMS treatment (Hendriks, Treffers, Verlaan-de Vries, Olsen, & Vertegaal, 2015).

The large reserve pool and ability to form polySUMO chains, makes SUMO2 an effective signal during heat shock (Flotho & Melchior, 2013; Saitoh & Hinchev, 2000; Su & Li, 2002). SUMO2 conjugation displays a rapid and dynamic redistribution during heat stress (Golebiowski et al., 2009). Here, global SUMO2/3 conjugation facilitates a multitude of protective responses. SUMO2 conjugation to chromatin-associated proteins ensures the stability of protein complexes (Seifert, Schofield, Barton, & Hay, 2015), which results in the restriction of transcriptional activity of heat shock induced genes (Niskanen et al., 2015). Rapid conjugation of SUMO2/3 to proteins during heat shock prevents protein aggregation by ensuring that proteins remain soluble thereby maintaining proteostasis (Liebelt et al., 2019).

SUMO expression is enhanced in the brain and heart during hypoxia (Comerford et al., 2003; Shao et al., 2004). Targets of altered SUMOylation during hypoxic conditions include HIF1 α , the principal inducer of hypoxic responses (Bae et al., 2004; Q. Cai, Verma, Kumar, Ma, & Robertson, 2010; J. Cheng, Kang, Zhang, & Yeh, 2007), other transcription factors and regulators of RNA stability (Chachami et al., 2019), and the SUMOylation machinery itself (Kunz et al., 2016). Cerebral and cardiac ischemias induce a global increase in SUMO conjugation (Chen et al., 2020; Cimarosti, Lindberg, Bomholt, Ronn, & Henley, 2008; Shao et al., 2004). In cardiomyocytes, hypoxia-induced changes in ion channel function promote proarrhythmic responses. Hypoxia increases SUMOylation of Nav1.5 in cardiomyocytes causing the channels to open in a normally inactivate state (Plant et al., 2020). This current, referred to as

I_{LATE} , prolongs the action potential. In cardiomyocytes, Kir2.1 currents stabilize the resting membrane potential and contribute to ventricular repolarization. Hypoxia-induced SUMOylation of Kir2.1 inhibits Kir2.1 currents through PIP2 in cardiomyocytes (Y. Xu et al., 2022). Altered SUMOylation has been reported in other diseased states of the heart including cardiac hypertrophy, where increased SUMO1 conjugation results in a protective phenotype, while overexpression of SUMO2 facilitates a pathological, hypertrophic phenotype (E. Y. Kim et al., 2015; A. Lee et al., 2014). In models of cardiac reperfusion injuries, protein components of the proteasomal degradation pathway, cardiac metabolism, and hypoxia and angiogenesis regulation display altered SUMO1 or SUMO2 conjugation (Hotz et al., 2020). Whether or not SUMOylation is protective during hypoxic conditions likely depends on the target's function.

1.4 Hypothesis

This work addresses two hypotheses. First, is HCN2 SUMOylation a mechanism for regulating HCN2 channel expression in nociceptors during persistent inflammation? In Chapter 2 and Chapter 3, HCN2 expression and HCN2 channel SUMOylation are quantified in cryosections of L4-L6 DRG neurons following CFA-induced inflammation in the rat hindpaw. Second, is PIAS3 an E3 SUMO ligase for ion channels? Experiments to test this hypothesis are performed in Chapter 4. Using a HEK cell model, the modulation of Kv4 channels by PIAS3 is characterized and the mechanism of action is identified. These experiments are then extended to cultured ventricular rat cardiomyocytes.

2 ALTERATIONS IN SUMOYLATION OF THE HYPERPOLARIZATION- ACTIVATED CYCLIC NUCLEOTIDE-GATED ION CHANNEL 2 DURING PERSISTENT INFLAMMATION

Publication: Forster LA, * **Jansen LR**,* Rubaharan M, Murphy AZ, Baro DJ. 2020. Alterations in SUMOylation of the hyperpolarization-activated cyclic nucleotide-gated ion channel 2 during persistent inflammation. *Eur J Pain*. doi:10.1002/ejp.1606

Contribution disclosure: LA. Forster, LR. Jansen, AZ Murphy, and DJ Baro were responsible for the conception and design of the research presented. M. Rubaharan performed animal experiments. LA. Forster and LR. Jansen contributed to the acquisition and analysis of the data. LA. Forster and LR. Jansen contributed equally*. LA. Forster, LR. Jansen and D. Baro were responsible for drafting the manuscript, and all authors were involved in revising the manuscript.

2.1 Abstract

Unilateral injection of Complete Freund's Adjuvant (CFA) into the intra-plantar surface of the rodent hindpaw elicits chronic inflammation and hyperalgesia in the ipsilateral hindlimb. Mechanisms contributing to this hyperalgesia may act over multiple time courses and can include changes in ion channel expression and post-translational SUMOylation. Hyperpolarization-activated, cyclic nucleotide-gated (HCN) channels mediate the hyperpolarization-activated current, I_h . An HCN2-mediated increase in C-nociceptor I_h contributes to mechanical hyperalgesia in the CFA model of inflammatory pain. Changes in HCN2 post-translational SUMOylation and protein expression have not been systematically documented for a given DRG throughout the time course of inflammation. This study examined HCN2 protein expression and post-translational SUMOylation in a rat model of CFA-induced hindpaw inflammation. L5 DRG cryosections were used in immunohistochemistry experiments and proximity ligation assays to investigate HCN2 expression and SUMOylation, respectively, on days 1 and 3 post-CFA. Unilateral CFA injection elicited a significant bilateral increase in HCN2 staining intensity in small diameter DRG neurons on day 1 post-CFA, and a significant bilateral increase in the number of small neurons expressing HCN2 but not staining intensity on day 3 post-CFA. HCN2 channels were hyper-SUMOylated in small diameter neurons of ipsilateral relative to contralateral DRG on days 1 and 3 post-CFA. Unilateral CFA injection elicits unilateral mechanical hyperalgesia, a bilateral increase in HCN2 expression and a unilateral increase in post-translational SUMOylation. This suggests that enhanced HCN2 expression in L5 DRG is not sufficient for mechanical hyperalgesia in the early stages of inflammation and that hyper-SUMOylation of HCN2 channels may also be necessary.

2.2 Significance

Nociceptor HCN2 channels mediate an increase in I_h that is necessary for mechanical hyperalgesia in a CFA model of chronic pain, but the mechanisms producing the increase in nociceptor I_h have not been resolved. The data presented here suggest that the increase in I_h during the early stages of inflammation may be mediated by an increase in HCN2 protein expression and post-translational SUMOylation.

2.3 Introduction

Nociceptor signaling is increased in chronic pain states due, in part, to maladjustments in sensory neuron ionic conductances (Berta, Qadri, Tan, & Ji, 2017; Gold & Gebhart, 2010; Pace et al., 2018; Reichling & Levine, 2009). In most cases, the molecular and cellular processes leading to this peripheral sensitization are poorly understood. Mounting evidence suggests that widespread alterations in ion channel SUMOylation may contribute to conductance changes underpinning hyperalgesia associated with chronic pain.

Small ubiquitin like modifier (SUMO) is a ~12kDa peptide that is reversibly conjugated to lysine (K) residues of target proteins (Flotho & Melchior, 2013). The majority of SUMOylation (~65%) occurs within identifiable consensus sequences (Hendriks, D'Souza, Chang, Mann, & Vertegaal, 2015). The phosphorylation status of a target protein often determines its ability to be SUMOylated (Dustrude et al., 2016). Additionally, the level of target protein SUMOylation depends upon the ratio of 2 opposing enzyme activities: conjugation by Ubc9 and deconjugation by isopeptidases, the best studied being the SENP family (isoforms 1-7) (Kunz, Piller, & Muller, 2018). A variety of E3 proteins can also stabilize Ubc9-target protein interactions to promote SUMOylation (Flotho & Werner, 2012; Koidl et al., 2016; Werner, Flotho, & Melchior, 2012). Of the 4 SUMO isoforms, SUMO1-3 are well-studied but the

physiological relevance of SUMO4 is unclear (Watts, 2013). SUMO2 and SUMO3 are 97% identical and are referred to as SUMO2/3. SUMO1 shares 47% identity with SUMO2/3. Non-mutually exclusive consequences of target protein SUMOylation include: 1) prevention of other modifications that occur on the same K (Anderson, Eom, & Stover, 2012); 2) binding to phosphoinositides (PIPs) concentrated in the trans-Golgi [PI(3)P] and plasma membrane [PI(3,4,5)P3] (Arendt et al., 2010; G. R. V. Hammond & Burke, 2020; Kunadt et al., 2015); 3) prevention of protein-protein interactions through steric hindrance (Dustrude et al., 2016); and most commonly, 4) promotion of protein-protein interactions through binding domains in partner proteins that recognize SUMO (Psakhye & Jentsch, 2012; Seifert et al., 2015).

Extracellular signaling and neuronal activity regulate the location and activity of the SUMOylation machinery and the SUMOylation status of target proteins (Craig et al., 2012; Hendriks, D'Souza, et al., 2015; Loriol et al., 2013; Parker, Forster, & Baro, 2019; Seifert et al., 2015). Both extracellular signals and nociceptor activity are altered during CFA-induced persistent inflammation, and a generalized increase in SUMOylation is observed in the DRG (Y. Wang et al., 2018b). SUMOylation of TRPV1 channels is necessary for thermal hyperalgesia during CFA-induced persistent inflammation, and increasing SUMOylation by genetic knock-out of SENP1 in sensory neurons exacerbates thermal hyperalgesia during CFA-induced persistent inflammation (Y. Wang et al., 2018b). SUMOylation of the NaV1.7 auxiliary subunit, CRMP2, prevents channel endocytosis (Dustrude et al., 2016). CRMP2 was hyper-SUMOylated in primary sensory afferents in a rat spared nerve injury model of chronic neuropathic pain, and blocking CRMP2 hyper-SUMOylation prevented mechanical and thermal hyperalgesia in this model (Dustrude et al., 2016; Dustrude, Wilson, Ju, Xiao, & Khanna, 2013; Francois-Moutal, Dustrude, et al., 2018; Moutal, Dustrude, et al., 2017). These data suggest that nociceptor ion

channel hyper-SUMOylation contributes to hyperalgesia during chronic inflammatory and neuropathic pain.

Several ion channel subunits can be SUMOylated. Existing data generally suggest that hyper-SUMOylation of ion channel subunits increases cell excitability. Enhancing K⁺ channel SUMOylation reduces outward currents mediated by Kv4 (M. A. Welch et al., 2019), Kv11 (Steffensen et al., 2018), Kv7 (Y. Qi et al., 2014; Xiong et al., 2017), Kv2 (Plant et al., 2011), and K2P1 (Plant et al., 2010; Rajan, Plant, Rabin, Butler, & Goldstein, 2005). To our knowledge, only Kv1.5 does not fit this pattern and is increased by hyper-SUMOylation (Benson et al., 2007), however, Kv1.5 is not highly expressed in nociceptors (Zheng et al., 2019). Conversely, inward conductances are generally enhanced by hyper-SUMOylation, including conductances mediated by HCN2 (Parker et al., 2017), NaV1.2 (Plant et al., 2016), NaV1.7 (Dustrude et al., 2016) and TRPV1 (Y. Wang et al., 2018a). While SUMO modulation of ion channels may be much more complex and vary according to which sites on the ion channel are SUMOylated (M. A. Welch et al., 2019), the data suggest a generalized increase in nociceptor ion channel SUMOylation could lead to increased excitability.

The nociceptor hyperpolarization-activated current (I_h) is increased in several models of chronic inflammatory and neuropathic pain (Djoughri et al., 2015; Emery, Young, Berrocso, Chen, & McNaughton, 2011; Schnorr, Eberhardt, Kistner, Rajab, Kasser, et al., 2014; Weng et al., 2012). I_h plays a pivotal role in shaping neuronal excitability and synaptic integration by influencing several neuronal activity features including membrane potential, firing threshold, resonance frequency, temporal summation, and synaptic strength (Hutcheon & Yarom, 2000; Shah, 2014; Wahl-Schott & Biel, 2009). Hyperpolarization-activated cyclic nucleotide gated ion channels (HCN) mediate I_h (Sartiani et al., 2017). There are four HCN isoforms. Genetic ablation

of HCN2 in primary sensory afferents prevented mechanical and thermal hyperalgesia in a chronic constriction injury model of neuropathic pain (Emery et al., 2011) and mechanical hyperalgesia in a CFA model of persistent inflammation (Schnorr, Eberhardt, Kistner, Rajab, Kasser, et al., 2014). HCN2 protein expression increases in small DRG neurons during CFA-induced persistent inflammation (Acosta et al., 2012; Weng et al., 2012). HCN2 is SUMOylated by both SUMO1 and SUMO2/3 in the rodent brain (Parker et al., 2017). SUMOylation of HCN2 at K669 increases channel surface expression and I_h in a heterologous expression system (Parker et al., 2017). Here we investigate changes in HCN2 expression and SUMOylation in rat L5 DRG on days 1 and 3 of CFA-induced inflammation.

2.4 Materials and Methods

2.4.1 *Animal Ethics*

Ethics approval was obtained from the Institutional Animal Care and Use Committee at Georgia State University, and all experiments were performed in compliance with Ethical Issues of the International Association for the Study of Pain and National Institutes of Health (NIH). Male Sprague-Dawley rats (Charles-River, MA) were pair-housed on a 12-hour light/dark cycle (lights on at 0700 hours) with ad libitum access to food and water.

2.4.2 *CFA model and tissue preparation*

Sixty-day old male Sprague-Dawley rats were injected with 200 μ l of CFA (Sigma, F5881, 1 ml contains 1 mg of heat-killed and dried *Mycobacterium tuberculosis* [strain H37Ra, ATCC 25177], 0.85 ml paraffin oil and 0.15 ml of mannide monooleate) into the mid-plantar surface of the right hindpaw. Control rats were handled, but did not receive CFA injections. Either 1 or 3 days later rats were anesthetized with 600 μ l of sodium pentobarbital (390 mg/ml) in phenytoin sodium (50 mg/ml) followed by an intracardiac injection of heparin (NDC 25021-

400-30, 1000 USP units/mL). Animals were perfused with ~200 ml of sodium nitrite saline followed by 350 ml of 4% paraformaldehyde. Hindpaws were measured. CFA-treated rats showed a significant increase in ipsilateral hindpaw width relative to contralateral hindpaw width ($p=0.0003$). Control rats showed no change ($p>0.9999$). After fixation, bilateral L5 DRG were identified by counting down from T13 (located at the last rib) to L6. L5 DRG were dissected and placed into 18% sucrose at 4°C overnight. The next day, the epineurium of each DRG was removed. DRG were embedded in 0.3% gelatin and sliced in 20 µm cryosections (Leica CM3050 S); slices were stored at 4°C for short-term storage (<2 months), or at -80°C for longer-term storage.

2.4.3 Antibodies and Reagents

The HCN2 polyclonal rabbit antibody (Alomone, APC-030, Jerusalem) concentration used was 1:200 for proximity ligation assays and 1:250 for immunohistochemistry (IHC) experiments, 5 µg for immunoprecipitations (IP), and 1:1000 for Western Blots. A secondary Alexa 488 goat anti-rabbit was used at 1:400 (Jackson ImmunoResearch, PA) for IHC experiments. For PLA, a monoclonal mouse antibody against SUMO1 (Santa Cruz, Sc-5308) was used at 1:100, and a monoclonal mouse antibody against SUMO2/3 (Developmental Studies Hybridoma Bank, SUMO-2 8A2) was used at a concentration of 1:70 and developed by Matinus, M. at John Hopkins School of Medicine, created by the NICHD of the NIH and maintained at The University of Iowa, Department of Biology, Iowa City, IA 52242. All chemicals were obtained through Sigma-Aldrich unless otherwise stated.

2.4.4 Immunohistochemistry

A cryosection was encircled with a hydrophobic pen (Vector Laboratories), washed once with 0.1 M PBS, twice with HBSS, and incubated with 3.5 µg/ml of Wheat Germ Agglutinin

CF® 594 (Biotium) to stain membranes. The cryosection was serially washed twice with HBSS, once with 0.1 M PBS, and permeabilized with 0.1 M PBS with 0.2% Triton X-100 (PBS-T). The cryosection was blocked for 30 minutes with 10% normal goat serum in PBS-T and incubated with diluted anti-HCN2 in PBS-T overnight at room temperature. The cryosection was serially washed three times with 0.1 M PBS and incubated with Alexa 488 goat anti-rabbit diluted in 0.1 M PBS for 3 hours at room temperature. The cryosection was washed 3x in 0.1 M PBS and incubated with 4', 6-diamidino-2-phenylindole (DAPI) (300 nM) for 5 minutes. Serial washes with 0.1 M PBS were repeated three times, and the cryosection was mounted with ProLong Gold antifade reagent (Thermo-Fisher Scientific). All incubations were performed in a humidity chamber with a minimum volume of 17 μ l per cryosection. IHC experiments were repeated on 7 experimental animals and 3 control animals for day 1, and 5 experimental animals and 4 control animals for day 3.

2.4.5 Immunohistochemistry analysis

Blind analyses were performed. DRG images were taken at 5x total magnification using an Olympus BX43 fluorescence microscope and cellSens software. Three images were taken per DRG. Images were analyzed with Photoshop. Each image was thresholded to remove the intensity of the sheath by successively increasing the tolerance of the magic wand tool. All remaining cells were considered HCN2 positive and were quantified if they showed a definitive nucleus and visible cell perimeter. Cells not meeting these criteria were ignored. All HCN2 positive cells were selected using the magnetic lasso tool and the diameter and gray mean values for each selection were obtained using the measurement feature. Cells were then classified by diameter: small $\leq 30 \mu\text{m}$, medium 31- 40 μm , large $> 40 \mu\text{m}$. The gray mean values for all cells in each neuronal size class were averaged and taken to be the mean intensity for the size class.

To measure frequency for each size class, the number of HCN2 positive cells in a class were divided by the total number of cells meeting the quantification requirements.

2.4.6 Proximity Ligation Assay

Proximity ligation assays were performed using Duolink® in situ Red kit (Sigma-Aldrich) following manufacturer's instructions. Briefly, DRG cryosections were washed once in 0.1 M PBS, twice in HBSS then incubated with 5 µg/ml Wheat Germ Agglutinin-FITC (Sigma-Aldrich) to stain membranes. DRG sections were washed twice with HBSS, once with 0.1 M PBS permeabilized with PBS-T. Each cryosection was blocked using 17 µl of Duolink® blocking solution for 30 minutes at 37°C. Primary antibodies were diluted in Duolink® antibody diluent, 17 µl was applied to each cryosection and incubated overnight at room temperature. Slides were washed three times for 15 minutes in 0.1 M PBS, and incubated with Duolink® anti-mouse minus and Duolink® anti-rabbit plus secondaries for 1 hour at 37°C. Slides were washed twice with Duolink® wash buffer A. The ligation reactions were performed at 37°C for 30 minutes. Slides were washed twice for 2 minutes with wash buffer A. The amplification reaction time was extended by 10% to 110 minutes at 37°C. Slides were washed twice for 10 minutes in wash buffer B then once in 0.1x wash buffer B before mounting with Vectashield non-hardening mounting medium (Vector laboratories, H-1000). Slides were sealed with clear nail varnish. All incubations were performed in a humidity chamber. All washes with PLA wash buffers A or B were performed in a minimum volume of 70 ml. PLA experiments using SUMO2/3 were repeated on 6 experimental animals and 3 control animals at 1 day, and on 7 experimental animals and 4 control animals at day 3. PLA experiments using SUMO1 were repeated on 6 experimental animals and 4 control animals at day 1, and 6 experimental animals and 3 control animals at day 3.

2.4.7 *PLA analysis*

Blind analyses were performed. Images were acquired with a Zeiss 700 confocal microscope using a 40x oil immersion objective within 5 days of the PLA experiment. Three sections were analyzed per DRG. For each section, a minimum of 3 z-stacks was acquired. Optical slices were 0.9 μm thick with an interval of 1 μm . Images were analyzed using the FIJI version of ImageJ. A maximum projection was created from 5 z-slices from the center of a cell. A projection contained a visible nucleus and clear cell boundaries and did not overlap with neighboring cells or fibers. Cells were outlined, and thresholded using the triangle method. The triangle method assumes that the intensity of the image is skewed in one direction and finds a value where the skew from background intensity is removed, leaving only signal above that value. Watershed analysis was performed to divide any coalesced signals. The analyze particle feature was used to obtain puncta number, mean pixel intensity and area for each punctum, as well as the area of the cell and Feret's diameter. Mean pixel intensity (MPI) of the puncta within 1 cell was obtained by a program developed by Alex Perez, to calculate the average mean puncta intensity within 1 cell and allow us to batch process large amounts of data.

2.4.8 *Rat DRG membrane preparation and denaturing immunoprecipitation*

Approximately 50 DRG were extracted from two rats and placed in autoclaved Dulbecco's phosphate buffer saline (DPBS) (2.7 mM KCl, 1.5 mM KH_2PO_4 , 136.9 mM NaCl, 8.9 mM Na_2HPO_4) on ice. DPBS was removed and the DRG were mechanically homogenized in 250 μl of ice cold homogenization buffer [0.3 M sucrose, 10 μl of 0.1 M PBS pH 7.4, 1 mM EDTA, 1:100 protease inhibitor cocktail (Sigma, cat. P8340)] supplemented with 20 mM NEM to prevent SUMO deconjugation. The homogenate was collected, and nuclei and cellular debris were pelleted by centrifugation at 14,000 RPM for 10 minutes at 4°C. The supernatant was

retained, and membranes were separated by ultracentrifugation in a tabletop ultracentrifuge at 40,000g for 90 min at 4°C. The supernatant was removed, and membranes were resuspended in 20 µl of denaturing buffer [1% SDS, 50 mM Tris-HCl pH 7.4, 5 mM DTT, 1:100 protease inhibitor cocktail (Sigma, cat. P8340), 20 mM NEM]. The resuspended membrane pellet was shaken for 1 hour at 4°C to aid in the resuspension of membrane proteins. The membrane fraction was then brought to volume of 200 µl with dH₂O to dilute the SDS prior to IPs. To further denature proteins, the sample was heated at 95°C for 10 minutes. The boiled sample was cooled on ice before addition of the IP antibody. ~1000 µg of protein was used for each IP with 5 µg of rabbit anti-HCN2 or 5 µg of normal IgG for negative controls. IPs were performed using the Classic Magnetic IP/Co-IP Kit (Pierce, cat. 88804) according to the manufacturer's instructions. IP products were eluted in a volume of 50 µl.

2.4.9 Western Blot

An HCN2 IP and a negative IgG control from the same membrane preparation (see above) were run side by side in sets of 3 on the same 12% SDS-polyacrylamide gel. After electrophoresis, proteins were transferred from the gel for 2 h at 45 AMP to a PVDF membrane (Immobilon-P, cat. #IPVH00010) using a semi-dry electroblotting system (OWL). The membrane was cut into 3 pieces and each piece comprised one set of HCN2 and IgG IP products. Membranes were blocked in 5% non-fat dry milk in TBS (50 mM Tris-HCl pH 7.4, 150 mM NaCl) for 1 h at room temperature (RT). Blots were washed 1x for 10 minutes with TTBS (TBS+ 0.1% Tween20), and then primary antibodies, prepared in 1% non-fat dry milk in TTBS, were added and incubated overnight at 4°C. Each set was probed with a different antibody that recognized HCN2, SUMO1 (Cell Signaling, 4930S, 1:1500) or SUMO2/3 (Abcam, ab3742, 1:750). Blots were washed 3x for 5 minutes in TTBS and then incubated with goat anti-rabbit

alkaline phosphatase conjugated secondary antibody (Jackson ImmunoResearch, 1:4000), prepared in 1% non-fat dry milk in TTBS, for 2 h with agitation at RT. Blots were washed 3x for 10 min with TTBS. The membranes were incubated with alkaline phosphatase substrate (Bio-Rad) for 5 minutes at RT, and then the membranes were exposed to X-ray film (MedSupply partners) and the chemiluminescent signals were visualized with a Kodak X-Omat 2000A imager.

2.4.10 Statistics

All statistical analyses were performed using GraphPad Prism. Data were tested for normality. Normal IHC data were analyzed with a one-way ANOVA followed by a Tukey's post-hoc test. Normal PLA data were analyzed with a paired t-test. Non-parametric data were analyzed with Kruskal-Wallis (KW) for IHC or Wilcoxon matched-pairs signed rank tests for PLA. All values are presented as the mean \pm SEM. $p < 0.05$ was considered statistically significant.

2.5 Results

2.5.1 Inflammation increases the level of HCN2 expression and the number of cells expressing HCN2.

Previous studies examined the effects of cutaneous hindlimb inflammation in L5 DRG on day 7 post-CFA and in L4 DRG on days 1 and 4 post-CFA (Acosta et al., 2012; Weng et al., 2012). This study examined the results of CFA-induced inflammation in L5 DRG on days 1 and 3 post-CFA. In the experimental treatment group, CFA was injected into the right hindpaw of each adult male Sprague-Dawley rat. In the control treatment group, rats were handled but not injected. Animals were perfused on day 1 or 3 post-CFA injection/handling. L5 DRG were dissected, cryosectioned (20 μ m) and used in IHC experiments. The specificity of the HCN2

antibody (anti-HCN2, Alomone Labs) was previously verified in a rigorous series of experiments (Acosta et al., 2012) and was confirmed here in a series of preliminary IHC experiments using antibody that was pre-absorbed with the immunogen provided by the manufacturer. Pre-absorption greatly diminished staining intensity (Figure 2-1A). As described in Materials and Methods, raw images of IHC experiments (Figure 2-1B, left panel) were processed, and HCN2-positive neurons were identified and circled (Figure 2-1B, right panel). Cells were classified into three groups according to diameter: small ($\leq 30 \mu\text{m}$), medium ($30 \mu\text{m} < x < 40 \mu\text{m}$), and large ($> 40 \mu\text{m}$). HCN2 immunoreactivity (IR) was measured as the mean pixel intensity for each cell and as the frequency of HCN2 expressing cells. The number of cells expressing HCN2 was quantified for each of the three cell sizes by dividing the number of HCN2 positive cells in each size category by the total number of cells in the DRG section (HCN2-positive and -negative) and multiplying by 100. This was termed frequency.

The mean pixel intensities measured on day 1 post-CFA were compared between control and experimental DRG (Figure 2-2B). The average mean pixel intensity for small diameter neurons in experimental animals significantly increased by ~50% in both contralateral (21.3 ± 1.4) and ipsilateral (22.8 ± 1.7) relative to control DRG (14.9 ± 0.8). The average mean pixel intensity for medium diameter neurons increased by ~40% in experimental (ipsilateral, 25.4 ± 2.6 ; contralateral, 23.2 ± 1.5) relative to control DRG (18.0 ± 1.3). The increase was statistically significant only for the ipsilateral DRG (Figure 2-2 legend). There were no significant differences in the average mean pixel intensity between large diameter neurons (contralateral, 25.1 ± 2.1 ; ipsilateral, 28.3 ± 3.8 ; control, 20.5 ± 2.2). A comparison of the mean frequency showed that there were no significant differences between control and experimental animals or between ipsilateral and contralateral DRG for any neuronal size class (Figure 2-2C). In general,

~55-65% of all DRG neurons examined here expressed HCN2, and small-diameter neurons had the greatest number of HCN2-positive cells (contralateral: small, $37.3 \pm 4.8\%$; medium, $12.4 \pm 1.8\%$ large, $13.1 \pm 2.0\%$) (ipsilateral: small, $34.1 \pm 5.6\%$; medium, $13.8 \pm 2.3\%$; large, $15.9 \pm 4.4\%$) (control: small, $22.3 \pm 5.7\%$; medium, $14.2 \pm 2.5\%$; large, $17.2 \pm 1.9\%$).

The situation changed by day 3 post-CFA such that there was a significant increase in the number but not intensity of cells expressing HCN2 (Figure 2-3). The average mean pixel intensities were no longer significantly different for any size class (Figure 2-3B), although there was still a slight elevation in contralateral (small, 21 ± 3.1 ; medium, 23.6 ± 3.7 ; large, 26.1 ± 4.7) and ipsilateral DRG (small, 19.6 ± 2.5 ; medium, 22.4 ± 3.5 ; large, 24.8 ± 4.3) relative to control DRG (small, 15 ± 1.9 ; medium, 16.9 ± 2.1 ; large, 18.7 ± 2.1). On the other hand, the number of cells expressing HCN2 significantly increased in small and medium but not large diameter neurons in experimental relative to control animals (Figure 2-3C). Mean frequency in both contralateral (small, $35.8 \pm 8.3\%$; medium, $17.2 \pm 1.7\%$) and ipsilateral DRG (small, $30.6 \pm 3.5\%$; medium, $15.8 \pm 1.4\%$) were significantly increased relative to control DRG (small, $11.9 \pm 2.4\%$; medium, $9.5 \pm 0.7\%$), but were not significantly different from one another.

In sum, unilateral hindpaw inflammation initially produced a significant bilateral increase in HCN2 protein expression in small diameter neurons. CFA-induced inflammation also produced a significant ipsilateral increase in medium diameter neurons. As inflammation progressed, expression levels returned back toward normal, but the number of small and medium diameter cells expressing HCN2 increased bilaterally.

2.5.2 HCN2 is SUMOylated in the rat DRG.

SUMOylation of HCN2 channels has never been examined in DRG neurons. To determine if HCN2 channels were SUMOylated in DRG neurons, denaturing

immunoprecipitation (IP) experiments were performed using DRG membrane preparations and an antibody against HCN2 followed by western blot experiments with antibodies against HCN2, SUMO2/3 and SUMO1. The experiment was repeated 3 times (i.e. 6 rats, see Materials and Methods). A representative experiment shows that all 3 antibodies recognized the same appropriately sized ~100kD band (Figure 2-4). This band was not observed in IP experiments using a non-specific rabbit IgG on the same membrane preparation. In order to prevent non-covalent interactions between proteins, i.e. co-IP, the membrane preparations were denatured with a high concentration of SDS (1%) and high heat treatment (95°C for 10 min) prior to the IPs (see Materials and Methods). These data indicate that SUMO1 and SUMO2/3 are covalently linked to HCN2 α -subunits in the rat DRG.

Next, *in situ* proximity ligation assays (PLA) were used to examine HCN2 channel SUMOylation in individual DRG neurons. Preliminary pre-absorption experiments on cryosectioned DRG confirmed the specificities of the SUMO1 (anti-SUMO1) and SUMO2/3 (anti-SUMO2/3) antibodies (Figure 2-5A). HCN2 channel SUMOylation was examined using anti-HCN2 and anti-SUMO2/3 in PLA on cryosectioned DRG (experimental). Primary antibodies were omitted in control PLA. SUMOylated HCN2 channels appeared as fluorescent puncta in confocal optical sections (Figure 2-5B, upper panels). Punctum area and intensity varied, which may reflect differences in the number of HCN2 channels represented by a punctum, e.g. solitary vs. clustered channels, and/or the extent of their SUMOylation. Puncta number and punctum mean pixel intensity were used as measures of the number of SUMOylated channels and the extent of channel SUMOylation, respectively. To measure HCN2 channel SUMOylation in a single cell, a confocal projection representing 5, ~1 μ m optical sections from the center of a cell was obtained. Note that this represents ~ 1/4 (small) to 1/8 (large) of the

volume of a neuron and that surface sections will be excluded, i.e., all plasma membrane staining lies along the perimeter of the cell. A cell was outlined and automatically thresholded to eliminate background (Figure 2-5B, bottom panels). FIJI was then used to measure the area of the cell as well as the number and intensity of puncta from within the circled region. Control and experimental PLA were performed on alternating sections of L5 DRG. DRG from 3 animals were analyzed. Results showed significantly more puncta/ μm^2 in experimental vs. control treatment groups (Figure 2-5C). These data indicated that HCN2 channels were decorated with SUMO2/3 in rat L5 DRG and that this method could be used to examine HCN2 channel SUMOylation in individual neurons.

2.5.3 Significantly more HCN2 SUMO2/3 conjugation is observed in small diameter neurons from ipsilateral DRG on day 1 but not day 3 post-CFA.

To test if HCN2 channels were hyper-SUMOylated during CFA-induced inflammation, CFA was injected into the right hindpaw of adult male rats. Animals were perfused 1 or 3 days post-CFA. Bilateral L5 DRG were dissected and cryosectioned. *In situ* PLA was performed on the cryosections using anti-HCN2 and anti-SUMO2/3. Control animals were handled but not injected. HCN2 channels were decorated with SUMO2/3 in small, medium, and large neurons from ipsilateral and contralateral DRG 1 day post-CFA (Figure 2-6A). The number of puncta per μm^2 was determined for the 3 size classes of neurons. Comparisons of control and experimental animals showed no significant differences and are not reported here. On the other hand, paired comparisons between contralateral and ipsilateral DRG from the same experimental animal revealed significant differences. Most likely, differences were revealed in the latter analyses because biological variability was reduced by intra-animal comparison.

A significant ~25% increase in puncta number was observed in small neurons from ipsilateral relative to contralateral DRG (Figure 2-6B). No significant differences were observed in medium or large diameter neurons in contralateral vs. ipsilateral DRG (Figure 2-6B). Paired t-tests on left vs. right DRG in the control treatment group indicated no significant differences (small, 0.24 ± 0.04 vs. 0.23 ± 0.03 , $p=0.5389$; medium, 0.23 ± 0.04 vs. 0.21 ± 0.06 , $p=0.6006$; large, 0.26 ± 0.03 vs. 0.23 ± 0.04 , $p=0.6340$; $n=3$ animals). Punctum intensity was divided by punctum area to obtain the mean pixel intensity per punctum, here termed puncta intensity. The average puncta intensity was calculated for each cell. Average puncta intensity was not significantly different between contralateral vs. ipsilateral DRG neurons for any size class (Figure 2-6C). Control animals showed no differences between left vs. right DRG (small, 47.82 ± 2.74 vs. 41.80 ± 4.32 , $p=0.25$; medium, 47.72 ± 2.79 vs. 42.68 ± 4.77 , $p=0.1694$; large, 48.96 ± 2.19 vs. 42.98 ± 5.32 , $p=0.2730$; $n=3$).

Analyses were performed for animals perfused at 3 days post-CFA (Figure 2-7A). There were no significant differences in HCN2-SUMO2/3 puncta number (Figure 2-7B) or intensity (Figure 2-7C) between contralateral vs. ipsilateral DRG neurons from experimental animals for any neuronal size class. There were also no significant differences between left vs. right DRG in the control treatment group for either puncta number (small, 0.38 ± 0.08 vs. 0.39 ± 0.11 , $p=0.8946$; medium, 0.43 ± 0.11 vs. 0.36 ± 0.12 , $p=0.2152$; large, 0.50 ± 0.10 vs. 0.41 ± 0.11 , $p=0.0708$; $n=4$) or puncta intensity (small, 71.23 ± 17.97 vs. 61.01 ± 12.95 , $p=0.1466$; medium, 69.65 ± 16.31 vs. 61.14 ± 12.65 , $p=0.1181$; large, 69.74 ± 17.88 vs. 61.03 ± 12.82 , $p=0.1987$; $n=4$).

In sum, the number of HCN2 channels decorated with SUMO2/3 was transiently increased by ~25% in small neurons from ipsilateral relative to contralateral DRG on day 1 but not 3 post-CFA. There were no significant changes in the extent of channel SUMOylation.

2.5.4 Conjugation of SUMO1 to HCN2 channels was reduced in medium and large diameter neurons on 1 day post CFA and increased in small neurons on day 3 post-CFA.

PLA experiments were repeated for experimental and control animals except that anti-SUMO1 was used. HCN2 channels decorated with SUMO1 were observed on day 1 post-CFA (Figure 2-8). Paired t-tests indicated that the mean number of HCN2-SUMO1 puncta was not significantly different in small neurons from contralateral vs. ipsilateral DRG, but puncta number was significantly reduced by ~30% in medium and large diameter neurons from ipsilateral relative to contralateral DRG (Figure 2-8B). There were no significant differences in mean puncta number between left vs. right DRG from control animals for any cell size (small, 0.35 ± 0.06 vs. 0.34 ± 0.09 , $p=0.7672$; medium, 0.31 ± 0.05 vs. 0.27 ± 0.08 , $p=0.3750$; large, 0.39 ± 0.12 vs. 0.31 ± 0.07 , $p=0.2184$; $n=4$). There were no significant differences in puncta intensity between contralateral vs. ipsilateral DRG for any neuronal size (Figure 2-8C). There were no significant differences in puncta intensity for left vs. right DRG from control animals (small, 55.22 ± 10.11 vs. 51.25 ± 7.35 , $p=0.6250$; medium, 55.83 ± 10.77 vs. 53.47 ± 6.94 , $p=0.8750$; large, 58.5 ± 11.15 vs. 55.65 ± 5.70 , $p>0.9999$; $n=4$).

SUMO1 conjugation to HCN2 channels was examined 3 days post-CFA (Figure 2-9). HCN2-SUMO1 puncta number was significantly increased by ~27% in small neurons from ipsilateral relative to contralateral DRG (Figure 2-9B). There were no significant differences in medium or large diameter neurons in ipsilateral relative to contralateral DRG (Figure 2-9B).

There were no significant differences in puncta number for left vs. right DRG from control animals (small, 0.28 ± 0.02 vs. 0.28 ± 0.08 , $p=0.9861$; medium, 0.23 ± 0.01 vs. 0.27 ± 0.10 , $p=0.7612$; large, 0.31 ± 0.03 vs. 0.33 ± 0.10 , $p=0.8797$; $n=3$). As in all other cases, there were no significant differences in puncta intensity for contralateral vs. ipsilateral DRG for any cell size (Figure 2-9C). Control animals also showed no differences in left vs. right DRG puncta intensity (small, 65.55 ± 16.13 vs. 48.64 ± 4.701 , $p=0.3539$; medium, 71.14 ± 23.03 vs. 48.51 ± 3.7 , $p=0.3559$; large, 67.96 ± 18.46 vs. 50.43 ± 2.37 , $p=0.3077$; $n=3$).

In sum, SUMO conjugation to HCN2 channels was increased in small diameter neurons from ipsilateral DRG on days 1 and 3 post-CFA. Dynamic changes varied with the SUMO isoform. Whereas conjugation to HCN2 channels with SUMO2/3 increased on day 1, conjugation with SUMO 1 increased on day 3. In medium and large diameter neurons, SUMO1 conjugation to HCN2 channels was transiently reduced on day 1 post-CFA.

2.6 Discussion

An HCN2-mediated increase in I_h is necessary for mechanical hyperalgesia experienced during persistent inflammation. The present study investigated how HCN2 channels in L5 DRG were altered during early stages of inflammation. The major finding of this study was that HCN2 protein expression was not sufficient for mechanical hyperalgesia. Moreover, HCN2 channel SUMOylation was significantly increased in small diameter neurons and decreased in medium and large diameter neurons in ipsilateral relative to contralateral DRG.

2.6.1 HCN2 protein expression and SUMOylation of HCN2 channel complexes are increased in small diameter neurons during CFA-induced inflammation.

Persistent inflammation is thought to be a primary mechanism whereby an acute injury leads to a chronic pain state (Dubin & Patapoutian, 2010; Emery, Young, & McNaughton, 2012;

Pinho-Ribeiro, Verri, & Chiu, 2017; Tsantoulas, Mooney, & McNaughton, 2016; Q. Xu & Yaksh, 2011). CFA administration elicits persistent inflammation (Millan et al., 1988; Stein, Millan, & Herz, 1988). In rats, a unilateral, intraplantar CFA injection significantly reduces the mechanical force necessary to produce ipsilateral paw withdrawal 1 to 14 days after inflammation. The observed mechanical hyperalgesia is not present in the contralateral paw (Goff, Burkey, Goff, & Jasmin, 1998; Hurley & Hammond, 2000; Millan et al., 1988; Schnorr, Eberhardt, Kistner, Rajab, Kasser, et al., 2014; Stein et al., 1988; Weng et al., 2012). The cutaneous inflammatory response is resolved by 17-21 days (W. M. Li et al., 2005). Inflammation alters several ionic currents in sensory neurons, including I_h , and specifically increases the excitability of C-fiber nociceptors (Herrmann et al., 2017; Pace et al., 2018; Takeda, Takahashi, & Matsumoto, 2014; Weng et al., 2012; Zemel, Ritter, Covarrubias, & Muqeem, 2018). I_h increases the excitability of DRG sensory neurons by limiting membrane hyperpolarization and facilitating depolarization (Yagi & Sumino, 1998). CFA-induced inflammation triggers an increase in the activation kinetics and maximal conductance of nociceptor I_h (Djoughri et al., 2015). Injections of pharmacological agents to block I_h as early as 1 day after CFA-induced inflammation prevent hyperalgesia (Schnorr, Eberhardt, Kistner, Rajab, Kasser, et al., 2014; Weng et al., 2012).

The mechanism(s) producing a CFA-induced increase in nociceptor I_h is unknown. In rat DRG sensory neurons, I_h is mediated largely by HCN isoforms 1 and 2, and to a lesser extent, HCN3 (L. L. Gao et al., 2012; Kouranova, Strassle, Ring, Bowlby, & Vasilyev, 2008; Weng et al., 2012), which can form homo- and hetero-tetramers. Channel complexes can also contain auxiliary subunits (Piskorowski, Santoro, & Siegelbaum, 2011; Santoro et al., 2011; Santoro et al., 2009; Saponaro et al., 2014). Genetic ablation of HCN2 from DRG sensory neurons

attenuated mechanical hyperalgesia measured on day 3 post-CFA (Schnorr, Eberhardt, Kistner, Rajab, Kasser, et al., 2014). Hindlimb inflammation elicited a transient increase HCN2 IR in small diameter neurons in ipsilateral rat L4 DRG on day 1 but not day 4 post-CFA, relative to uninjected controls (Acosta et al., 2012). A significant decrease was also observed in large diameter neurons on day 4 post-CFA (Acosta et al., 2012). A second study examined the effects of hindlimb inflammation on ipsilateral L5 DRG neurons 7 days post-CFA; it showed a significant increase in HCN2 IR in small diameter neurons and a significant increase in the number of small and medium diameter neurons expressing HCN2, but no change in HCN1 or HCN3 expression relative to uninjected controls (Weng et al., 2012). The current study shows a significant bilateral increase in HCN2 staining intensity in small and medium diameter L5 DRG neurons on day 1 post-CFA relative to uninjected controls. In addition, there is a significant bilateral increase in the number of cells expressing HCN2 on day 3 post-CFA. We did not investigate if this increase in L5 DRG IR was accompanied by an increase in channel surface expression. Future studies will confirm if a CFA-induced increase in nociceptor I_h is accompanied by an increase in nociceptor HCN2 surface expression. The bilateral changes were unexpected since CFA injection was unilateral. Unilateral peripheral nerve damage can result in unilateral hyperalgesia but bilateral changes in DRG cytokine and cytokine receptor mRNA and protein expression (Brazda, Klusakova, Svizenska, Veselkova, & Dubovy, 2009; Dubovy, Brazda, Klusakova, & Hradilova-Svizenska, 2013; Jancalek, Dubovy, Svizenska, & Klusakova, 2010; Jancalek, Svizenska, Klusakova, & Dubovy, 2011) and NaV1.8 mRNA (Oaklander and Belzberg 1997). Such changes are thought to be due to a generalized inflammatory response. Several mechanisms could underlie bilateral effects (Koltzenburg et al., 1999).

Our data suggest that an increase in HCN2 protein expression is not sufficient for mechanical hyperalgesia because, unilateral injection of CFA produces unilateral hyperalgesia (Hurley & Hammond, 2000; Stein et al., 1988) but a bilateral increase in HCN2 protein expression (Figures 2 & 3). Altered expression of additional ion channels and/or other proteins may be necessary for hyperalgesia (Pace et al., 2018). Alternatively, additional post-translational modifications to HCN2 channels may be required. Recent studies demonstrated that enhanced ion channel SUMOylation can contribute to hyperalgesia in models of chronic pain (Francois-Moutal et al., 2018; Moutal et al., 2017; Wang et al., 2018a). Post-translational SUMOylation can regulate ion channel biophysical properties, trafficking and surface expression (Benson et al., 2007; Chamberlain et al., 2012; X. Q. Dai et al., 2009; Dustrude et al., 2016; Martin, Nishimune, Mellor, & Henley, 2007; Parker et al., 2017; Plant et al., 2010; Plant et al., 2016; Plant, Zuniga, Araki, Marks, & Goldstein, 2012; Y. Qi et al., 2014; Rajan et al., 2005; Steffensen et al., 2018; Y. Wang et al., 2018b; M. A. Welch et al., 2019; Xiong et al., 2017). Our data indicate that unilateral CFA injection produces unilateral hyper-SUMOylation of HCN2 in small diameter neurons from L5 DRG. HCN2 SUMOylation produces an increase in channel surface expression and I_h in a heterologous expression system (Parker et al., 2017), but the effect of enhanced DRG HCN2 SUMOylation observed here is unknown.

Because HCN2 α -subunits are SUMOylated in the DRG (Figure 4), the most parsimonious interpretation of the PLA experiments is that SUMOylation of HCN2 α -subunits is enhanced during inflammation. However, in order to produce a fluorescent punctum in a PLA, the HCN2 and SUMO proteins need to be within 40nM of one another so that their antibodies can interact to generate a punctate fluorescent signal. HCN channels can exist as heterotetramers in multiprotein complexes with auxiliary proteins like TRIP8b (Santoro et al., 2009) and MINT

(Kimura, Kitano, Nakajima, & Nakanishi, 2004), which also have predicted SUMOylation sites. This means that the increase in PLA puncta number could also represent increased SUMOylation of other HCN isoforms and/or auxiliary subunits that make-up the HCN2 channel complex. Indeed, it is well documented that a cell stressor can evoke group SUMOylation, whereby several proteins in a physically linked group are non-specifically SUMOylated, as opposed to targeting one specific protein within the group (Jentsch & Psakhye, 2013).

The increase in SUMOylated HCN2 channel complexes is a modest ~27%, but it is fairly common for low levels of SUMOylation to exert substantial regulatory effects (Benson et al., 2007; Flotho & Melchior, 2013). Nevertheless, there are examples of much greater increases in SUMOylation, for example, CRMP2 SUMOylation in the sciatic nerve, spinal dorsal horn and glabrous skin appears to increase by as much as ~300% in a rat model of neuropathic pain (Moutal, Dustrude, et al., 2017). Small diameter DRG neurons can be classified into at least six cell types (Li et al., 2016; Usoskin et al., 2015), and it is possible that a specific nociceptor cell type representing a small fraction of the population shows a much larger increase in HCN2 SUMOylation. Since the cell type(s) exhibiting the CFA-induced enhancement of HCN2 protein expression and HCN2 channel SUMOylation were not identified, we cannot conclude that increased expression and SUMOylation are coincident in the same cell or that the inflammation-induced increase in nociceptor I_h depends upon a 2-step process.

There are four SUMO isoforms and three were examined in this study. Conjugation of SUMO2/3 vs. SUMO1 to HCN2 channel complexes was differentially regulated as inflammation progressed: SUMO2/3 but not SUMO1 conjugation to HCN2 channels was significantly increased on day 1 post-CFA, and the opposite was true on day 3 post-CFA. The sole SUMO conjugating enzyme, Ubc9, does not show a preference for SUMO isoforms and interacts with a

similar affinity for all isoforms (Knipscheer, van Dijk, Olsen, Mann, & Sixma, 2007), but the SENP family of SUMO isopeptidases that mediate SUMO deconjugation can exhibit SUMO isoform specificity and can be differentially localized by post-translational modification (Kunz et al., 2018). Likewise, diverse E3 proteins that stabilize interactions between Ubc9 and its targets can also exhibit SUMO isoform specificity (Cappadocia, Pichler, & Lima, 2015; Koidl et al., 2016; Tatham et al., 2005). Together, these data support the emerging ideas that inflammatory mediators regulate the nociceptor SUMOylation machinery, and that this regulation may effect alterations in multiple ionic conductances during nociceptor sensitization.

2.6.2 SUMOylation of HCN2 channel complexes is decreased in medium and large diameter neurons during CFA-induced inflammation.

SUMO1 conjugation to HCN2 channel complexes was transiently decreased in medium and large diameter neurons from ipsilateral L5 DRG on day 1 of inflammation. This regulation could potentially contribute to hyperalgesia which peaks on day 1 (Millan et al., 1988; Stein et al., 1988). Medium and large neurons could contribute directly to hyperalgesia as nociceptors (Dubin & Patapoutian, 2010; Nagi et al., 2019), or they could indirectly influence nociceptor activity through presynaptic mechanisms and/or other circuit effects (Braz, Solorzano, Wang, & Basbaum, 2014; D. Guo & Hu, 2014; Mendell, 2014). It will be important to identify these neurons and how HCN2 channel deSUMOylation regulates their activity.

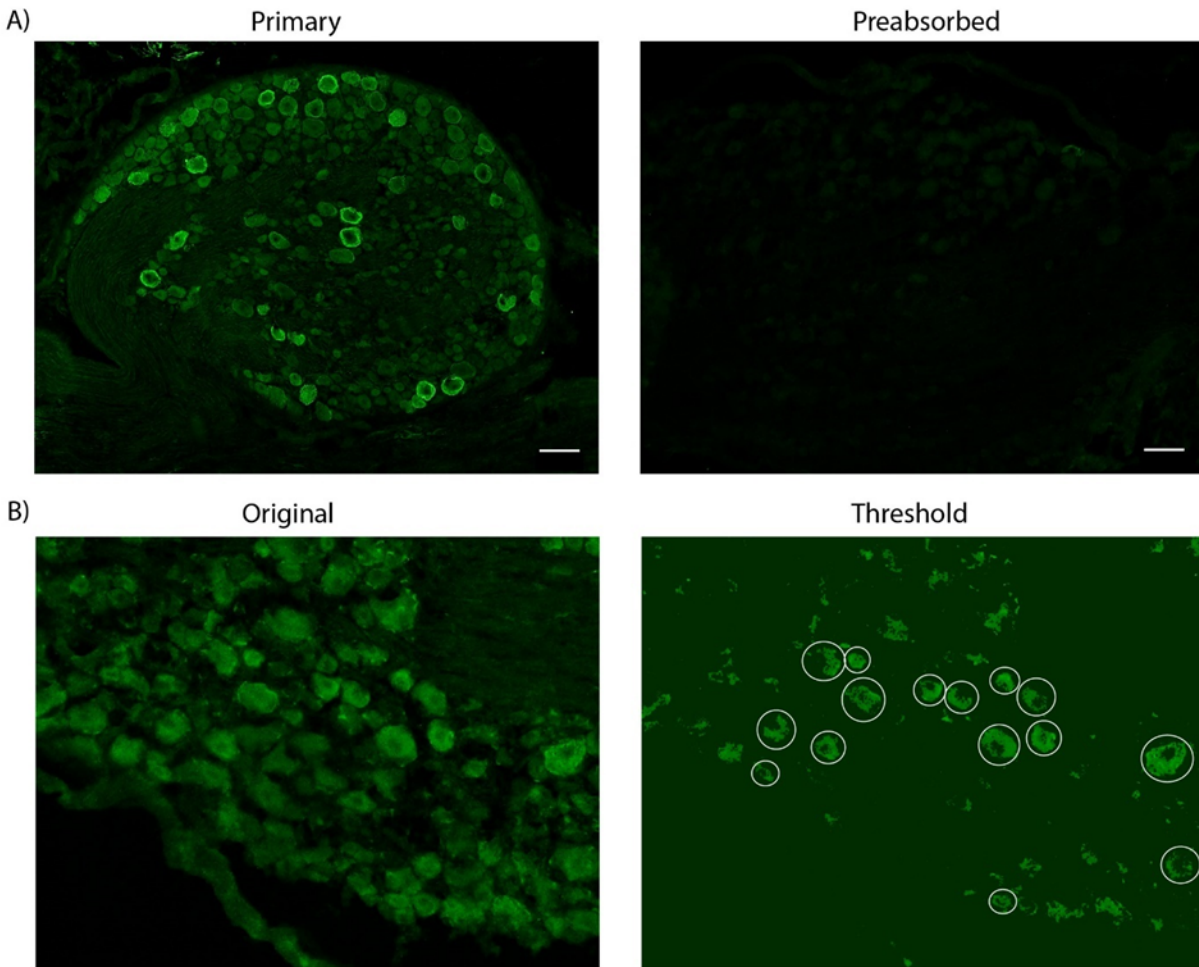


Figure 2-1 Validation of anti-HCN2 and quantification of HCN2 positive cells.

A) Representative IHC. Experiments using antibody and pre-absorbed antibody show anti-HCN2 specificity. Scale bars are 100 μm . B) Representative analysis. Sections show cells before and after thresholding. Cells having an obvious nucleus and plasma membrane, and therefore meeting the criteria for analysis, are circled.

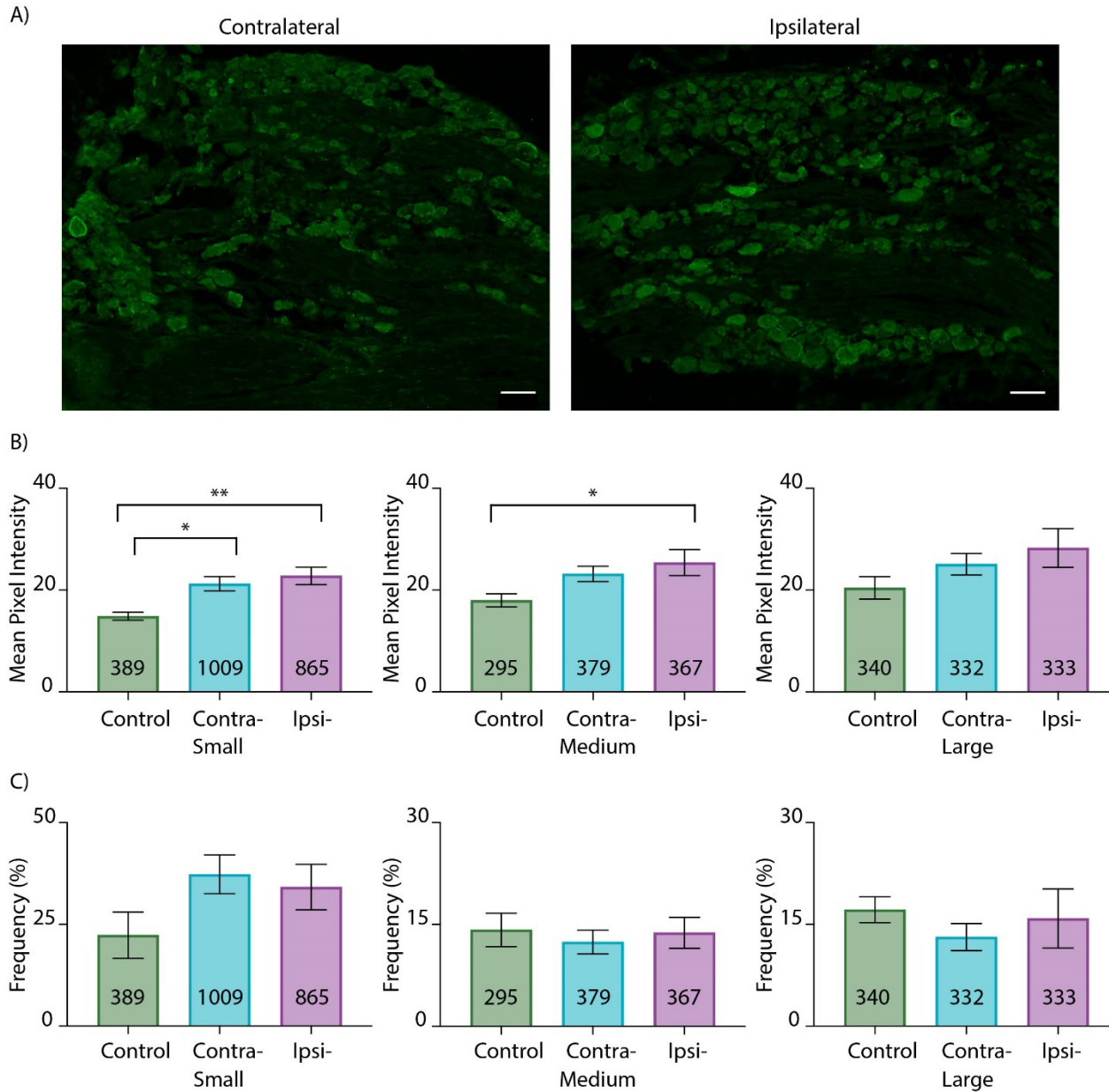


Figure 2-2 CFA-induced inflammation alters HCN2 protein expression on 1 day post-CFA.

A) Representative images of HCN2 IR in contralateral and ipsilateral L5 sections 1 day post-CFA injection. Scale bars are 100 μ m. B) HCN2 expression is elevated in experimental compared to control DRG. Average mean pixel intensities \pm SEMs are plotted for three size classes of DRG neurons. A one way ANOVA with a Tukey's post-hoc test that makes all possible comparisons shows HCN2 IR is significantly elevated in small cells for experimental vs.

control treatment groups ($F(2,17)=8.468$; $p=0.0028$). Asterisks indicate which two-way comparisons were significant. A one way ANOVA with a Tukey's post-hoc shows HCN2 IR is significantly elevated in medium cells for ipsilateral vs. control treatment groups ($F(2,17)=3.748$; $p=0.0448$). Asterisks indicate which pairwise comparisons were significant: *, $p<0.05$; **, $p<0.01$. A one way ANOVA shows that HCN2 IR was not significantly different between large cells from experimental and control DRG ($F(2,17)=1.794$; $p=0.1963$). C) HCN2 frequency is unaltered 1 day post-CFA injection. Bar plots of the frequency of HCN2 positive neurons in each size category ($[\text{HCN2-expressing cells per category} \div \text{total number of cells in all categories}] \times 100$). Statistical tests show there were no significant differences between experimental and control animals for any cell type (small; $KW(2,17)=3.603$; $p=0.1682$; medium; $F(2,17)=0.1860$; $p=0.8317$; large; $KW(2,17)=1.999$; $p=0.3824$).

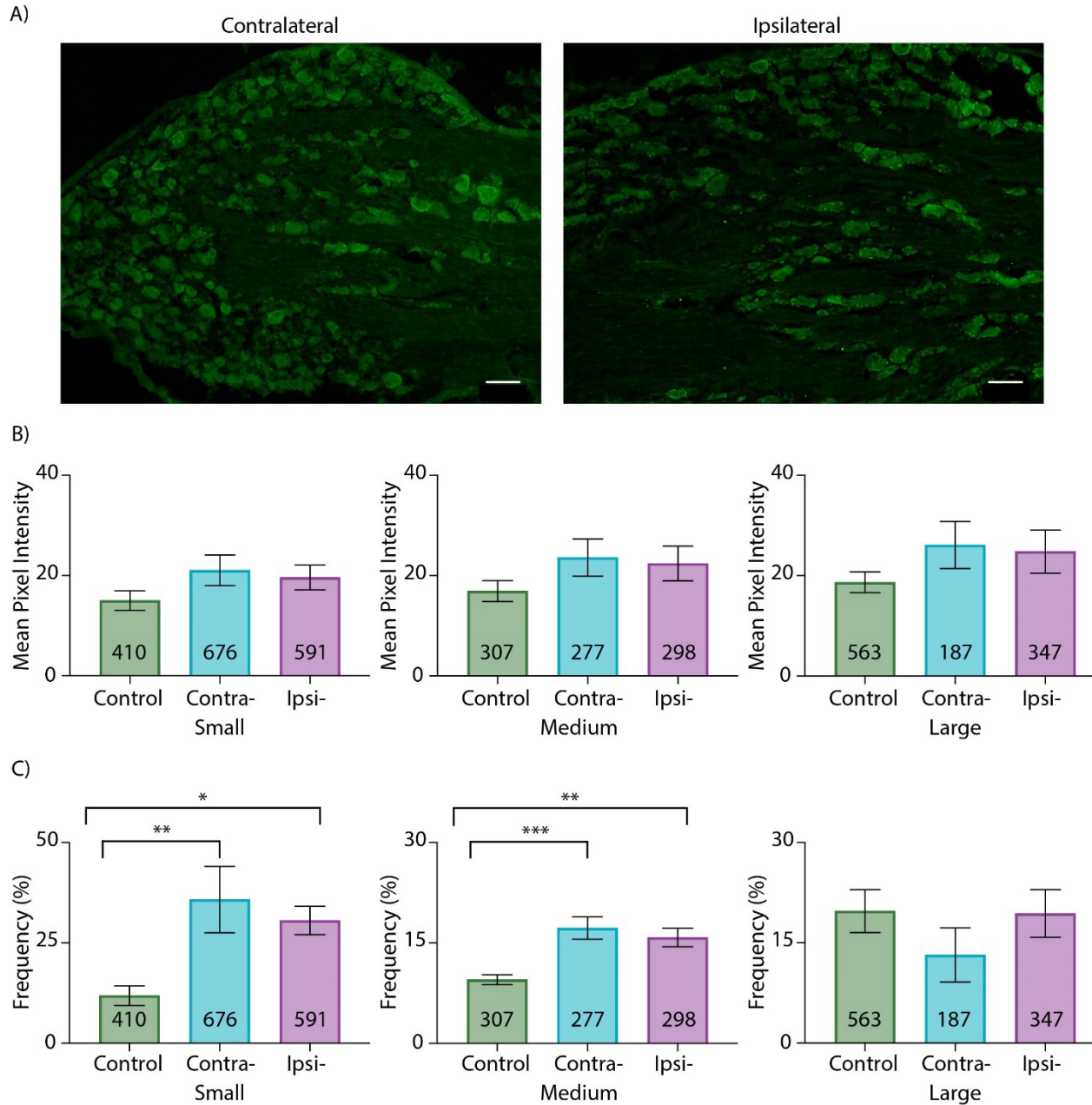


Figure 2-3 HCN2 protein expression is altered on day 3 post-CFA.

A) Representative images of HCN2 IR in contralateral and ipsilateral L5 sections 3 days post-CFA. Scale bars are 100 μ m. B) The intensity of HCN2 IR is unaltered 3 days post-CFA. Bar plots of mean pixel intensity. One way ANOVAs show no significant differences between treatment groups for any size category (small; $F(2,15)=1.893$; $p=0.1849$; medium;

$F(2,15)=1.667$; $p=0.2220$; large; $F(2,15)=1.499$; $p=0.2550$). C) HCN2 frequency is significantly increased in small and medium diameter neurons in experimental compared to control animals. Bar plots of the frequency of HCN2 IR in each size class ([HCN2-expressing cells per category ÷ total number of cells in all categories] x 100). A one way ANOVA with a Tukey's post-hoc test shows HCN2 frequency is significantly elevated in small cells for experimental vs. control treatment groups ($F(2,15)=8.022$; $p=0.0043$). Asterisks indicate which two-way comparisons were significant. A one way ANOVA with a Tukey's post-hoc test shows HCN2 frequency is significantly elevated in medium cells for experimental vs. control treatment groups ($F(2,15)=13.51$; $p=0.0004$). Asterisks indicate significant differences in pairwise comparisons: *, $p<0.05$; **, $p<0.01$; ***, $p<0.001$. A Kruskal-Wallis test shows HCN2 frequency is not significantly different between large cells for experimental vs. control treatment groups ($KW(2,15)=3.058$; $p=0.2251$).

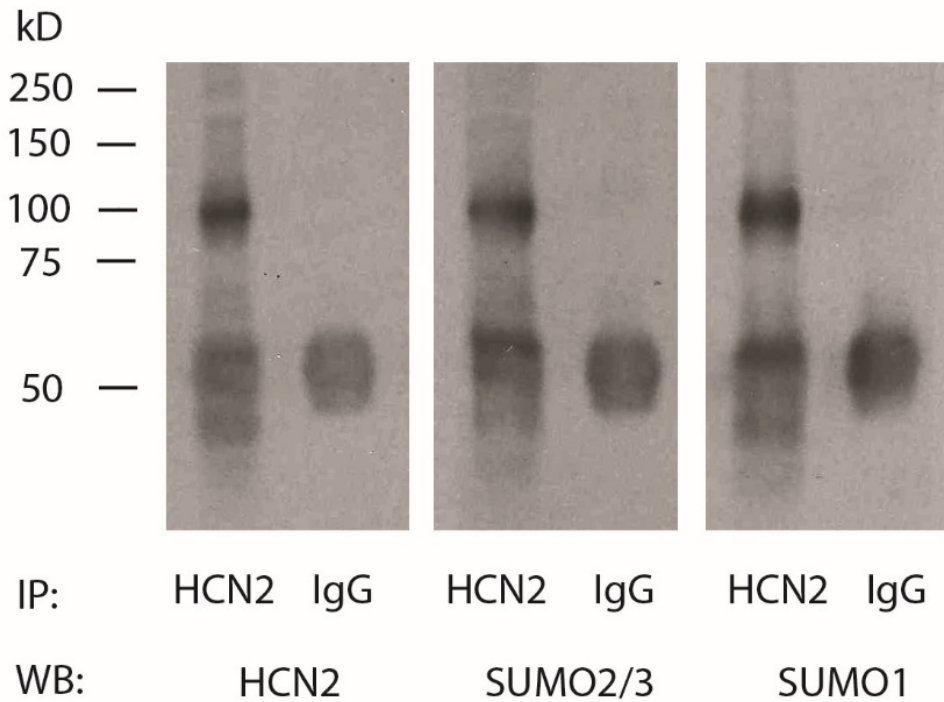


Figure 2-4 HCN2 is SUMOylated in rat DRG.

Denaturing immunoprecipitation (IP) experiments were performed on a DRG membrane preparation with an antibody against HCN2 or IgG (control). IP products from 1 membrane preparation were run in triplicate on an SDS-polyacrylamide gel followed by western blotting (WB). The blot was cut into 3, and probed for HCN2, SUMO2/3 and SUMO1. The experiment was repeated using 3 different DRG membrane preparations. A representative result from one experiment is shown. All 3 WB antibodies recognized the same ~100kD protein in the HCN2 IP product but not the IgG IP product. The data indicate that SUMO1 and SUMO2/3 are covalently linked to HCN2 since they remained bound under denaturing conditions. The ~50kD band present in all lanes represents the IP antibody.

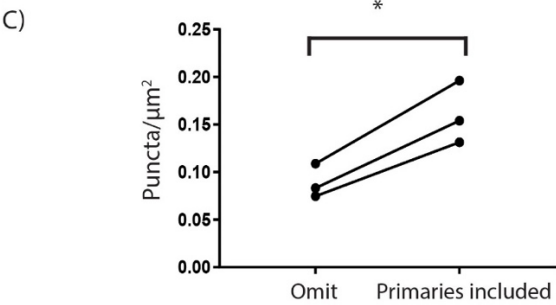
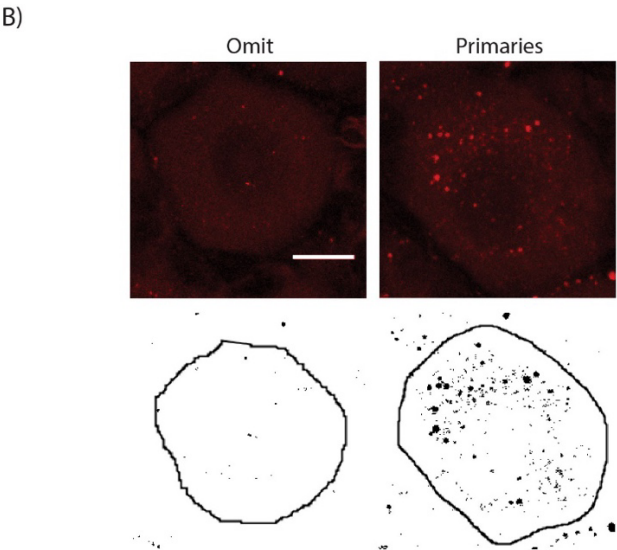
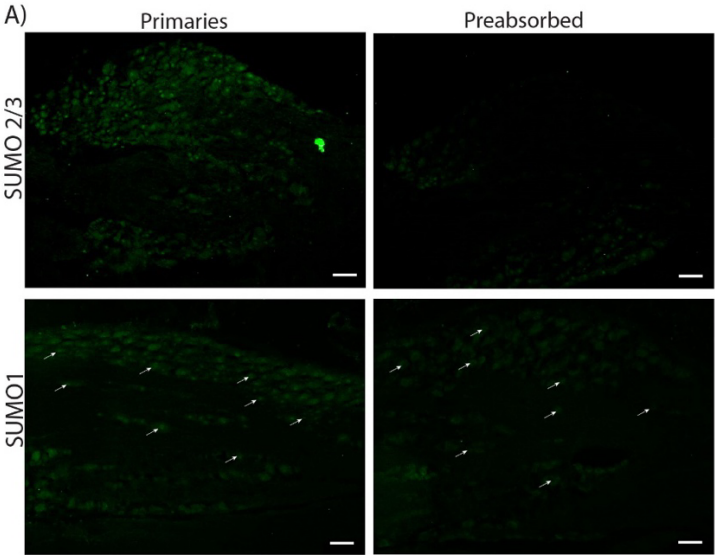


Figure 2-5 Measuring HCN2 channel SUMOylation.

A) Verification of SUMO antibodies. Antibodies were (right) or were not (left) preabsorbed with the corresponding peptide for SUMO2/3 (upper panel) or SUMO1 (lower

panel). SUMO is predominately expressed in nuclei. Note the loss of nuclear staining following preabsorption, e.g. white arrows in bottom panel. Scale bars are 100 μm . B) Method for quantifying HCN2 channel SUMOylation. *In situ* PLA was performed on DRG cryosections with (experimental) or without (control) antibodies against SUMO2/3 and HCN2. Upper panel shows a 5 μm projection of confocal optical slices through representative cells from control and experimental treatment groups. Each image represents a projection of 5 slices in continuous succession that together encompass the center of the cell. Each optical section is 0.9 μm with a z-stack interval of 1 μm . Note that the red puncta indicating SUMOylated HCN2 channels were largely absent when antibodies were omitted. Scale bar is 10 μm . The cells were circled and thresholded, and the resulting image is shown in the lower panel. Black puncta within the circled region were counted using the analyze particle tool on imageJ and normalized by the area (μm^2) of the circle. Note that all black puncta, regardless of size were counted. C) HCN2 channels are SUMOylated in DRG neurons. Plots of puncta per μm^2 show there are significantly more puncta when primary antibodies for HCN2 and SUMO2/3 were included (0.08 ± 0.01 vs. 0.16 ± 0.02 , $p=0.0149$, paired t-test, $n=3$, 70 and 62 cells analyzed in total). The lines indicate that the cells were from the same experiment, i.e. alternate sections from a single DRG on the same slide receiving the same PLA reagents and treated in an identical fashion.

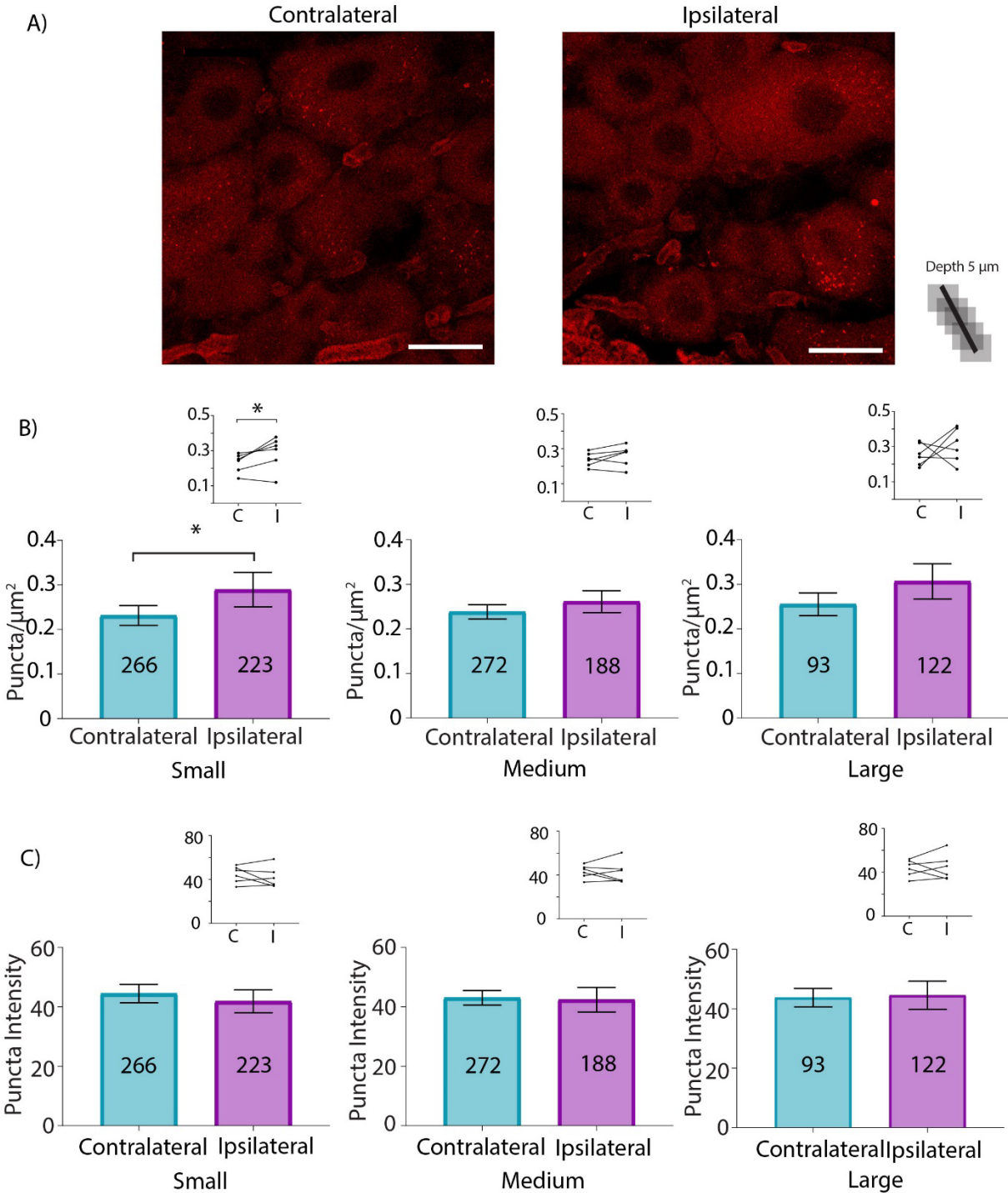


Figure 2-6 SUMO2/3 conjugation to HCN2 channels is increased in small diameter neurons from ipsilateral relative to contralateral DRG at 1 day post-CFA.

A) Representative PLA. Scale bars are 25 μm . Note that this image provides an overview, but for the purpose of quantification, individual projections were made for each cell, e.g. Figure

2-5B. B) Plots of mean number of puncta/ μm^2 for all DRG from 6 CFA treated animals on day 1 post-CFA. The number inside the bar represents the total number of cells analyzed. Inset: Each line compares the means for contralateral and ipsilateral DRG from one animal. Paired t-tests indicate the number of puncta significantly increased for small but not medium or large neurons in ipsilateral compared to contralateral DRG (small, 0.23 ± 0.02 vs. 0.29 ± 0.04 , $p=0.0499$; medium, 0.24 ± 0.02 vs. 0.26 ± 0.02 , $p=0.2120$; large, 0.26 ± 0.03 vs. 0.31 ± 0.04 , $p=0.4259$). C) Plots of mean puncta intensity on day 1 post-CFA. Paired t-tests indicate mean puncta intensities were not significantly different between ipsilateral and contralateral DRG for any size category (small, 44.47 ± 3.1 vs. 41.86 ± 3.9 , $p=0.4495$; medium, 43.06 ± 2.5 vs. 42.43 ± 4.1 , $p=0.8503$; large, 43.74 ± 3.1 vs. 44.51 ± 4.8 , $p=0.8518$).

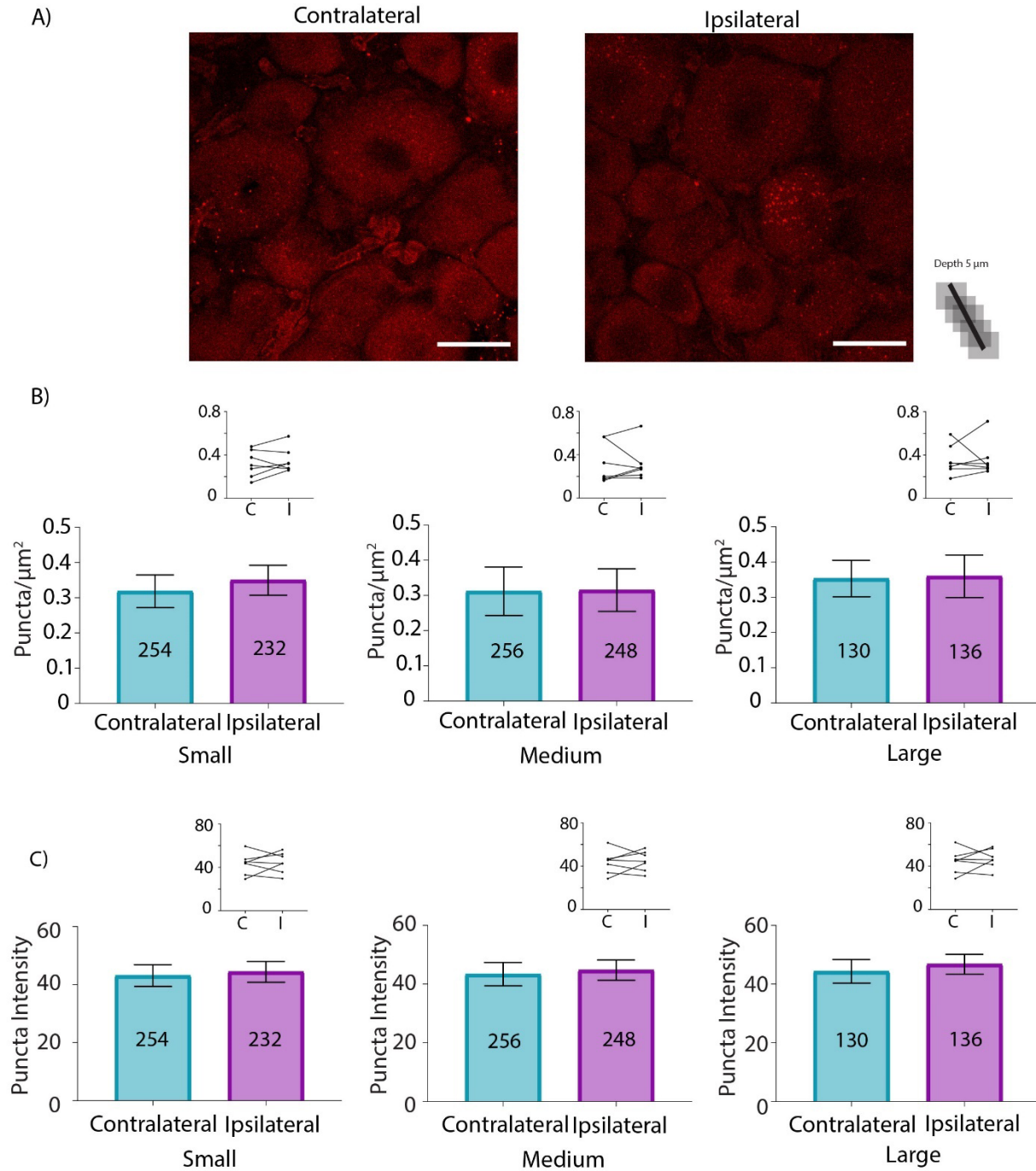


Figure 2-7 SUMOylation of HCN2 channels by SUMO2/3 does not change 3 days post-CFA.

A) Representative PLA. Scale bars are 25 μm . Note that this image provides an overview, but for the purpose of quantification, individual projections were made for each cell, e.g. Figure

2-5B. B) Plots of mean number of puncta/ μm^2 for all DRG from 7 CFA treated animals on day 3 post-CFA. The number inside the bar represents the total number of cells analyzed. Inset: Each line compares means for contralateral and ipsilateral DRG from one animal. Wilcoxon matched-pair tests indicate no significant difference in puncta number for small, medium, or large diameter cells (small, 0.32 ± 0.05 vs. 0.35 ± 0.04 , $p=0.375$; medium, 0.31 ± 0.07 vs. 0.32 ± 0.06 , $p=0.5781$; large, 0.35 ± 0.05 vs. 0.36 ± 0.06 , $p=0.8125$). C) Plots of mean puncta intensity on day 3 post-CFA. Paired t-tests indicate mean puncta intensities were not significantly different for any size category in ipsilateral compared to contralateral DRG (small, 43.13 ± 3.73 vs. 44.4 ± 3.56 , $p=0.731$; medium, 43.4 ± 3.98 vs. 44.78 ± 3.45 , $p=0.7087$; large; 44.35 ± 4.04 vs. 46.75 ± 3.36 , $p=0.5670$).

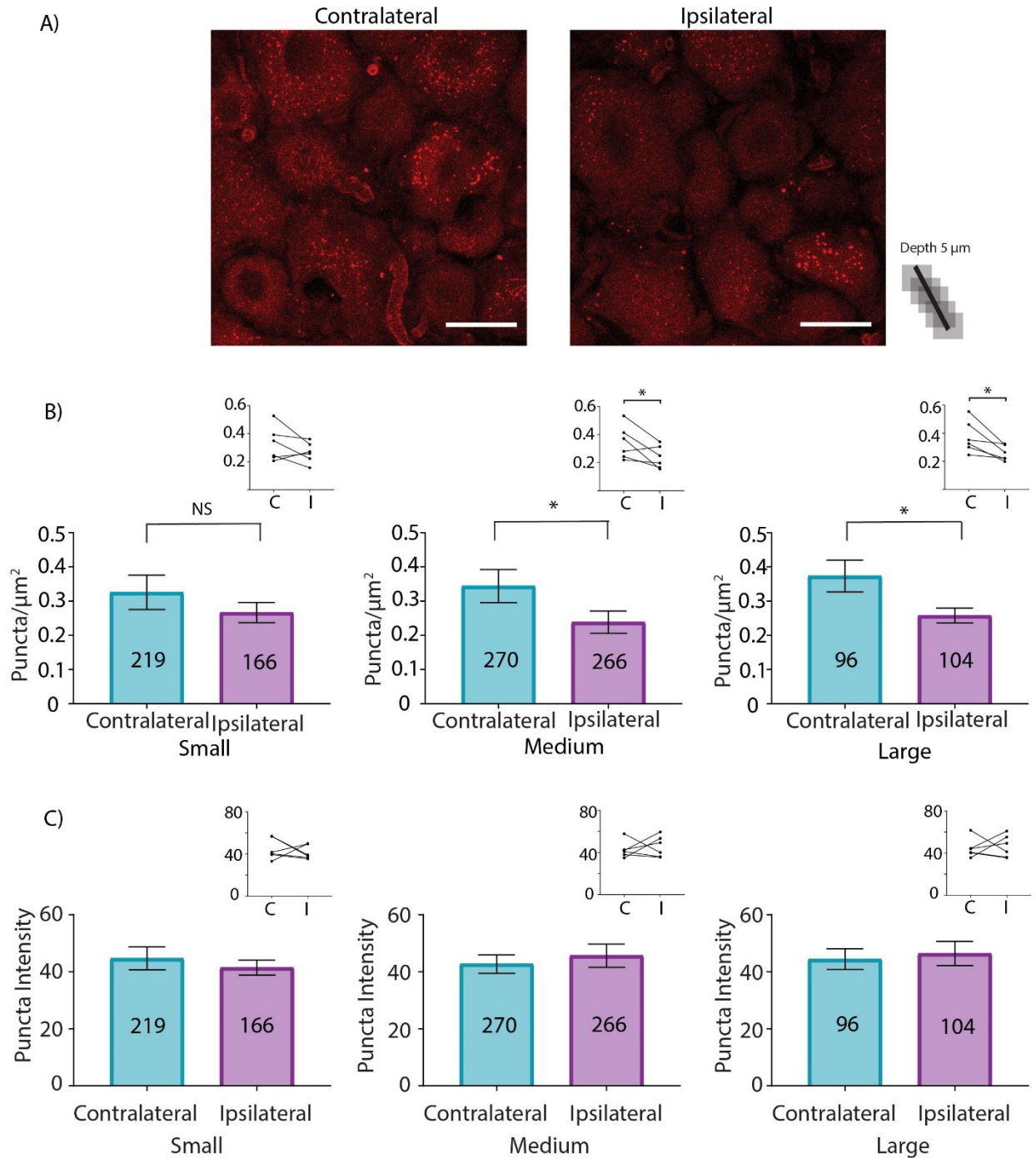


Figure 2-8 HCN2 channel SUMOylation by SUMO1 is diminished in medium and large diameter neurons from ipsilateral relative to contralateral DRG at 1 day post-CFA.

A) Representative PLA. Scale bars are 25 μm . Note that this image provides an overview, but for the purpose of quantification, individual projections were made for each cell, e.g. Figure

2-5B. B) Plots of mean number of puncta/ μm^2 for all DRG from 6 CFA treated animals on day 1 post-CFA. The number inside the bar represents the total number of cells analyzed. Inset: Each line compares means for contralateral and ipsilateral DRG from one animal. Paired t-tests indicate medium and large diameter cells contain significantly fewer puncta in the ipsilateral DRG relative to the contralateral DRG (small, 0.33 ± 0.05 vs. 0.27 ± 0.03 , $p=0.2058$; medium, 0.34 ± 0.05 vs. 0.24 ± 0.03 , $p=0.0480$; large, 0.37 ± 0.05 vs. 0.26 ± 0.02 , $p=0.0238$). C) Plots of mean puncta intensity on day 1 post-CFA. Paired t-tests indicate mean puncta intensities were not significantly different for any size category in ipsilateral compared to contralateral DRG (small, 44.68 ± 4.03 vs. 41.48 ± 2.66 , $p=0.5986$; medium, 42.7 ± 3.24 vs. 45.65 ± 4.06 , $p=0.6299$; large, 44.44 ± 3.68 vs. 46.39 ± 4.27 , $p=0.7631$).

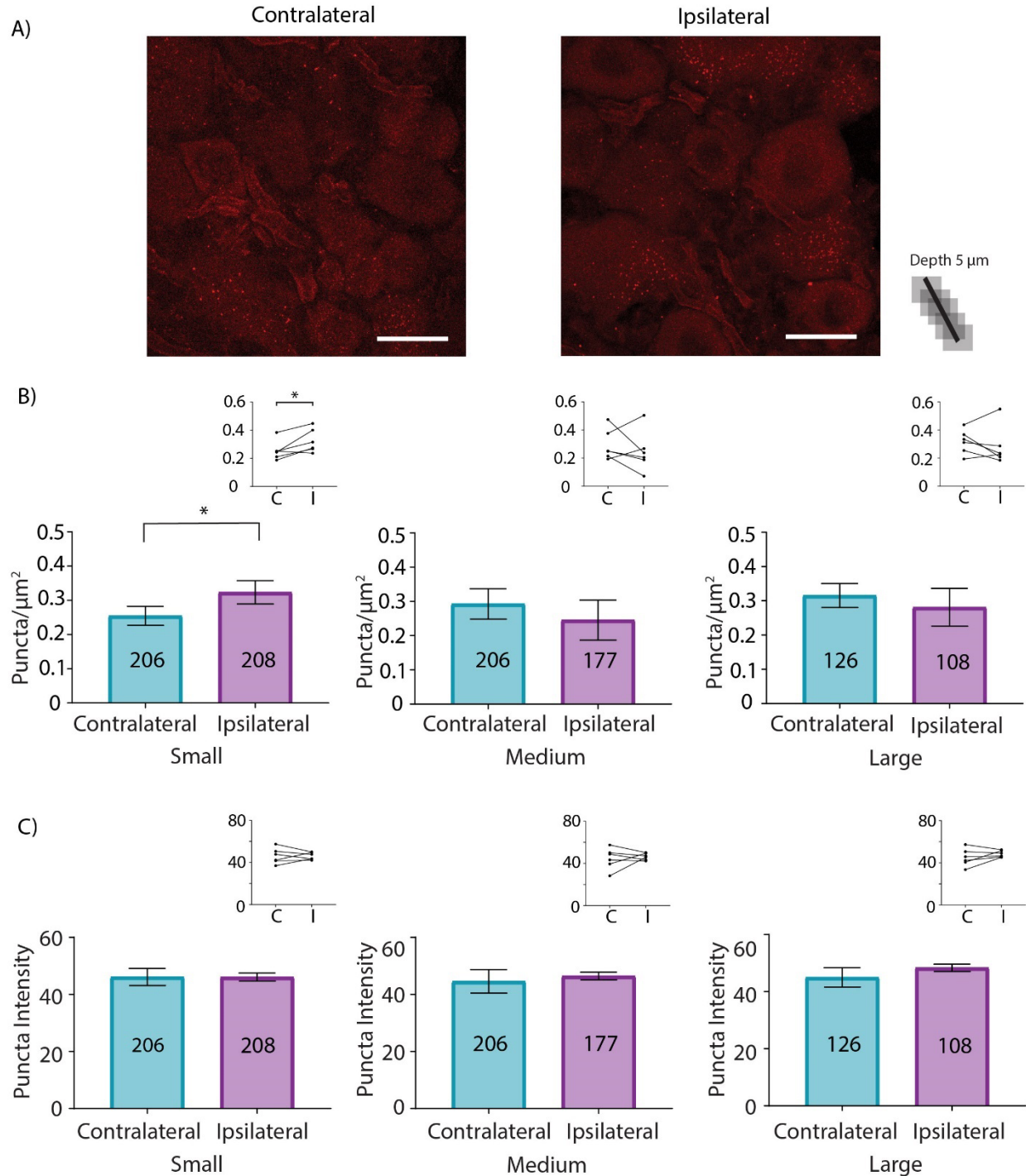


Figure 2-9 HCN2 channel SUMOylation by SUMO1 is increased in small neurons from ipsilateral relative to contralateral DRG at 3 days post-CFA

A) Representative PLA. Scale bars are 25 μm . Note that this image provides an overview, but for the purpose of quantification, individual projections were made for each cell, e.g. Figure

2-5B. B) Plots of mean puncta/ μm^2 for all DRG from 6 CFA treated animals on day 3 post-CFA. The number inside the bar represents the total number of cells analyzed. Inset: Each line compares means for contralateral and ipsilateral DRG from one animal. Significantly more puncta were observed in ipsilateral relative to contralateral DRG as indicated by paired t-tests or non-parametric alternative* (small, 0.25 ± 0.03 vs. 0.32 ± 0.03 , $p=0.0285$; medium, 0.29 ± 0.05 vs. 0.25 ± 0.06 , $p=0.4310$; large*, 0.32 ± 0.03 vs. 0.28 ± 0.06 , $p=0.5625$). C) Plots of mean puncta intensity on day 3 post-CFA. Paired t-tests indicate mean puncta intensities were not significantly different for any size category in ipsilateral compared to contralateral DRG (small, 46.14 ± 3.0 vs. 46.08 ± 1.41 , $p=0.9826$; medium, 44.58 ± 4.12 vs. 46.45 ± 1.32 , $p=0.6612$; large, 44.99 ± 3.38 vs. 48.35 ± 1.27 $p=0.2758$).

3 CHANGES IN PERIPHERAL HCN2 CHANNELS DURING PERSISTENT INFLAMMATION

Publication: **Jansen, L. R.**, * Forster, L. A., * Smith, X. L., Rubaharan, M., Murphy, A. Z., & Baro, D. J. (2021). Changes in peripheral HCN2 channels during persistent inflammation. *Channels (Austin)*, 15(1), 165-179. doi:10.1080/19336950.2020.1870086

Contribution disclosure: LR. Jansen, LA. Forster, AZ Murphy, and DJ Baro were responsible for the conception and design of the research presented. M. Rubaharan performed animal experiments. LR. Jansen, LA. Forster, and XL. Smith contributed to the acquisition and analysis of the data. LR. Jansen and LA. Forster contributed equally*. LR. Jansen, LA. Forster, and D. Baro were responsible for drafting the manuscript, and all authors were involved in revising the manuscript.

3.1 Abstract

Nociceptor sensitization following nerve injury or inflammation leads to chronic pain. An increase in the nociceptor hyperpolarization-activated current, I_h , is observed in many models of pathological pain. Pharmacological blockade of I_h prevents the mechanical and thermal hypersensitivity that occurs during pathological pain. Alterations in the Hyperpolarization-activated Cyclic Nucleotide-gated ion channel 2 (HCN2) mediate I_h -dependent thermal and mechanical hyperalgesia. Limited knowledge exists regarding the nature of these changes during chronic inflammatory pain. Modifications in HCN2 expression and post-translational SUMOylation have been observed in the Complete Freund's Adjuvant (CFA) model of chronic inflammatory pain. Intra-plantar injection of CFA into the rat hindpaw induces unilateral hyperalgesia that is sustained for up to 14 days following injection. The hindpaw is innervated by primary afferents in lumbar DRG, L4-6. Adjustments in HCN2 expression and SUMOylation have been well-documented for L5 DRG during the first 7 days of CFA-induced inflammation. Here, we examine bilateral L4 and L6 DRG at day 1 and day 3 post-CFA. Using L4 and L6 DRG cryosections, HCN2 expression and SUMOylation were measured with immunohistochemistry and proximity ligation assays, respectively. Our findings indicate that intra-plantar injection of CFA elicited a bilateral increase in HCN2 expression in L4 and L6 DRG at day 1, but not day 3, and enhanced HCN2 SUMOylation in ipsilateral L6 DRG at day 1 and day 3. Changes in HCN2 expression and SUMOylation were transient over this time course. Our study suggests that HCN2 is regulated by multiple mechanisms during CFA-induced inflammation.

3.2 Introduction

Persistent inflammation and/or nerve injury can lead to chronic pain. This debilitating condition is characterized by allodynia (pain in response to non-noxious stimuli), hyperalgesia (increased sensitivity to noxious stimuli), and spontaneous painful and/or burning sensations in the absence of stimuli (Dubin & Patapoutian, 2010; Emery et al., 2012; Kuner & Flor, 2016; Pinho-Ribeiro et al., 2017; Tsantoulas et al., 2016; Q. Xu & Yaksh, 2011). Chronic pain is underpinned by widespread reorganization of the pain circuitry, including changes to component neurons. While component neurons throughout the pain circuit can be altered (Boadas-Vaello, Homs, Reina, Carrera, & Verdu, 2017; L. Du, Wang, Cui, He, & Ruan, 2013a, 2013b), here we focus specifically upon nociceptors.

Nociceptors are peripheral sensory neurons that initiate pain signalling upon detecting noxious temperatures, pressures and chemicals (Dubin & Patapoutian, 2010). Nociceptor somata are located in the Dorsal Root Ganglia (DRG) and trigeminal ganglia. A single process projects from the soma; it bifurcates, and one process extends to the periphery and the other innervates the central nervous system. Nociceptors are functionally classified by their conduction velocities: C-fibers have small-diameter, unmyelinated axons; $A\delta$ nociceptors have small to medium diameter, lightly myelinated axons; and, there is also a class of $A\beta$ nociceptors that have larger diameter myelinated axons (Djoughri & Lawson, 2004; Nagi et al., 2019). The range of conduction velocities for each of these 3 classes varies with the species, but for the sake of comparison, the peak conduction velocities for C-, $A\delta$ - and $A\beta$ -fibers in a typical guinea pig compound action potential are approximately 0.6m/s, 3.3m/s and 9.6m/s, respectively (Djoughri & Lawson, 2004). Neurons within each class are functionally subdivided according to their threshold to noxious chemical, mechanical, and thermal stimuli. Recently, unbiased RNA

sequencing approaches have been included in classification schemes (C. L. Li et al., 2016; Usoskin et al., 2015), and several principal nociceptor cell types have been identified, each with a unique transcriptome, size and sensory function.

Nociceptors become hyper-excitabile in chronic pain states elicited by nerve damage (neuropathic pain) and/or persistent, unresolved inflammation (inflammatory pain). This sensitization not only changes nociceptor responses to noxious and non-noxious stimuli, but also drives pathological changes to CNS components of the pain circuitry. Nociceptor sensitization is due, in part, to persistent alterations in a number of ionic currents that act to reduce threshold and increase cell excitability (Berta et al., 2017; Gold & Gebhart, 2010; Pace et al., 2018; Reichling & Levine, 2009; Tibbs, Posson, & Goldstein, 2016; Zemel et al., 2018). The hyperpolarization-activated, non-specific cation current, I_h , is a slowly depolarizing current that functions to enhance nociceptor excitability (Yagi & Sumino, 1998). Under normal conditions, I_h plays a limited role in pain transmission, and pain thresholds are largely unaffected by pharmacological inhibition or genetic ablation of I_h (Emery et al., 2011; Schnorr, Eberhardt, Kistner, Rajab, Kasser, et al., 2014; Takasu, Ono, & Tanabe, 2010). However, during sensitization, I_h transitions into a pivotal role in pain signalling. In multiple models of chronic pain, nociceptor I_h amplitude is increased, and pharmacological agents that block I_h reduce nociceptor excitability and return pain thresholds to baseline (Chaplan et al., 2003; Dalle & Eisenach, 2005; D. H. Lee, Chang, Sorkin, & Chaplan, 2005; Luo et al., 2007; Richards & Dilley, 2015; Schnorr, Eberhardt, Kistner, Rajab, Kasser, et al., 2014; Sun, Xing, Tu, Han, & Wan, 2005; Tibbs et al., 2016; Tsantoulas et al., 2017; Tsantoulas et al., 2016; X. Wang et al., 2016; Weng et al., 2012; Yao, Donnelly, Ma, & LaMotte, 2003). In addition, blocking I_h during chronic pain can also reduce the release of inflammatory mediators and glial activation (H. Huang, Zhang, & Huang, 2019).

The family of hyperpolarization activated, cyclic nucleotide gated ion channels, isoforms 1-4 (HCN 1-4), mediate I_h . These pore-forming α -subunits are assembled into homo- and hetero-tetrameric channels that are largely permeable to K^+ and Na^+ , and may also display a small permeability for Ca^{2+} (Sartiani et al., 2017; Wahl-Schott & Biel, 2009). Channels open upon hyperpolarization, but isoforms differ in their activation kinetics: HCN1 is the fastest and HCN4 is the slowest. All isoforms possess a cyclic nucleotide binding domain (CNBD), which when bound by cAMP shifts the voltage dependence of activation to more positive potentials. Isoforms show varying degrees of cAMP sensitivity, with HCN2 and HCN4 exhibiting the largest depolarizing shift in voltage dependence upon binding cAMP. Homo- and hetero-tetrameric channels composed largely of HCN1 and HCN2, and to a lesser extent, HCN3, conduct nociceptor I_h (L. L. Gao et al., 2012; Kouranova et al., 2008; Weng et al., 2012).

Studies utilizing genetic ablation of specific HCN isoforms have begun to identify isoform-specific contributions to chronic pain. HCN1 contributes to cold allodynia during neuropathic pain (Momin, Cadiou, Mason, & McNaughton, 2008). HCN2 (Emery et al., 2011; Schnorr, Eberhardt, Kistner, Rajab, Kasser, et al., 2014), but not HCN1 (Momin et al., 2008) or HCN3 (Lainez, Tsantoulas, Biel, & McNaughton, 2019) contributes to mechanical and thermal hyperalgesia; however, the role of HCN2 varies with the model under study. When Complete Freund's Adjuvant (CFA) was injected into the plantar surface of the hindpaw to elicit persistent inflammation, HCN2 knock out in sensory afferent neurons prevented mechanical but not thermal hyperalgesia on day 3 post-CFA (Schnorr, Eberhardt, Kistner, Rajab, Kasser, et al., 2014). In contrast, ablation of HCN2 in sensory afferents prevented thermal but not mechanical hyperalgesia from 30min to 3hr after intra-plantar injection of the potent inflammatory mediator, PGE2 (Emery et al., 2011). Moreover, genetic ablation of HCN2 in primary sensory afferents

prevented both mechanical and thermal hyperalgesia from 2 to 21 days after the induction of neuropathic pain by chronic constriction of the sciatic nerve (Emery et al., 2011). Loss of HCN2 in primary sensory afferents also significantly reduced the pain behavior that is typically observed 1hr after intra-plantar injection of 4% formalin (licking, biting and paw lifting), and that is thought to be due to release of inflammatory mediators (Emery et al., 2011). These data suggest that there are likely to be numerous mechanisms that regulate HCN2 channels over multiple time courses, and that each mechanism may be differentially activated in a cell-type-specific manner and according to the catalyst(s) that triggers the pain state.

Current analgesic strategies to reduce I_h focus mainly on the development of isoform selective HCN channel blockers, e.g. small molecules that preferentially block channels containing HCN1 and/or HCN2 subunits (Dini et al., 2018; Resta et al., 2018). More generally, knowledge about the molecular mechanisms that alter ionic currents during pathological pain is being exploited to develop novel anti-nociceptive drugs tailored to a specific modulatory mechanisms (Francois-Moutal, Scott, et al., 2018; Moutal, Yang, et al., 2017). Several intracellular signalling pathways are known to drive nociceptor sensitization (Basbaum, Bautista, Scherrer, & Julius, 2009; J. K. Cheng & Ji, 2008; Djouhri, Dawbarn, Robertson, Newton, & Lawson, 2001; Hucho & Levine, 2007), but details on their modulation of HCN2 channels are limited.

A variety of molecular mechanisms may underpin the increase in nociceptor I_h during chronic pain states. Altered nociceptor HCN2 channel expression has been observed in multiple subcellular compartments during pathological pain, including the soma, peripheral terminals, central terminals, and along axons in nerves (Acosta et al., 2012; Papp, Hollo, & Antal, 2010; Schnorr, Eberhardt, Kistner, Rajab, Kasser, et al., 2014; Smith et al., 2015; Weng et al., 2012). In

some models of neuropathic pain, somatic nociceptor HCN2 protein expression appeared to decrease despite an increased I_h (Chaplan et al., 2003; Jiang et al., 2008; Y. Liu, Feng, & Zhang, 2015). In these cases, the decrease in expression may represent compensation for prolonged nociceptor hyperexcitability, or redistribution of the channels from soma to axon. In other models of inflammatory pain, both I_h and HCN2 protein expression increased (Acosta et al., 2012; Cho, Staikopoulos, Furness, & Jennings, 2009; L. A. Forster, Jansen, Rubaharan, Murphy, & Baro, 2020; Papp et al., 2010; Richards & Dilley, 2015; Schnorr, Eberhardt, Kistner, Rajab, Kasser, et al., 2014; Smith et al., 2015; Weng et al., 2012). In most instances, it was not clear if altered expression represented an adjustment to transcription, translation, and/or post-translational modifications that modify channel turnover. The rat model of CFA-induced chronic inflammatory pain highlights the idea that multiple mechanisms may be regulating HCN2 channels over different time courses. Unilateral, intra-plantar CFA injection elicits persistent inflammation and chronic pain in the ipsilateral hindlimb that is resolved by 14-21 days (W. M. Li et al., 2005; Millan et al., 1988). HCN2 expression is enhanced in multiple subcellular compartments leading to mechanical hyperalgesia (Acosta et al., 2012; Papp et al., 2010; Schnorr, Eberhardt, Kistner, Rajab, Kasser, et al., 2014; Weng et al., 2012). A detailed immunohistochemical examination of somatic HCN2 protein expression in lumbar 5 (L5) DRG neurons that innervate the hindlimb showed that HCN2 immunoreactivity significantly increased on day 1 post-CFA in small and medium neurons relative to control animals that did not receive CFA injections (L. A. Forster et al., 2020). HCN2 staining intensity then returned to baseline by day 3, but the number of neurons expressing HCN2 significantly increased (L. A. Forster et al., 2020). By days 5-7 post-CFA, HCN2 staining intensity was once again significantly increased, and the number of neurons expressing HCN2 remained elevated relative to controls (Weng et al.,

2012). In these studies, DRG neurons were only identified by soma size, and it is not known if all changes occurred in one cell type, or if HCN2 expression was altered in different cell types at distinct time points. It is noteworthy that changes in somatic HCN2 protein expression on days 1 and 3 post-CFA were bilateral, while chronic pain only occurs in the ipsilateral hindlimb (Millan et al., 1988; Schnorr, Eberhardt, Kistner, Rajab, Kasser, et al., 2014). This suggests that an increase in HCN2 protein expression may be necessary, but that the supplemental channels are not sufficient to produce pathological pain. One possibility is that a second ipsilateral mechanism acts on the supplemental HCN2 channels to alter their function and/or subcellular location.

It is well documented that HCN2 channel function is regulated by cAMP. Binding of cAMP to the channel's CNBD significantly shifts voltage dependence to more positive potentials, which will increase I_h under physiological conditions. DRG cAMP levels are elevated in models of chronic pain, and enhanced cAMP concentrations lower nociceptive thresholds and lead to hyperalgesia (Taiwo & Levine, 1991; Tsantoulas et al., 2017; Tsantoulas et al., 2016). Agonists of Gi/o-coupled receptors that reduce cAMP produce analgesia (Resta et al., 2016). In some models of neuropathic pain, genetic ablation of PKA had no effect on hyperalgesia, suggesting that direct binding of cAMP to the channel CNBD could increase I_h (Herrmann et al., 2017; Malmberg et al., 1997). In contrast, PKA is necessary for CFA-induced inflammatory pain (Herrmann et al., 2017). Knocking out either HCN2 or PKA prevented CFA-induced pathological pain, but deletion of the CNBD domain from the HCN2 channel had no effect on pain thresholds (Herrmann et al., 2017). Furthermore, on days 5-7 post-CFA, C-fiber but not A δ nociceptors showed enhanced excitability due to a significant increase in I_h activation kinetics and amplitude, but there was no change in I_h voltage dependence of activation (Djoughri et al., 2015; Weng et al., 2012). PKA is known to phosphorylate HCN2 (Herrmann et al., 2017). Thus,

the existing data suggest that CFA-induced persistent inflammation triggers cAMP activation of PKA, and perhaps, PKA phosphorylation of HCN2, which somehow leads to an increase in I_h .

HCN2 α -subunits interact with several auxiliary subunits that modify channel function, stability and surface expression (Brandt et al., 2009; Kimura et al., 2004; Michels et al., 2008; Nawathe et al., 2013; Qu et al., 2004; Santoro et al., 2004). Protein-protein interactions can be regulated by post-translational SUMOylation (Flotho & Melchior, 2013). Small Ubiquitin-like MOdifier (SUMO) peptides are post-translationally conjugated to lysine residues on target proteins, e.g., HCN2. The SUMO moiety can then promote or prevent interactions between the target and its interacting partners. There are 4 SUMO isoforms (SUMO1-4): SUMO2 & SUMO3 (SUMO2/3) are ~97% identical; SUMO1 shares 47% identity with SUMO2/3; the physiological relevance of SUMO 4 is unclear. The majority of SUMOylation (~65%) occurs within identifiable consensus sequences (Hendriks, D'Souza, et al., 2015), and HCN2 has several putative SUMOylation sites (Parker et al., 2017). HCN2 SUMOylation at K669 increased channel surface expression and I_h maximal conductance in a heterologous expression system (Parker et al., 2017). Inflammation causes a global increase in the SUMOylation of DRG proteins, and experimentally enhanced SUMOylation in sensory neurons produced pathological pain (Y. Wang et al., 2018a). In a rat model of CFA-induced inflammatory pain, HCN2 SUMOylation was increased in small DRG neurons on days 1 and 3 post-CFA (later times not examined) (L. A. Forster et al., 2020). A target protein's phosphorylation status often determines its ability to be SUMOylated (Dustrude et al., 2016; Flotho & Melchior, 2013). Activation of the adenylyl cyclase-cAMP-PKA axis in an identified pattern generating neuron permitted the post-translational SUMOylation that led to an enhanced I_h (Parker et al., 2019). Thus, inflammatory mediators acting through PKA could alter the phosphorylation status of HCN2 channels to

permit their SUMOylation, which could enhance surface expression. SUMOylation of HCN2 channels is dynamically regulated as inflammation progresses. SUMO2/3 conjugation to HCN2 increased at day 1 post-CFA, and SUMO1 conjugation to HCN2 increased at day 3 post-CFA (L. A. Forster et al., 2020). These data imply that inflammatory mediators regulate HCN2 interaction with components of the SUMOylation machinery that show target and SUMO-isoform specificity (Flotho & Melchior, 2013).

The rat hindpaw is innervated by sensory neurons in L4-L6 DRG. We previously reported the effects of CFA injection on HCN2 expression and SUMOylation in L5 DRG. Here, we complete the study and document changes in HCN2 expression and SUMOylation in L4 and L6.

3.3 Materials and Methods

3.3.1 Animal Ethics

Ethics approval was obtained from the Institutional Animal Care and Use Committee at Georgia State University and all experiments were performed in compliance with the Ethical Issues of the International Association for the Study of Pain and the National Institutes of Health (NIH). 60-day old, male Sprague-Dawley rats were pair housed in a 12-hr light/dark cycle (lights on at 0700 hr) with ad libitum access to food and water.

3.3.2 CFA Model and Tissue Preparation

A detailed description is found in Forster et al (L. A. Forster et al., 2020). Briefly, 60-day old, male Sprague Dawley rats were injected with 200 μ l of CFA into the mid-plantar surface of the right hindpaw. Control animals were handled, but not injected. 1 or 3 days later, animals were anesthetized, injected with heparin and perfused. Animals were fixed with 4%

paraformaldehyde. Bilateral L4 and L6 DRG were extracted and placed into an 18% sucrose solution at 4°C overnight. The following day, the epineurium was removed and DRG were embedded in 0.3% gelatin and sliced into 20 µm cryosections.

3.3.3 Antibodies and Reagents

The antibodies, dilution factors and applicable experiments are found in Forster et al (L. A. Forster et al., 2020).

3.3.4 Immunohistochemistry and Analysis

IHC was performed as previously described (L. A. Forster et al., 2020). For each DRG, three 5x magnification images were taken. Blind analysis was performed on Photoshop. Images were thresholded to remove the intensity of the sheath. All cells above threshold with a definitive nucleus and visible cell perimeter were HCN2+ cells. Cells below threshold but meeting these quantification requirements were considered HCN2-. HCN2+ cells were sorted into classes by diameter: small ≤ 30 µm, medium 30- 40 µm and large > 40 µm. All gray mean values within a size class were averaged and is represented as the mean pixel intensity of that size class. The number of HCN2+ cells within a size class were divided by the sum of all HCN2+ and HCN2- cells and is represented as the frequency of that class. IHC experiments were repeated on 6 or 7 experimental animals and 4 or 5 control animals for L4 and L6 DRG at day 1 and day 3.

3.3.5 Proximity Ligation Assay

PLAs were performed using Duolink[®] In Situ Red Kit and manufacturer's guidelines as previously described (L. A. Forster et al., 2020). Images were captured with a Zeiss 700 confocal microscope using a 40x oil immersion objective. Three cryosections were examined per DRG

with a minimum of 3 z-stacks per cryosection. Blind analyses were performed using the FIJI version of ImageJ. Cells with a visible nucleus, clear cell boundaries and no overlap with neighboring cells or fibers were selected for quantification. Maximum intensity projections of 5 z-slices from the middle of the cells were created. Cells were outlined and thresholded using the triangle method. Watershed analysis divided coalesced signals. For each cell, the average number of puncta was divided by the cell area to obtain puncta/ μm^2 . The mean pixel intensity (MPI) within 1 cell was processed by a program created by Alex Perez. PLA experiments were repeated on 6 experimental and 3 control DRG for L4 and L6 DRG at day 1 and day 3.

3.3.6 Statistics

All statistical analyses were performed using GraphPad Prism. All data were tested for normality. The data for left and right DRG from each control animal were combined because paired t-tests indicated left and right DRG showed no significant differences. IHC data were analyzed with a one-way ANOVA followed by Tukey's post-hoc or Kruskal-Wallis followed by Dunn's post-hoc. Multiple comparison tests showed no significant differences in HCN2 SUMOylation between control and experimental DRG, therefore control data are not shown. Normal PLA data were measured using paired t-tests between ipsilateral and contralateral DRG. Non-parametric PLA data were analyzed with Wilcoxon-matched pairs. All values are presented as mean \pm SEM. $p < 0.05$ was considered statistically significant.

3.4 Results

3.4.1 *HCN2 expression and SUMOylation in L4 DRG neuron on days 1 and days 3 post-CFA*

CFA was injected into the right hindpaw of experimental animals to elicit persistent inflammation, while control animals were handled, but not injected. Bilateral L4 and L6 DRG were dissected at day 1 or day 3 post-CFA and cryosectioned for immunohistochemistry (IHC) or proximity ligation assays (PLA), as previously described (L. A. Forster et al., 2020). The IHC experiments were used to measure the level of HCN2 expression in a given cell (mean pixel intensity) and the percent of HCN2 expressing cells (frequency) in small ($\leq 30 \mu\text{m}$), medium (30- 40 μm) and large ($> 40 \mu\text{m}$) neurons. Values for left and right control DRG were not significantly different from each other; therefore, left and right values were combined and the datum for one control animal represents the average for left and right DRG. PLA experiments measured the number of SUMOylated HCN2 channels (puncta/ μm^2) or the extent to which HCN2 channels were SUMOylated (puncta intensity) in ipsilateral relative to contralateral DRG.

Figure 3-1 shows representative cryostat sections and the results for L4 DRG 1 day post-CFA. A significant ~53% increase in HCN2 IR was observed in both ipsilateral and contralateral small cells relative to control (contralateral: 22.5 ± 1.5 ; ipsilateral: 23.4 ± 1.5 ; control: 15.0 ± 1.8) (Figure 3-1b). There were no significant differences in medium or large cell IR (Medium contralateral: 24.0 ± 2.0 ; ipsilateral: 25.8 ± 2.3 ; control: 18.4 ± 3.0) (Large contralateral: 27.2 ± 1.9 ; ipsilateral: 28.2 ± 2.8 ; control: 20.4 ± 3.6). In contrast, Figure 3-1c shows that CFA-injection produced a bi-lateral increase in the number of medium and large, but not small cells expressing HCN2 (Small contralateral: 37.3 ± 5.0 ; ipsilateral: 38.6 ± 5.6 ; control: 25.0 ± 5.5) (Medium contralateral: 19.1 ± 1.3 ; ipsilateral: 19.9 ± 2.1 ; control: 12.7 ± 1.0) (Large contralateral: $20.8 \pm$

1.7; ipsilateral: 20.6 ± 1.5 ; control: 13.1 ± 2.5). These experiments did not reveal any CFA-induced change in post-translational SUMOylation of HCN2 channels. There were no significant differences in the number or intensity of puncta between ipsilateral and contralateral L4 DRG 1 day post-CFA for any size class (Figure 3-1e,f).

These experiments did not reveal any CFA-induced change in HCN2 expression or post-translational SUMOylation in L4 DRG on day 3 post-CFA. There were no significant differences in HCN2 mean pixel intensity (Figure 3-2a) or frequency (Figure 3-2b) for any size class. The number (Figure 3-2c) and intensity (Figure 3-2d) of puncta were similar in ipsilateral and contralateral L4 DRG.

3.4.2 HCN2 expression and SUMOylation in L6 DRG neurons on days 1 and day 3 post-CFA

In the L6 DRG 1 day post-CFA, HCN2 expression bilaterally increased in experimental small cells relative to controls (Figure 3-3a). The mean pixel intensity was ~65% greater for experimental compared to control animals (contralateral: 25.5 ± 1.8 ; ipsilateral: 27.6 ± 2.2 ; control: 16.1 ± 1.1). Although mean pixel intensity increased in experimental vs. control for both medium and large cells, it was not statistically significant. There were no significant changes in HCN2 frequency for any size class (Small contralateral: 44.3 ± 4.2 ; ipsilateral: 54.1 ± 4.7 ; control: 42.1 ± 4.2) (Medium contralateral: 17.3 ± 1.9 ; ipsilateral: 17.6 ± 1.8 ; control: 16.0 ± 2.1) (Large contralateral: 13.3 ± 1.9 ; ipsilateral: 11.7 ± 1.3 ; control: 14.0 ± 2.8) (Figure 3-3b). There was a small but significant increase in the number of SUMOylated HCN2 channels in medium and large neurons (Figure 3-3c). The differences were isoform specific with SUMO 1 vs. SUMO 2/3 modification increasing in medium vs. large cells, respectively. There were no significant changes in puncta intensity (Figure 3-3d).

In the L6 DRG on day 3 post-CFA, there were no significant differences in HCN2 immunoreactivity (Figure 3-4a) or frequency (Figure 3-4b) for any L6 DRG neuronal size class. There were no significant changes in the number of SUMOylated HCN2 channels (Figure 3-4c). In contrast, HCN2 SUMO2/3 puncta intensity was significantly increased in ipsilateral small and medium cells, but not in large cells (Figure 3-4d).

3.5 Discussion

In this work, we investigated HCN2 expression and SUMOylation in L4 and L6 DRG at days 1 and 3 post-CFA injection. Using IHC, we found a bilateral increase in HCN2 mean pixel intensity in small neurons from L4 and L6 DRG at day 1, but expression levels returned to baseline by day 3. The number of medium and large neurons expressing HCN2 also transiently increased in L4 DRG on day 1 post-CFA. Using PLA, we found that HCN2 SUMOylation increased in L6 DRG at days 1 and 3. The number of SUMOylated HCN2 channels increased in medium and large cells at day 1, whereas the extent of HCN2 SUMOylation was enhanced in small and medium cells at day 3.

The patterns of change in HCN2 expression and SUMOylation are distinct for each of the lumbar DRG (Tables 1&2). This is not surprising given that for each DRG a different fraction of neurons project to the hindpaw. Whereas most neurons in the L5 DRG project to the hindpaw (Rigaud et al., 2008; Swett, Torigoe, Elie, Bourassa, & Miller, 1991), afferents in the L4 DRG project to the hindlimb, knee and hip joint (Nakajima et al., 2008; Rigaud et al., 2008; Salo & Theriault, 1997), and the neurons in L6 DRG mainly innervate visceral organs (Herrity, Rau, Petruska, Stirling, & Hubscher, 2014; Rigaud et al., 2008; Swett et al., 1991). Changes occurred in all size classes of neurons, which is consistent with the fact that both C-fiber and A β fibers respond to CFA-induced inflammation (Belkouch et al., 2014).

Despite the fact that neurons in L4-L6 DRG differentially innervate the hindpaw, Table 1 shows that most changes in HCN2 expression occurred to the same extent in ipsi- and contra-lateral DRG for all 3 lumbar levels. This generalized change suggests that altered expression of HCN2 is likely to be a systemic response to CFA injection (Koltzenburg, Wall, & McMahon, 1999), which is not sufficient for the development of inflammatory pain at these time points. In contrast, Table 2 shows increased SUMOylation is observed exclusively in the ipsilateral side and may make a more direct contribution to the pain phenotype. In that respect, and given that SUMOylation of HCN2 is known to enhance surface expression of the channel (Parker et al., 2017), it may be that in DRGs where SUMOylation is increased, surface expression of HCN2 is also increased without necessarily altering total expression. Alternatively, SUMOylation of HCN2 may have a direct effect on the gating of the channel. There are several examples of SUMOylation altering ion channel biophysical properties (Benson et al., 2007; X. Q. Dai et al., 2009; Plant et al., 2010; Plant et al., 2016; Steffensen et al., 2018; Y. Wang et al., 2018a; Meghyn A. Welch, Lori A. Forster, Selin I. Atlas, & Deborah J. Baro, 2019; Xiong et al., 2017). In our previous study, enhanced HCN2 SUMOylation in HEK cells did not alter I_h voltage dependence or kinetics (Parker et al., 2017). However, this result must be interpreted in the context of significant experimental caveats. First, since SUMO regulates protein-protein interactions, the effect of HCN2 SUMOylation will depend upon the available complement of interacting proteins, and the HCN2 interactome varies between cell types. Second, in our HEK cell experiments the level of HCN2 SUMOylation was altered in an uncontrolled fashion simply by increasing the cytosolic concentration of SUMO and the SUMO conjugating enzyme, Ubc9. HCN2 has multiple putative SUMOylation sites, but this manipulation increased SUMOylation at just a single site, so all potential effects of enhanced SUMOylation may not have been

observed. Third, modulators play a permissive role in SUMOylation (Parker et al., 2019), and the phosphorylation state of a protein determines which sites can be SUMOylated (Dustrude et al., 2016; Flotho & Melchior, 2013). Thus, inflammatory mediators that alter phosphorylation states will likely produce a distinct pattern of HCN2 SUMOylation and associated effects that would not be replicated in the HEK cell experiments.

Emerging data suggest that altered SUMOylation may drive changes in several ion channels during nociceptor sensitization. The SUMOylation status of hundreds of proteins in a single cell is altered in response to a cellular stressor (Hendriks, D'Souza, et al., 2015; Seifert et al., 2015). Chronic inflammation resulted in hyper-SUMOylation of the heat sensing TRPV1 channel, which lowered the temperature threshold of activation and led to thermal hyperalgesia (Y. Wang et al., 2018a). CRMP2, a subunit of the NaV1.7 channel, is hyper-SUMOylated in a rat model of chronic neuropathic pain, which enhances the sodium current; and, blocking CRMP2 hyper-SUMOylation in DRG neurons prevented mechanical and thermal hyperalgesia (Dustrude et al., 2016; Dustrude et al., 2013; Francois-Moutal, Dustrude, et al., 2018; Moutal, Dustrude, et al., 2017). A ~2-fold change in CRMP2 SUMOylation was observed in sciatic nerve, dorsal horn and glabrous skin during neuropathic pain (Moutal, Dustrude, et al., 2017) suggesting that larger changes in HCN2 SUMOylation may be observed in subcellular compartments such as axons and terminals relative to somata. Additional ion channels are known to be SUMOylated including Kv4 (Meghyn A. Welch et al., 2019), Kv11 (Steffensen et al., 2018), Kv7 (Y. Qi et al., 2014; Xiong et al., 2017), Kv2 (Plant et al., 2011), K2P1 (Plant et al., 2010; Rajan et al., 2005), Kv1.5 (Benson et al., 2007), NaV1.2 (Plant et al., 2016) and NaV1.5 (Plant et al., 2020). Their SUMOylation patterns have not yet been ascertained during chronic pain.

In sum, CFA-induced inflammation results in HCN2-dependent mechanical hyperalgesia. Inflammation-induced alterations in lumbar DRG sensory neurons include altered HCN2 expression and post-translational SUMOylation. Multiple mechanisms regulate HCN2 during the time course of CFA-induced inflammation. Identification of these mechanisms and the cell type in which they occur are worth further study.

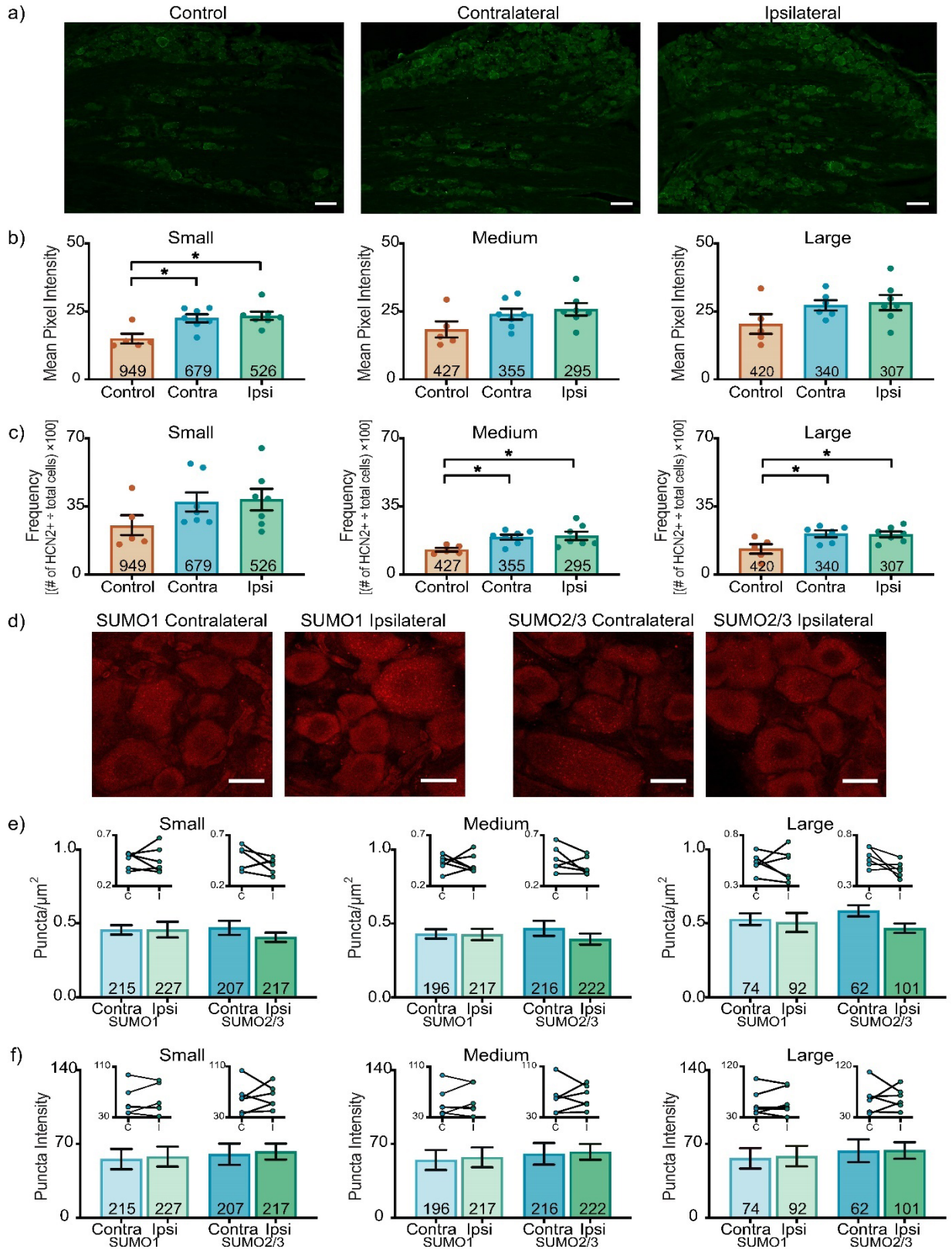


Figure 3-1 HCN2 protein expression but not SUMOylation is altered in the L4 DRG 1 day post-CFA.

A) Representative images of HCN2 IR. Scale bars are 100 μm . B) HCN2 mean pixel intensity is elevated in small diameter DRG neurons. Average mean pixel intensity \pm SEM is shown for three size classes of DRG neurons (small: $\leq 30 \mu\text{m}$; medium: 30- 40 μm ; large: $> 40 \mu\text{m}$). Each dot represents the mean for one animal. Note that data for left and right DRG from each control were combined, because paired t-tests indicated left and right DRG showed no significant differences. The total number of cells examined for all animals within the treatment group is indicated in the bar. Asterisks indicate significance, $*p < 0.05$. Small cells: Kruskal-Wallis with Dunn's post-hoc test (2,16)=7.750; $p=0.014$; medium cells: one-way ANOVA $F(2,16)=2.378$; $p=0.125$; large cells: one-way ANOVA $F(2,15)=2.158$; $p=0.150$. C) The percent of medium and large diameter neurons expressing HCN2 increases 1 day post-CFA. Plot of percent HCN2 positive cells for each size class (frequency = # HCN2 positive cells for that size class \div total cell number for all classes). Bars indicate mean \pm SEM. Asterisks indicate significance, $*p < 0.05$. Small cells: Kruskal-Wallis (2,16)= 3.441; $p=0.184$; medium cells: one-way ANOVA with Tukey's post hoc test $F(2,16)= 4.901$; $p=0.022$; large cells: one-way ANOVA with Tukey's post hoc test $F(2,15)= 5.188$; $p=0.019$. D) Representative confocal projections (5 μm) from PLA experiments. Scale bars are 25 μm . E) The number of SUMOylated HCN2 channels is unaltered 1 day post-CFA. The number of puncta/ μm^2 for HCN2 SUMO1 (light bars) and SUMO2/3 (dark bars) conjugation is shown for three size classes of DRG neurons (small: $\leq 30 \mu\text{m}$; medium: 30- 40 μm ; large: $> 40 \mu\text{m}$). SUMO1; small: 0.458 ± 0.054 vs 0.456 ± 0.032 , $p=0.979$, paired t-test; medium: 0.424 ± 0.038 vs 0.429 ± 0.032 , $p>0.999$, Wilcoxon-matched pairs; large: 0.505 ± 0.065 vs 0.528 ± 0.039 , $p=0.740$, paired t-test; SUMO2/3; small: 0.405 ± 0.031 vs 0.469 ± 0.048 , $p=0.271$, paired t-test; medium: 0.394 ± 0.037 vs 0.467 ± 0.050 , $p=0.181$, paired t-test; large: 0.467 ± 0.032 vs 0.584 ± 0.038 , $p=0.068$, paired t-test. Inset:

compares the means for contralateral and ipsilateral DRG for each animal. F) SUMOylated HCN2 Puncta Intensities are unaltered 1 day post-CFA. Plot of average puncta intensity \pm SEM for each size class. SUMO1; small: 57.86 ± 9.486 vs 55.55 ± 9.556 , $p=0.615$, paired t-test; medium: 57.24 ± 9.442 vs 54.76 ± 9.484 , $p=0.643$, paired t-test; large: 58.37 ± 9.707 vs 56.34 ± 9.626 , $p=0.679$, paired t-test; SUMO2/3; small: 62.71 ± 7.576 vs 60.19 ± 10.08 , $p=0.785$, paired t-test; medium: 62.44 ± 7.471 vs 60.60 ± 10.21 , $p=0.824$, paired t-test; large: 63.80 ± 7.816 vs 63.46 ± 10.79 , $p=0.975$, paired t-test.

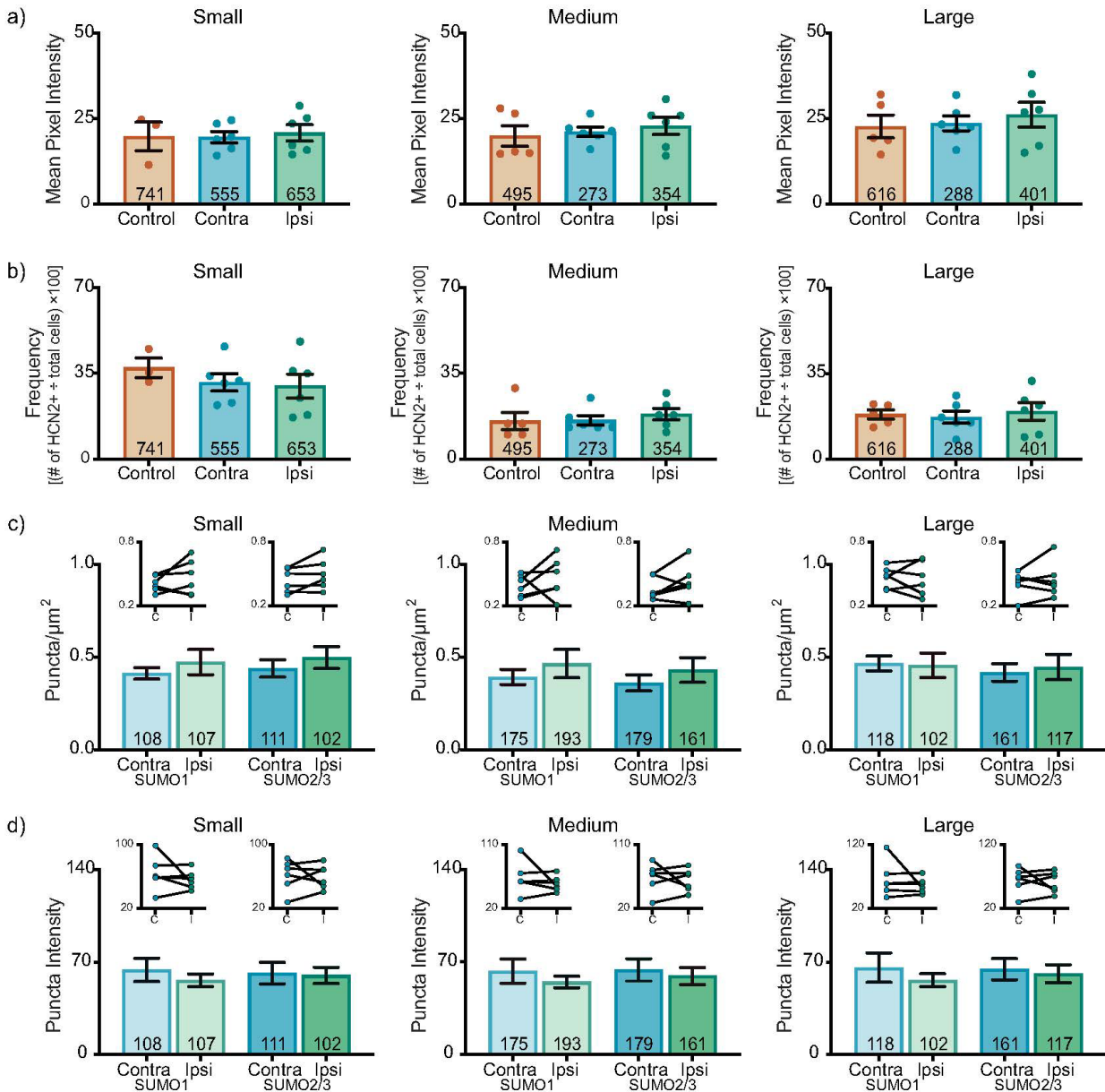


Figure 3-2 HCN2 protein expression and HCN2 SUMOylation are unaltered in the L4 DRG 3 days post CFA.

A) HCN2 mean pixel intensities do not change 3 days post-CFA. Average mean pixel intensity \pm SEM is shown for three size classes of DRG neurons (small: $\leq 30 \mu\text{m}$; medium: $30-40 \mu\text{m}$; large: $> 40 \mu\text{m}$). Each dot represents the mean for one animal. Note that data for left and right DRG from each control were combined, because paired t-tests indicated left and right DRG showed no significant differences. The total number of cells examined for all animals within the

treatment group is indicated in the bar. Small cells: one-way ANOVA $F(2,12)=0.090$; $p=0.915$; medium cells: Kruskal-Wallis $(2,14)=0.438$; $p=0.819$; large cells: one-way ANOVA $F(2,14)=0.330$; $p=0.725$. B) The percent of HCN2 expressing cells does not change 3 days post-CFA. Plot of percent HCN2 positive cells for each size class (frequency = # HCN2 positive cells for that size class \div total cells number for all classes). Bars are mean \pm SEM. Small cells: one-way ANOVA $F(2,12)=0.581$; $p=0.574$; medium cells: Kruskal-Wallis $(2,14)=1.358$; $p=0.531$; large cells: one-way ANOVA $F(2,14)=0.176$; $p=0.840$. C) The number of SUMOylated HCN2 channels is unaltered in L4 DRG neurons. The number of puncta/ μm^2 for HCN2 SUMO1 (light bars) and SUMO2/3 (dark bars) conjugation is shown for three size classes of DRG neurons (small: $\leq 30 \mu\text{m}$; medium: $30-40 \mu\text{m}$; large: $> 40 \mu\text{m}$). SUMO1; small: 0.473 ± 0.068 vs 0.412 ± 0.031 , $p=0.307$, paired t-test; medium: 0.465 ± 0.076 vs 0.393 ± 0.041 , $p=0.418$, paired t-test; large: 0.456 ± 0.066 vs 0.466 ± 0.040 , $p=0.847$, paired t-test; SUMO2/3; small: 0.479 ± 0.059 vs 0.438 ± 0.047 , $p=0.121$, paired t-test; medium: 0.431 ± 0.067 vs 0.361 ± 0.043 , $p=0.236$, paired t-test; large: 0.446 ± 0.069 vs 0.417 ± 0.047 , $p=0.562$, paired t-test. Inset: compares the means for contralateral and ipsilateral DRG for each animal. D) SUMOylated HCN2 Puncta Intensities are unaltered in L4 DRG neurons. Plot of average puncta intensity \pm SEM for each size class. SUMO1; small: 56.16 ± 4.766 vs 64.04 ± 8.799 , $p=0.382$, paired t-test; medium: 54.92 ± 4.379 vs 63.08 ± 9.142 , $p=0.400$, paired t-test; large: 56.32 ± 4.917 vs 65.79 ± 11.18 , $p=0.423$, paired t-test; SUMO2/3; small: 59.62 ± 6.125 vs 61.62 ± 8.081 , $p=0.836$, paired t-test; medium: 59.44 ± 6.444 vs 64.02 ± 8.447 , $p=0.609$, paired t-test; large: 61.18 ± 6.817 vs 64.59 ± 7.984 , $p=0.691$, paired t-test.

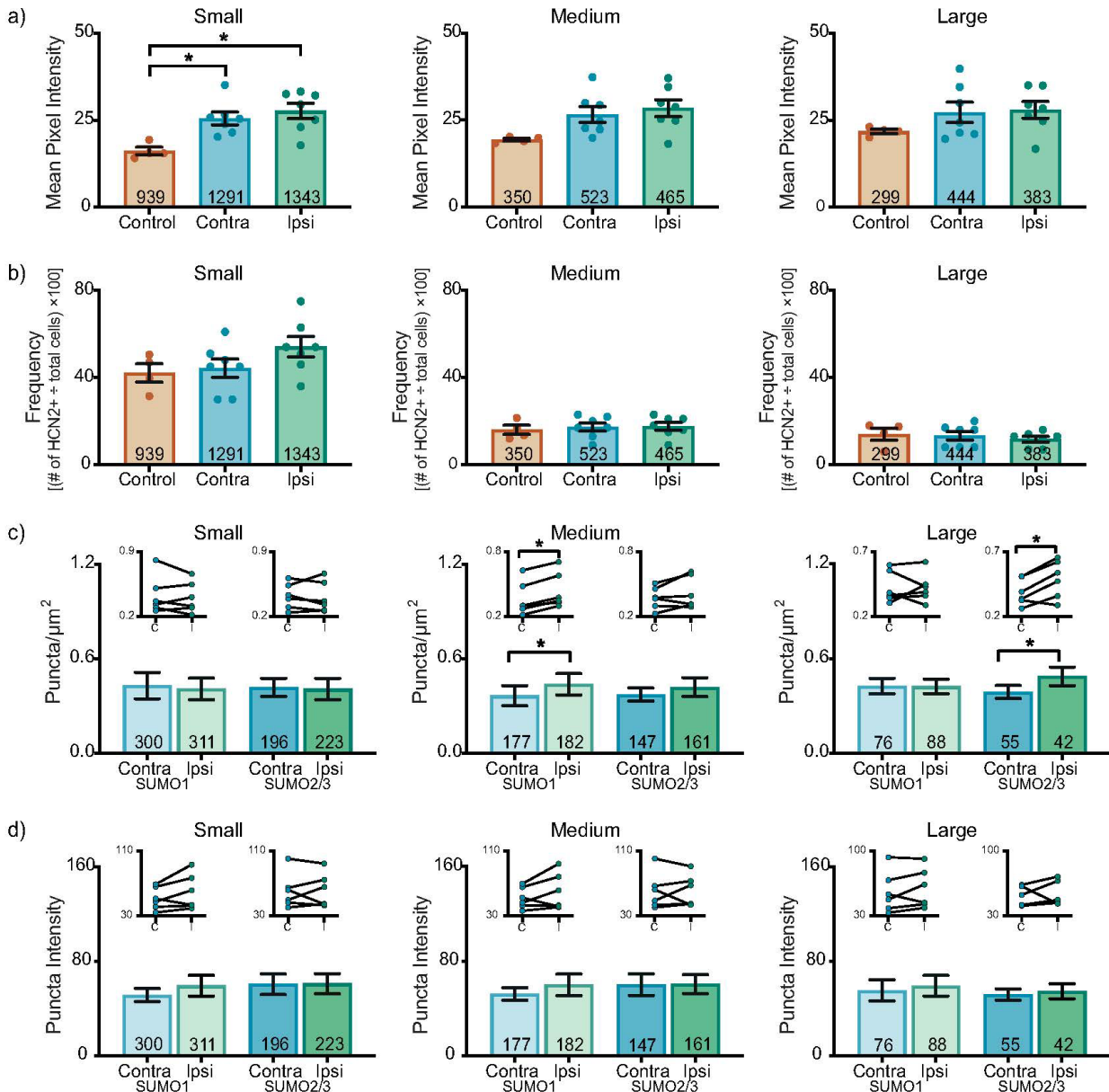


Figure 3-3 HCN2 protein expression and HCN2 SUMOylation are enhanced in the L6 DRG 1 day post-CFA.

A) HCN2 mean pixel intensity is elevated in small diameter neurons. Average mean pixel intensity \pm SEM is shown for three size classes of DRG neurons (small: $\leq 30 \mu\text{m}$; medium: $30\text{--}40 \mu\text{m}$; large: $> 40 \mu\text{m}$). Each dot represents the mean for one animal. Note that data for left and right DRG from each control were combined, because paired t-tests indicated left and right DRG showed no significant differences. The total number of cells examined for all animals within the

treatment group is indicated in the bar. Asterisks indicate significance, * $p < 0.05$. Small cells: one-way ANOVA with Tukey's post-hoc $F(2,15)=7.422$; $p=0.0060$; medium cells: one-way ANOVA $F(2,15)=3.542$; $p=0.055$; large cells: one-way ANOVA $F(2,15)=1.338$; $p=0.292$. B) The percent of HCN2 expressing cells is unaltered 1 day post-CFA. Plot of percent HCN2 positive cells for each size class (frequency = # HCN2 positive cells for that size class \div total cells number for all classes). Bars indicate mean \pm SEM. Small cells: one-way ANOVA $F(2,15)=1.980$; $p=0.173$; medium cells: one-way ANOVA $F(2,15)=0.147$; $p=0.865$; large cells: one-way ANOVA $F(2,15)=0.365$; $p=0.700$. C) The number of SUMOylated HCN2 channels increases in medium and large diameter neurons. The number of puncta/ μm^2 for HCN2 SUMO1 (light bars) and SUMO2/3 (dark bars) conjugation is shown for three size classes of DRG neurons (small: $\leq 30 \mu\text{m}$; medium: $30-40 \mu\text{m}$; large: $> 40 \mu\text{m}$). Bars indicate the mean \pm SEM. Asterisks indicate significance, * $p < 0.05$. SUMO1; small: 0.408 ± 0.068 vs 0.429 ± 0.083 , $p=0.574$, paired t-test; medium: 0.438 ± 0.068 vs 0.365 ± 0.064 , $p=0.031$, Wilcoxon matched-pairs; large: 0.424 ± 0.046 vs 0.426 ± 0.049 , $p=0.961$, paired t-test; SUMO2/3; small: 0.407 ± 0.069 vs 0.418 ± 0.057 , $p=0.752$, paired t-test; medium: 0.419 ± 0.060 vs 0.372 ± 0.042 , $p=0.189$, paired t-test; large: 0.488 ± 0.059 vs 0.388 ± 0.042 , $p=0.018$, paired-test. Inset: compares the means for contralateral and ipsilateral DRG for each animal. D) SUMOylated HCN2 Puncta Intensities are unaltered 1 day post-CFA. Plot of average puncta intensity \pm SEM for each size class. SUMO1; small: 59.42 ± 8.867 vs 51.48 ± 5.557 , $p=0.137$, paired t-test; medium: 59.92 ± 9.085 vs 52.20 ± 5.315 , $p=0.189$, paired t-test; large: 59.39 ± 8.740 vs 55.49 ± 9.037 , $p=0.316$, paired t-test; SUMO2/3; small: 61.16 ± 8.501 vs 60.61 ± 8.770 , $p=0.916$, paired t-test; medium: 60.58 ± 8.002 vs 60.13 ± 9.115 , $p=0.936$, paired t-test; large: 54.74 ± 6.259 vs 51.96 ± 4.790 , $p=0.655$, paired t-test.

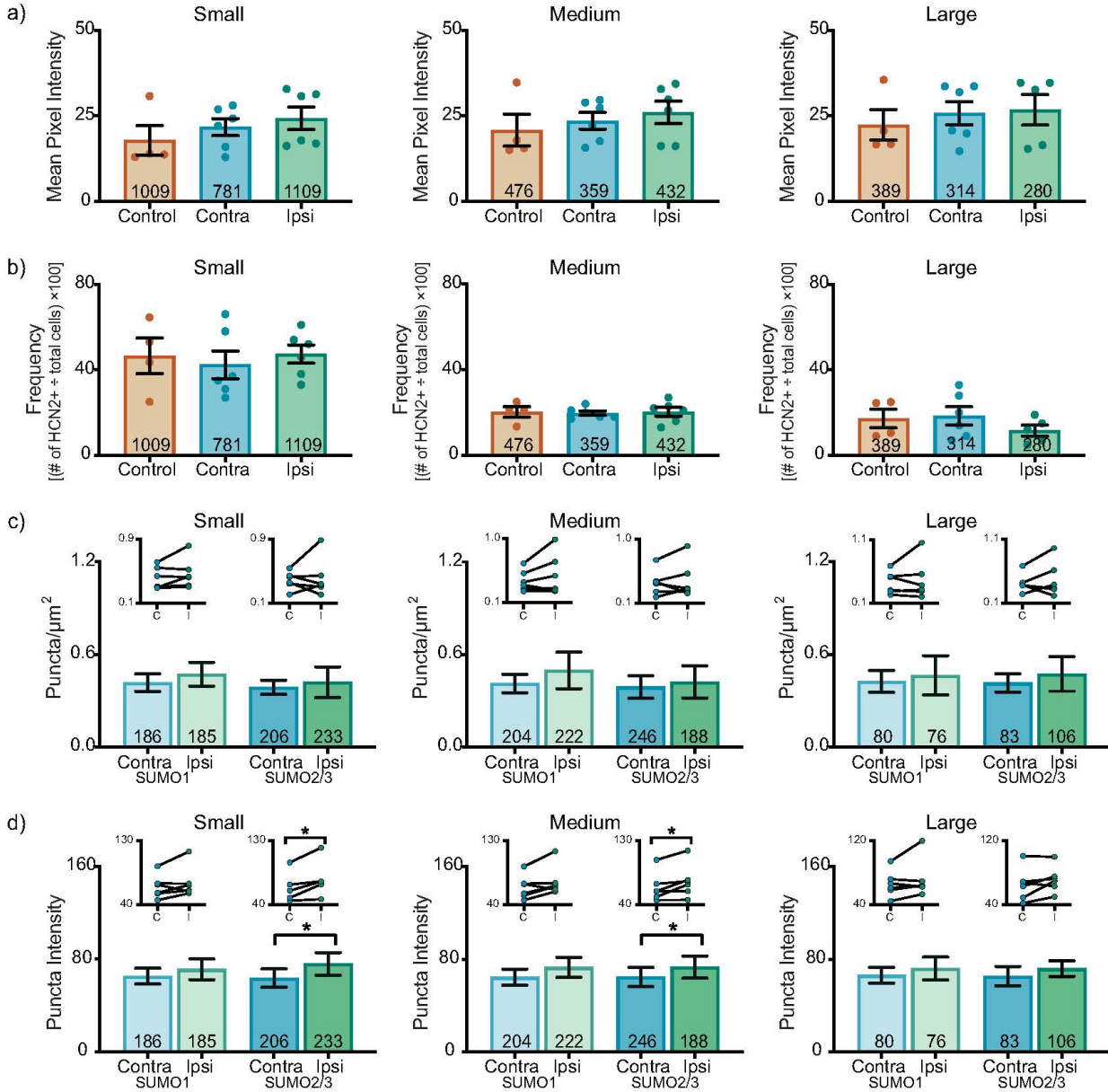


Figure 3-4 HCN2 SUMOylation but not protein expression is altered in the L6 DRG 3 days post-CFA.

A) HCN2 mean pixel intensities do not change 3 days post-CFA. Average mean pixel intensity \pm SEM is shown for three size classes of DRG neurons (small: $\leq 30 \mu\text{m}$; medium: 30-40 μm ; large: $> 40 \mu\text{m}$). Each dot represents the mean for one animal. Note that data for left and right DRG from each control were combined, because paired t-tests indicated left and right DRG

showed no significant differences. The total number of cells examined for all animals within the treatment group is indicated in the bar. Small cells: Kruskal-Wallis (2,13)=2.842; p=0.252; medium cells: Kruskal-Wallis (2,13)=1.309; p=0.543; large cells: Kruskal-Wallis (2,12)=0.061; p=0.977. B) The percent of HCN2 expressing cells does not change 3 days post-CFA. Plot of percent HCN2 positive cells for each size class (frequency = # HCN2 positive cells for that size class ÷ total cells number for all classes). Bars indicate mean ± SEM. Small cells: one-way ANOVA F(2,13)=0.206; p=0.817; medium cells: one-way ANOVA (2,13)=0.043; p=0.958; large cells: one-way ANOVA F(2,12)=0.932; p=0.420. C) The number of HCN2 SUMOylated channels is unaltered 3 days post-CFA. The number of puncta/μm² for HCN2 SUMO1 (light bars) and SUMO2/3 (dark bars) conjugation is shown for three size classes of DRG neurons (small: ≤ 30 μm; medium: 30- 40 μm; large: > 40 μm). SUMO1; small: 0.473 ± 0.077 vs 0.418 ± 0.057, p= 0.211, paired t-test; medium: 0.498 ± 0.118 vs 0.413 ± 0.06, p=0.219, paired t-test; large: 0.466 ± 0.127 vs 0.427 ± 0.071, p=0.593, paired t-test; SUMO2/3; small: 0.423 ± 0.099 vs 0.389 ± 0.046, p=0.678, paired t-test; medium: 0.424 ± 0.104 vs 0.392 ± 0.073, p=0.563, Wilcoxon matched-pairs, large: 0.475 ± 0.112 vs 0.417 ± 0.059, p=0.563, Wilcoxon matched-pairs. Inset: compares the means for contralateral and ipsilateral DRG for each animal. D) SUMOylated HCN2 Puncta Intensities are increased in small and medium cells. Plot of average puncta intensity ± SEM for each size class. SUMO1; small: 71.29 ± 8.984 vs 65.37 ± 6.805, p= 0.219, Wilcoxon matched-pairs; medium: 73.03 ± 8.633 vs 64.59 ± 6.927, p=0.094, Wilcoxon matched-pairs; large: 72.02 ± 9.835 vs 66.21 ± 6.770, p=0.313, Wilcoxon matched-pairs; SUMO2/3; small: 75.83 ± 9.743 vs 63.63 ± 7.899, p=0.031, Wilcoxon matched-pairs; medium: 73.25 ± 9.620 vs 64.71 ± 8.353, p=0.046, paired t-test; large cells: 71.93 ± 6.724 vs 65.46 ± 8.374, p=0.148, paired t-test.

Table 1 Fold Change in Mean HCN2 Expression in L4-L6 DRG

Fold Change in Mean HCN2 Expression in Experimental DRG relative to Control DRG						
HCN2 Expression	Small		Medium		Large	
	Contralateral DRG	Ipsilateral DRG	Contralateral DRG	Ipsilateral DRG	Contralateral DRG	Ipsilateral DRG
Mean Pixel Intensity Day 1						
L4	1.5 (\pm 0.10)	1.6 (\pm 0.10)	1.3 (\pm 0.11)	1.4 (\pm 0.12)	1.3 (\pm 0.09)	1.4 (\pm 0.14)
L5	1.4 (\pm 0.10)	1.5 (\pm 0.12)	1.3 (\pm 0.08)	1.4 (\pm 0.14)	1.2 (\pm 0.10)	1.4 (\pm 0.19)
L6	1.6 (\pm 0.11)	1.7 (\pm 0.14)	1.4 (\pm 0.12)	1.5 (\pm 0.12)	1.3 (\pm 0.13)	1.3 (\pm 0.11)
Frequency Day 1						
L4	1.5 (\pm 0.20)	1.5 (\pm 0.22)	1.5 (\pm 0.11)	1.6 (\pm 0.17)	1.6 (\pm 0.13)	1.6 (\pm 0.11)
L5	1.7 (\pm 0.21)	1.5 (\pm 0.25)	1.0 (\pm 0.08)	1.1 (\pm 0.15)	0.8 (\pm 0.12)	0.9 (\pm 0.25)
L6	1.1 (\pm 0.10)	1.3 (\pm 0.11)	1.1 (\pm 0.12)	1.1 (\pm 0.11)	1.0 (\pm 0.14)	0.8 (\pm 0.10)
Mean Pixel Intensity Day 3						
L4	1.0 (\pm 0.08)	1.1 (\pm 0.12)	1.1 (\pm 0.07)	1.1 (\pm 0.13)	1.0 (\pm 0.10)	1.2 (\pm 0.16)
L5	1.4 (\pm 0.20)	1.3 (\pm 0.16)	1.4 (\pm 0.22)	1.3 (\pm 0.20)	1.4 (\pm 0.25)	1.3 (\pm 0.23)
L6	1.2 (\pm 0.14)	1.4 (\pm 0.18)	1.1 (\pm 0.12)	1.2 (\pm 0.16)	1.1 (\pm 0.15)	1.2 (\pm 0.20)
Frequency Day 3						
L4	0.8 (\pm 0.10)	0.8 (\pm 0.13)	1.0 (\pm 0.12)	1.2 (\pm 0.15)	0.9 (\pm 0.14)	1.1 (\pm 0.20)
L5	3.0 (\pm 0.70)	2.6 (\pm 0.30)	1.8 (\pm 0.17)	1.7 (\pm 0.15)	0.7 (\pm 0.21)	1.0 (\pm 0.18)
L6	0.9 (\pm 0.14)	1.0 (\pm 0.09)	1.0 (\pm 0.05)	1.0 (\pm 0.10)	1.1 (\pm 0.25)	0.7 (\pm 0.15)

Bold values = $p < 0.05$
 \pm SEM are shown in parenthesis.

Table 2 Fold Change in Mean HCN2 SUMOylation in L4-L6 DRG

Fold Change in Mean HCN2 SUMOylation in Ipsilateral DRG relative to Contralateral DRG						
HCN2 SUMOylation	Small		Medium		Large	
	SUMO1	SUMO2/3	SUMO1	SUMO2/3	SUMO1	SUMO2/3
Puncta/ μm^2 Day 1						
L4	1.0 (\pm 0.12)	0.9 (\pm 0.07)	1.0 (\pm 0.09)	0.8 (\pm 0.08)	1.0 (\pm 0.12)	0.8 (\pm 0.05)
L5	0.8 (\pm 0.10)	1.3 (\pm 0.17)	0.7 (\pm 0.10)	1.1 (\pm 0.10)	0.7 (\pm 0.06)	1.2 (\pm 0.16)
L6	1.0 (\pm 0.16)	1.0 (\pm 0.16)	1.2 (\pm 0.18)	1.1 (\pm 0.16)	1.0 (\pm 0.11)	1.3 (\pm 0.15)
Puncta Intensity Day 1						
L4	1.0 (\pm 0.17)	1.0 (\pm 0.13)	1.0 (\pm 0.17)	1.0 (\pm 0.13)	1.0 (\pm 0.17)	1.0 (\pm 0.12)
L5	0.9 (\pm 0.06)	0.9 (\pm 0.09)	1.1 (\pm 0.10)	1.0 (\pm 0.10)	1.0 (\pm 0.10)	1.0 (\pm 0.11)
L6	1.2 (\pm 0.17)	1.0 (\pm 0.14)	1.1 (\pm 0.17)	1.0 (\pm 0.13)	1.1 (\pm 0.16)	1.1 (\pm 0.12)
Puncta/ μm^2 Day 3						
L4	1.1 (\pm 0.16)	1.1 (\pm 0.14)	1.2 (\pm 0.19)	1.2 (\pm 0.18)	1.0 (\pm 0.14)	1.1 (\pm 0.16)
L5	1.3 (\pm 0.13)	1.1 (\pm 0.13)	0.8 (\pm 0.20)	1.0 (\pm 0.19)	0.9 (\pm 0.18)	1.0 (\pm 0.17)
L6	1.1 (\pm 0.18)	1.1 (\pm 0.25)	1.2 (\pm 0.29)	1.1 (\pm 0.27)	1.1 (\pm 0.30)	1.1 (\pm 0.27)
Puncta Intensity Day 3						
L4	0.9 (\pm 0.07)	1.0 (\pm 0.10)	0.9 (\pm 0.07)	0.9 (\pm 0.10)	0.9 (\pm 0.08)	0.9 (\pm 0.11)
L5	1.0 (\pm 0.03)	1.0 (\pm 0.08)	1.0 (\pm 0.03)	1.0 (\pm 0.08)	1.1 (\pm 0.03)	1.1 (\pm 0.08)
L6	1.1 (\pm 0.14)	1.2 (\pm 0.15)	1.1 (\pm 0.13)	1.1 (\pm 0.15)	1.1 (\pm 0.15)	1.1 (\pm 0.10)

Bold values = $p < 0.05$

\pm SEM are shown in parenthesis.

4 PIAS3 IS AN E3 SUMO LIGASE FOR KV4 CHANNELS

Unpublished: Jansen, L. R., Welch, M. A., Plant, L. D., & Baro, D. J. PIAS3 is an E3 SUMO ligase for Kv4 channels. *In preparation.*

Contribution disclosure: LR. Jansen, MA. Welch, LD. Plant, and DJ Baro were responsible for the conception and design of the research presented. LR. Jansen, MA. Welch, and DJ Baro contributed to the acquisition and analysis of the data. LR. Jansen and D. Baro were responsible for drafting the manuscript.

4.1 Introduction

The Protein Inhibitor of Activated STAT3 (PIAS3) is an E3 ligase that facilitates the covalent attachment of the small ubiquitin modifier protein (SUMO) to target lysine residues. PIAS3 contains 6 conserved domains: a DNA-binding SAP domain, a nuclear localization PINIT domain, a RING-like SP-RING domain, an S/T Stretch, and 2 SUMO Interacting Motif (SIM) domains (Lussier-Price et al., 2020; Pichler et al., 2017). SIM domains non-covalently bind to SUMO peptides. All E3 SUMO ligases utilize their SIM domains to stabilize the thioester bond between the donor SUMO and Ubc9, the sole E2 SUMO conjugating enzyme in a closed configuration for efficient target SUMOylation (Lascorz et al., 2022; Lussier-Price et al., 2020; Mascle et al., 2013). PIAS3 was identified in 2000 as an E3 SUMO ligase for nuclear transcription factors (E. S. Johnson & Gupta, 2001; Kahyo et al., 2001; Kotaja et al., 2002; Schmidt & Muller, 2002; Takahashi et al., 2001), however work by Wible and colleagues during the late 1990's suggests that PIAS3 may act as an E3 SUMO ligase for voltage-gated K⁺ (Kv) channels. Wible and colleagues referred to PIAS3 as the K⁺ Channel Associated Protein (KChAP), as it interacted with Kv1.2, and 4 α subunits in either yeast two hybrid assays or co-immunoprecipitation experiments with rat heart lysates (Kuryshv et al., 2000; Wible et al., 1998). In heterologous systems, KChAP co-expression increased Kv1.3, Kv2.1, and Kv4.3 currents, decreased Kv1.2 and Kv1.4 currents and had no effect on Kv1.5 currents (Kuryshv et al., 2000; Kuryshv et al., 2001; Wible et al., 1998). Wible and colleagues could not determine KChAP's mechanism of action, but did identify a ~100 amino acid fragment of the protein that mediated these effects (Kuryshv et al., 2000). It is now known that this fragment only contains the SIM1 domain of PIAS3. Thus far, no E3 SUMO ligases have been identified for ion channels.

Hypoxia results in enhanced global SUMOylation through upregulation of the SUMOylation machinery (Comerford et al., 2003; Shao et al., 2004). In cardiomyocytes, hypoxia induced SUMOylation of Nav1.5 and Kir2.1 results in proarrhythmic effects. Kv4.2 and Kv4.3 channels mediate I_{toF} in ventricular cardiomyocytes (Plant et al., 2020; Y. Xu et al., 2022). I_{toF} regulates the activity of the myocardium by controlling the repolarization phases of the cardiac action potential in rodents and in most higher order animals (Niwa & Nerbonne, 2010). Loss of I_{toF} has been shown to increase the action potential duration and increase intracellular calcium through L-type Ca^{2+} channels which peak during phase 2 of the cardiac action potential (Kaprielian et al., 1999; H. Xu et al., 1999). Hypoxia has been shown to regulate I_{toF} currents in neonatal rat cardiomyocytes through an undetermined mechanism (W. Guo, Kamiya, & Toyama, 1995).

Acute adrenergic activation downregulates I_{toF} in cardiomyocytes through PKA-mediated phosphorylation of the channel (Gallego et al., 2005). In both heterologous systems and hippocampal neurons, PKA-mediated phosphorylation of Kv4.2 at S552 results in decreased currents and enhanced internalization of the channel (R. S. Hammond et al., 2008; Schrader et al., 2002). PKA has been shown to block the SUMO modulation of Kv4-mediated I_A in invertebrate neurons, and gate target SUMOylation for other ion channels (Dustrude et al., 2016; Parker et al., 2019). Downstream of S552, is an established SUMO site K579 (M. A. Welch et al., 2019). When Kv4.2 is expressed as ternary complex, that is with its auxiliary subunits KCHIP2a and DPP10, enhanced SUMOylation at this site increases maximal conductance and surface expression by enhancing Rab11a-dependent slow recycling of the channel after endocytosis (L. A. Forster, Jansen L.R., Baro D.J; Welch et al., 2021).

In this study, we determine if PIAS3 acts as an E3 SUMO ligase for Kv4.2 channels in HEK cells and in cultured ventricular cardiomyocytes. We further determine if the phosphorylation status of Kv4.2 influences its ability to be SUMOylated in these systems.

4.2 Materials and Methods

Table 3 Primer Sequences

Primer	Sequence
Kv4.2g-S552A Forward	5'-CAATGTGTCGGGAAGCCATAGAGGCGCTGTGCAAGAACTC-3'
Kv4.2g-S552A Reverse	5'-CAATGTGTCGGGAAGCCATAGAGGCGCTGTGCAAGAACTC-3'
Kv4.2g-S552E Forward	5'-CGGGAAGCCATAGAGGCGAGGTGCAAGAACTCAG-3'
Kv4.2g-S552E Reverse	5'-CTGAGTTCTTGCACCTCGCCTCTATGGCTTCCCG-3'

4.2.1 Antibodies

Antibodies used: mouse HA (Invitrogen, 26183) 1:3000 WB, guinea pig Kv4.2 (Alomone Labs APC-023-GP) 5ug/mL IP, rabbit Kv4.2 (Alomone Labs APC-023) 1:400 PLA, mouse Kv4.2 (Neuromab 75-361) 1:2000 WB, rabbit Kv4.3 (Alomone Labs APC-014) 1:400 PLA, mouse Pan-KChIP (Neuromab 75-006) 1:1000 WB, mouse PIAS3 (Santa Cruz sc-48339) 1:100 WB, rabbit SUMO1 (Proteintech 10329-1-AP) 1:500 WB, mouse SUMO1 (Santa Cruz Sc-130275) 1:200 WB 1:100 PLA, SUMO2 (Proteintech, 11251-1-AP) 1:500 WB, rabbit SUMO2 (Cell Signaling, 18H8) 1:1000 WB, mouse SUMO2 (Developmental Studies Hybridoma Bank, 8A2) 1:70 PLA, mouse TAT (Abcam ab63957) 1:100 IHC, rabbit Ubc9 (Cell Signaling, 18H8) 1:500 WB.

4.2.2 Cell Culture

Human Embryonic Kidney 293 (HEK293) cells were purchased from American Type Culture Collection (cat. no CRL-1573, lot number 2869494). HEK parental lines were cultured in Eagle's Minimum Essential Medium (EMEM, Corning, cat. no 10009CV), supplemented with 10% Fetal Bovine Serum and 1% penicillin/streptomycin. HEK stable lines were cultured in the same media supplemented with 200 μ M gentamicin. All HEK293 cells were limited to passage 15.

Neonatal ventricular rat cardiomyocytes were purchased from Lonza (cat. no R-CM-561). 1 mL of cardiomyocytes was resuspended by drop-wise addition of 9 mL of Rat Cardiomyocyte Growth Medium (RCGM). Cells were seeded at equal volumes (\sim 1.4mL) onto 7x, 35mm dishes each containing 4x, 15mm laminin coated coverslips (Invitrogen cat. 23017015; 20 μ g/mL) and 0.6 ml of RCGM. 4 hours after seeding, 80% of the media was replaced with RCGM supplemented with 200 μ M bromodeoxyuridine (BrdU) to limit fibroblast proliferation. For long-term culture, 50% of the media was removed and replaced with fresh RCGM + 200 μ M BrdU every 3 days.

4.2.3 Plasmids

A plasmid encoding a mouse Kv4.2 channel with GFP fused to the C-terminus (Kv4.2g) was kindly provided by Dax Hoffman. Site-directed mutagenesis was used to mutate Kv4.2g-S552 into a phosphodeficient (Kv4.2g-S552A) and phosphomimetic (Kv4.2g-S552E) plasmid using the PCR primers listed in Table 3. Mutations were verified with Sanger Sequencing. Kv4.2g-K579R, a SUMO-deficient mutant was previously created (Welch et al., 2021). GFP was removed from Kv4.2g or its mutants using restriction digest with SalI and NotI to create a Kv4.2, GFP-null plasmid. HA-KChIP2a and HA-DPP10c were previously described (Welch et al.,

2021). FLAG-PIAS3 was purchased from Addgene (#152070). SUMO2 was a gift from Edward Yeh (Addgene, #17360), and Ubc9, a gift from Peter Howley (Addgene, #14438). An mCherry2-Cl plasmid was a gift from Michael Davidson (Addgene, #54563). A dominant negative version of Rab11a (Rab11aS25N) was obtained from Addgene (#46786). For siRNA experiments, siGenome Human UBE2I siRNA SMARTpool and non-targeting siRNA pool #2 were purchased from Dharmacon.

4.2.4 Calcium Phosphate Transfections

HEK cells were seeded at ~80% density 24 hours prior to transfection. 10 µg or 62 µg of DNA were prepared in 220 µL or 440 µL of 1x TE Buffer, followed by 30 µL or 60 µL of 2 M CaCl₂, and then dropwise addition of 250 µL or 500 µL of 2X HBS (275 mM NaCl, 10 mM KCl, 12 mM dextrose, 1.4 mM Na₂HPO₄, 40 mM HEPES, pH 7.05-7.10). The transfection media were added to the cells and removed after 4 hours. Kv4.2g, KChIP2a, and DPP10 were transfected at a ratio of 1:1 to form the ternary complex. PIAS3 and mCherry was used at a ratio of 1:1 in electrophysiology experiments and 5:1 for immunoprecipitation (IP) and western blot (WB) experiments. siRNAs were used at 25 nM. The average transfection efficiency (transfected cells/total cells) obtained with this protocol is ~60%. Cells were either passaged to coverslips 24 hours post-transfection or lysed after 72 hours.

4.2.5 TAT-PIAS3 peptide synthesis

The flag-PIAS3 plasmid was restriction digested and ligated into the pCDNA3 TAT-HA vector, a gift from Matija Peterlin (Addgene, #14654) to make a TAT-PIAS3 construct. This construct was used as a backbone to create a TAT-PIAS3-SIM1 mutant by mutating the SIM1 domain of PIAS3 to a stretch of Alanines. Mutations were verified by Sanger Sequencing. TAT protein synthesis has been previously described (Parker et al., 2019). Briefly, TAT-PIAS3 or

TAT-PIAS3-SIM1 mutant was transformed in BL21 E. coli cells (Agilent). A single colony was grown overnight in broth containing ampicillin (100 $\mu\text{g}/\text{mL}$). The overnight culture was then added to broth containing 500 μM isopropyl β -D-1-thiogalactopyranoside (IPTG) for 5 hours and cells were pelleted and washed with 1x PBS (137 mM NaCl, 2.7 mM KCl, 10 mM Na_2HPO_4 , 1.8 mM KH_2PO_4 , pH 7.4). Pellets were resuspended in Buffer Z (8 M urea, 100 mM NaCl, 20 mM HEPES, pH 8.0) and then sonicated on ice. The sonicate was cleared with centrifugation and then equilibrated with 10 mM imidazole. The cleared sonicate was incubated with Ni-NTA agarose resin, and the peptide was eluted with increasing concentration of imidazole (100 mM, 250 mM, 500 mM, 1 M). The fractions were passed through a PD-10 desalting column and eluted in 1x PBS. Peptide concentrations were determined using a Nanodrop 2000.

4.2.6 Electrophysiology

Whole cell patch clamp recordings were performed on HEK cells plated on Poly-L-Lysine (100 $\mu\text{g}/\text{mL}$) coated coverslips. Cells were continuously superfused with extracellular saline (141 mM NaCl, 4.7 mM KCl, 1.2 mM MgCl_2 , 1.8 mM CaCl_2 , 10 mM glucose, 10 mM HEPES, pH 7.4, osmolarity ~ 300 mOsm/L). In some cases, cells were superfused with 8-bromo cAMP (100 μM) during the recording for a maximum of 30 minutes. To measure the acute effects of PIAS3, transfected HEK cells were incubated with equal volumes of either PBS, TAT-PIAS3 (50 mM) or TAT-PIAS3-SIM1 mutant (50 mM) for 30 minutes at 37°C and 5% CO_2 prior to recording. Transfected cells were identified by GFP or mCherry expression and were patched with borosilicate glass pipettes (~ 2 -3 $\text{M}\Omega$) filled with intracellular saline (140 mM KCl, 1.2 mM MgCl_2 , 1 mM CaCl_2 , 10 mM EGTA, 2 mM MgATP, 10 mM HEPES, pH 7.2, osmolarity ~ 290 mOsm/L), and connected to a Multiclamp 700B Amplifier (Axon Industries).

Whole cell capacitance was measured upon break-in. Fast and slow capacitance and series resistance were compensated. I_A was elicited with a series of 1 s pre-pulses to -90 mV each followed by a 250 ms test-pulse from -50 mV to $+50$ mV in 10 mV increments. To isolate I_A , an offline subtraction was performed using a pre-pulse to -30 mV. I_A steady state inactivation was elicited using a 1.4 s voltage step from -110 mV to -10 mV in 10 mV increments, each followed by test pulse to $+20$ mV. I_h was elicited from HEK cells stably expressing an HCN2-GFP fusion protein using a series of 5 s hyperpolarizing voltage steps from -50 mV to -120 mV in 10 mV increments. Steady state peak current was measured by subtracting the initial fast leak current from the slowly activating I_h current for each voltage step. For I_A and I_h , the maximal conductance (G_{max}) and the voltage of half-activation ($V_{50 \text{ act}}$) were determined by plotting conductance against the voltage and fitting the data with a first-order Boltzmann equation. For I_A , the fast (t_f) and slow (t_s) time constants of inactivation were determined by fitting the decay current for the $+50$ mV test pulse with a two-term exponential equation. For I_A , the V_{50} of half-inactivation was determined by plotting the current against the voltage and fitting to a first-order Boltzmann equation. In all cases, bar graphs represent the mean \pm SEM. Unpaired t-test or one-way ANOVA with post hoc were used to determine significant difference among treatment groups.

4.2.7 Immunoprecipitation

72 hours post transfection, HEK cells were lysed in RIPA buffer (1% NP40, 50mM Tris-HCl pH7.4, 150mM NaCl, 0.1% SDS, 0.5% DOC, 2mM EDTA, 20mM NEM, 1:100 protease inhibitor) for 30 minutes at 4°C . Lysates were collected and debris was pelleted by centrifugation for 10 minutes at 14,000 rpm. The protein concentrations of the resulting supernatants were determined using the Pierce BCA Assay kit. Equal amounts of protein were incubated with an

anti-Kv4.2 or anti-IgG antibody overnight at 4°C. Kv4.2 was immunoprecipitated using the Pierce Classic Magnetic IP/Co-IP Kit according to manufacturer's instructions. IP elutions were carried out in Pierce low pH Elution Buffer at 100 µL/mg of protein.

4.2.8 Western Blot Assays

Kv4.2 IP products and siRNA lysates were fractionated using SDS-PAGE and then transferred onto a PVDF membrane using a wet electroblotting system. siRNA lysates were incubated with SYPRO RUBY protein blot stain prior to WB experiments and imaged with an Axion Biosystems 6000. Membranes were blocked in 5% non-fat milk in TBS (50 mM Tris-HCl pH7.4, 150 mM NaCl) for 3 hrs at room temperature, and then incubated with primary antibody in 1% non-fat milk in T-TBS (TBS + 0.1% Tween20) overnight at 4°C. The next day, membranes were washed and incubated with an Alkaline Phosphatase conjugated secondary antibody in 1% non-fat milk in T-TBS for 2 hrs at room temperature. Membranes were washed and incubated with AP substrate (Biorad) and the chemiluminescent signal imaged with Axion Biosystems 6000. To determine the fraction of SUMOylated protein, membranes were probed first with a SUMO antibody, then stripped using a mild stripping buffer (200 mM glycine, 0.1% SDS, and 1% Tween 20, pH 2.2) and re-probed with a primary antibody against the protein of interest. ImageJ was used for WB analysis. The optical density (OD) of the SUMO signal was divided by that of the OD for protein to determine the fraction of SUMOylated protein. To determine the knockdown of Ubc9 in siRNA lysates, the Ubc9 signal was divided by the total lysate (entire lane) OD. T-tests were used to determine significance and bars represent mean ± SEM.

4.2.9 Immunohistochemistry

HEK cells were incubated with equal volumes of PBS or TAT-PIAS3 (50 nM) for 30 minutes at 37°C and 5% CO₂. Cells were then washed 1x in 1x PBS and fixed in 4% PFA solution. Cells were permeabilized with 1x PBS and 0.05% Triton X-100 and then blocked with a 10% normal goat serum for 30 minutes at room temperature (RT). Cells were incubated overnight with a mouse anti-HIV TAT at 4°C. The next day, cells were incubated with Goat-anti-mouse DyLight 405 for 2 hours at RT, followed by serial washes in 1x PBS. Cells were coverslipped with Vectashield and imaged using a Keyence BZ-X series fluorescent microscope with a channel filter for DAPI.

4.2.10 Proximity Ligation Assay

A variety of setups were used in this experiment to maximize reagent usage. Cardiomyocyte incubations with treatment groups occurred in 24-well plates with 1 coverslip and 500 µl of RCGM per well. All washes, fixation, WGA and DAPI incubations, and permeabilizations occurred in 35mm dishes with 2 ml volumes at RT on a shaking platform. Incubations with primary antibodies and DUOLink products occurred in a humidity chamber where coverslips were placed onto slides marked with a hydrophobic pen. 75 µl/coverslip was used for primary incubations and 40 µl/coverslip were used for all DUOLink incubations.

First, cardiomyocytes were treated with 1 of 5 groups: PBS, TAT-PIAS3 (50 nM), TAT-PIAS3-SIM1 mutant (50 nM), 8-bromo cAMP (100 µM) or 8-bromo cAMP (100 µM) + TAT-PIAS3 (50 nM) for 30 minutes at 37°C and 5% CO₂. Next, coverslips were washed with 1x PBS for 2 minutes and then fixed with a 4% PFA solution for 10 minutes. Coverslips were then washed with 1x PBS for 2 minutes before incubation with WGA-CF®594 (Biotium Aldrich 3.3 µg/mL) for 10 minutes. Coverslips were washed with 1x PBS for 2 minutes and then

permeabilized with 1x PBS with 0.05% Triton X-100 3x at 5-minute intervals. Coverslips were blocked in 35mm dishes with 1 mL of Duolink blocking solution for 30 minutes at 37°C. After the block, coverslips were incubated with primary solutions overnight at 4°C. Primary solutions contained either rabbit Kv4.2 (1:400) or rabbit Kv4.3 (1:400) and mouse SUMO1 (1:100) and mouse SUMO2 (1:70) diluted in Duolink antibody diluent. The next day, coverslips were washed with 1x PBS 3x at 5-minute intervals, and then 2x in DUOLink Wash Buffer A. Coverslips were incubated with Duolink rabbit plus and mouse minus probes diluted 1:5 in Duolink antibody diluent for 1 hour at 37°C. Coverslips were washed 2x in Wash Buffer A and then incubated with the Duolink ligase reaction for 30 minutes at 37°C. Coverslips were washed 2x in Wash Buffer A, and then incubated with the Duolink amplification reaction for 2 hours at 37°C. Coverslips were washed 2x in Wash Buffer B for 10 minutes, 1x in 0.01x Wash Buffer B for 1 minute, and then incubated with DAPI (300 nM) for 5 minutes. Coverslips were washed with 1x PBS and mounted with 7 µl of non-hardening VectaShield.

4.2.11 Proximity Ligation Analysis

PLA experiments were imaged with a Keyence BZ-X series fluorescent microscope with multichannel filters for DAPI and TRITC. PLA experiments were repeated $n = \geq 3$ per treatment group. For analysis, PLA images were thresholded in ImageJ using the triangle method as previously described (L. A. Forster et al., 2020). Cardiomyocytes were outlined and the area and the raw integrated density of the puncta within a selection were recorded. Raw Integrated density was divided by area for each group. The data was compared using a one-way ANOVA with Tukey's post-hoc to determine significant difference.

4.3 Results

4.3.1 *PIAS3 increases Kv4.2 I_A at K579 in the TC by increasing Rab11a-dependent slow recycling.*

To test our hypothesis that PIAS3 is an E3 SUMO ligase for Kv4.2 channels, we first investigated if/how PIAS3 modulates I_A. We conducted whole cell patch clamp recordings in HEK cells transiently transfected with the Kv4.2g TC with or without a plasmid for PIAS3. We used a voltage protocol with a pre-pulse to -90 mV followed by test pulses from -50 mV to +50 mV to measure the voltage dependence of activation (Figure 4-1A). We used a voltage protocol with steps from -110 mV to -30 mV, each followed by test pulse to +20 mV to measure the voltage dependence of steady state inactivation (Figure 4-1B). PIAS3 overexpression significantly increased I_A g_{max} by 60% compared to the Kv4.2g TC (Figure 4-1C). This effect mimicked the results reported in our previous study where either SUMO and Ubc9 overexpression or acute application of SUMO peptides via the patch pipette increased I_A g_{max} by ~30-60% compared to the Kv4.2g TC (Figure 4-1C). To determine if this effect was due to PIAS3 acting within the same pathway as SUMO and Ubc9 or an independent pathway, we co-expressed these three plasmids with the Kv4.2g TC. There was no additive effect on I_A g_{max} following co-expression of these plasmids, suggesting that PIAS3 augments I_A through SUMOylation (Figure 4-1C). PIAS3 had no effect on the V₅₀ of activation or on the time constants of inactivation but induced a significant leftward shift in the V₅₀ of inactivation thereby slowing channel closing (Figure 4-1D, table 4). This effect was not evident in SUMO and Ubc9 studies nor in previous studies examining PIAS3 (Kuryshv et al., 2000; Kuryshv et al., 2001; M. A. Welch et al., 2019; Welch MA, 2021; Wible et al., 1998).

To determine if the PIAS3-mediated increase in I_A was due to SUMOylation of the α subunit, we repeated whole cell patch clamp recordings using a SUMO-deficient Kv4.2g-K579R TC. The mutant TC blocked the effects of PIAS3 on I_A (Figure 4-1E). PIAS3 co-expression had no significant effect on the V_{50} of activation or V_{50} of inactivation in Kv4.2g-K579R TC, nor on the time constants of inactivation (Figure 4-1F, table 5). These data indicated that the PIAS3-mediated increase in I_A was due to Kv4.2g-K579 SUMOylation. This is consistent with our previous study showing that SUMO and Ubc9 augment I_A by enhancing SUMOylation of Kv4.2g- K579 in the TC.

We previously showed that enhanced SUMOylation of Kv4.2 at K579 increases surface expression and I_A by augmenting Rab11a-dependent slow recycling of the channel after endocytosis (L. A. Forster, Jansen L.R., Baro D.J; Welch MA, 2021). Rab11a GTPases regulate slow recycling by moving cargo from the sorting endosomes to the recycling endosome compartment and back to the plasma membrane (Allgood & Neunuebel, 2018). We asked if the PIAS3-mediated increase in I_A required Rab11a-dependent slow recycling. HEK cells were transfected with the Kv4.2g TC with or without PIAS3 and with or without Rab11aS25N, a plasmid encoding a dominant negative version of Rab11a which blocks slow recycling. Co-expression of Rab11aS25N with the Kv4.2g TC had no significant effect on I_A g_{max} compared to the Kv4.2g TC alone (Figure 4-2). However, inhibiting Rab11a-dependent slow recycling significantly blocked the PIAS3-mediated increase in I_A g_{max} by ~65% (Figure 4-2). These data suggested that like SUMO and Ubc9, the PIAS3-mediated increase in I_A was due to K579 channel SUMOylation augmenting Rab11a-dependent slow recycling downstream of endocytosis. Together, these data show that PIAS3 recapitulates the effects of SUMO and Ubc9 on Kv4.2 I_A in the TC.

4.3.2 *PIAS3 requires its E3 SUMO ligase properties to modulate I_A .*

E3 SUMO ligases facilitate target SUMOylation, in part, by utilizing internal SIM domains to position the donor SUMO in an optimal position for discharge on to the target lysine (Lascorz et al., 2022). PIAS3 has two internal SIM domains. SIM1 is adjacent to the SP-RING domain while SIM2 immediately precedes the last residue in the C-terminus (Lussier-Price et al., 2020). Previous studies reported that a ~100 amino acid fragment of the PIAS3 protein beginning at the end of the SP-RING domain was responsible for the increase in I_A (Kuryshv et al., 2000). As the SIM1 domain is found within this fragment, we asked if the SIM1 domain is necessary for PIAS3-mediated increase in I_A . To test this, we cloned PIAS3 into an N-terminal TAT-HA-HIS vector to produce a TAT-PIAS3 construct (Figure 4-3A). TAT-conjugated proteins use the cell penetrating properties of the TAT protein transduction domain to enter the cell (Walrant, Cardon, Burlina, & Sagan, 2017). We used site-directed mutagenesis to mutate the SIM1 domain to a stretch of Alanines creating a TAT-PIAS-SIM1 mutant construct (Figure 4-3B). These constructs produced membrane permeable, recombinant proteins that were incubated with HEK Kv4.2g TC cells for 30 minutes at 37°C prior to recording. Acute treatment with TAT-PIAS3 (50 nM) proteins significantly increased I_A g_{max} by ~50% compared to PBS control (Figure 4-3C). This increase was lost when cells were acutely treated with the TAT-PIAS3-SIM1 mutant (50 nM) protein. This indicated that the SIM1 domain of PIAS3 is required for its effects on I_A (Figure 4-3C). We confirmed that TAT-PIAS3 proteins entered HEK cells using immunohistochemistry (Figure 4-3D).

E3 SUMO ligases simultaneously interact with the substrate, donor SUMO, and Ubc9, during the Ubc9-mediated transfer of SUMO to the target lysine (Lascorz et al., 2022). As such, we hypothesized that the PIAS3-mediated increase in I_A requires Ubc9. We transfected HEK

cells with the Kv4.2g TC with or without PIAS3 and with or without siRNAs for Ubc9 (25 nM) or a control siScramble (25 nM). Knocking down Ubc9 in the Kv4.2g TC had no effect on I_A g_{max} compared to the siScramble (Figure 4-3D). However, knockdown of Ubc9 significantly prevented the PIAS3-mediated increase in I_A g_{max} (Figure 4-3D). We confirmed the efficiency of siRNA experiments by probing for Ubc9 in lysates from cells transfected with siUbc9 or siScramble (Figure 4-3E). On average, we obtained a significant 62% knockdown. These data suggest that PIAS3 augments I_A by acting in concert with Ubc9 to enhance SUMOylation of the channel at K579.

4.3.3 PIAS3 increases Kv4.2-K579 SUMOylation but not HA-KChIP2a or HA-DPP10 SUMOylation in the TC.

We sought to confirm that PIAS3 increases Kv4.2 channel SUMOylation at K579 in the TC. HEK cells were transfected with the Kv4.2 TC with or without PIAS3. For these experiments, a Kv4.2 plasmid without GFP was used, as GFP may be SUMOylated. Kv4.2 was immunoprecipitated (IP) from cell lysates and IP products were used in WB experiments to determine the fraction of SUMOylated channel. PIAS3-induced a significant 3.6x fold increase in the number of SUMO1 decorations on Kv4.2 (Figure 4-4A, B). Experiments were repeated with the SUMO deficient Kv4.2g-K579R TC to determine if the increase in SUMO1 decoration occurred at K579. PIAS3 had no significant effect on SUMO1 decoration of Kv4.2g-K579R channels (Figure 4-4C, D). These data confirm our hypothesis that PIAS3 increases Kv4.2 SUMOylation at K579. We previously showed that SUMO and Ubc9 increased SUMO2 decoration of Kv4.2 channels in the TC, while SUMO1 decoration was not examined (Welch MA, 2021). In these experiments, PIAS3 had no significant effect on baseline SUMO2 decoration of Kv4.2 or Kv4.2-K579R channels (data not shown). As SIM domains have been

shown to exert selective preference for SUMO isoforms, our data suggests that the SIM1 of PIAS3 more favorably interacts with a SUMO1 charged Ubc9 to augment Kv4.2 SUMOylation (Gonzalez-Prieto et al., 2021; Namanja et al., 2012).

E3 SUMO ligases are often recruited to protein complexes inducing en masse SUMOylation in a process that is referred to as group SUMOylation (Celen & Sahin, 2020; Sahin, de The, & Lallemand-Breitenbach, 2022; Vertegaal, 2022). We asked if HA-KChIP2a and HA-DPP10 are targets for PIAS3 in the TC. We used Kv4.2 IPs to probe for the SUMOylation status of these proteins in co-IP experiments. The blots show that HA-KChIP2a is decorated by SUMO1 and SUMO2 in the lysate and supernatant (unbound protein of IP) fractions of transfected HEK cells (Figure 4-5A, B). HA-KChIP2a is not decorated by SUMO1 or SUMO2 in the co-IP fractions of HEK cells transfected with either the Kv4.2g TC or Kv4.2g TC and PIAS3 (Figure 4-5A, B). These data suggest that HA-KChIP2a in the TC is not a target of PIAS3 as SUMOylation may prevent its association with protein complexes. We probed the SUMOylation status of HA-DPP10 using co-IP experiments. HA-DPP10 proteins were decorated by SUMO1 in the TC (Figure 4-5C). PIAS3 had no significant effect on HA-DPP10 SUMO1 decoration compared to baseline (Figure 4-5D). HA-DPP10 proteins were also decorated by SUMO2 in the TC (Figure 4-5E). HA-DPP10 SUMO2 decoration was not significantly altered by PIAS3 overexpression (Figure 4-5F). These data confirm that Kv4.2-K579 is the only target of PIAS3-mediated SUMOylation in the TC.

4.3.4 PIAS3 augments HCN2-mediated I_h .

We asked if PIAS3 can modulate the currents of other voltage-gated ion channels. We transiently transfected a HEK HCN2 stable line with mCherry or PIAS3 and mCherry. PIAS3 expression increased I_h by ~60% compared to mCherry transfected cells (Figure 4-6A). This is

consistent with the 60% increase in I_A in Kv4.2g TC cells. To determine if the PIAS3-mediated increase in I_h occurred through SUMOylation, SUMO2/3 peptides were added in the patch pipette of PIAS3 transfected cells. Acute treatment with SUMO did not produce an additive effect in these cells, suggesting that PIAS3 augments I_h by acting as a part of the SUMOylation machinery (Figure 4-6B). To determine if PIAS3 targets K669, experiments were repeated in a SUMO deficient HEK-HCN2-K669R stable line. I_h was not significantly different in mCherry or PIAS3 and mCherry transfected cells (Figure 4-6C, D). These data suggest that PIAS3 increases I_h by enhancing SUMOylation at K669. Therefore, PIAS3 may be an E3 SUMO ligase for HCN2 channels.

4.3.5 PKA-mediated phosphorylation at S552 blocks PIAS3-mediated SUMOylation of Kv4.2g in the TC.

PKA-mediated phosphorylation of Kv4.2 at S552, a site just upstream of K579, induces internalization of the channel (R. S. Hammond et al., 2008; Schrader et al., 2002). As phosphorylation can control the ability of a target lysine to be SUMOylated (Dustrude et al., 2016; Zhao, Xia, Cheng, Zhu, & Li, 2020), we asked if PKA-mediated phosphorylation at S552 blocks PIAS3-mediated SUMOylation of K579 in the TC. We used site-direct mutagenesis to create a phosphodeficient (Kv4.2g-S552A) and phosphomimetic (Kv4.2g-S552E) Kv4.2g plasmid (Figure 4-7A). We first examined the effects of PKA activation on I_A in the TC using bath application of 8-bromo cAMP, a membrane permeable cAMP analog. PKA activation had no effect on I_A compared to the TC alone. However, PKA activation significantly blocked ~60% of the PIAS3-mediated increase in I_A (Figure 4-7B). To test if this was due to PKA-induced phosphorylation at S552 we repeated whole-cell patch clamp experiments with the Kv4.2g-S552 mutants. Neither mutation had a significant effect on I_A compared to the wildtype Kv4.2g (Figure

4-7C, D). PIAS3 significantly increased I_A by ~60% in Kv4.2g-S552A TC cells superfused with 8-bromo cAMP compared to cells expressing the Kv4.2g-S552A TC alone (Figure 4-7C). I_A was not significantly different in cells co-expressing the Kv4.2g-S552E TC and PIAS3 compared to the Kv4.2g-S552E TC alone. No further effect was evident in these cells following superfusion with 8-bromo cAMP (Figure 4-7D). These data suggested that the S552A TC blocked the effects of 8-bromo cAMP, while the S522E TC mimicked and occluded the effects of 8-bromo cAMP. This indicates that PKA-induced phosphorylation at S552 blocks the PIAS3-mediated increase in channel SUMOylation. We confirmed this using IP and WB experiments. HEK cells were transfected with the S552E TC with and without PIAS3. Note GFP was removed from this plasmid as well. Kv4.2 IP products were used in WB experiments to determine the fraction of SUMOylation of Kv4.2. The S552E TC prevented PIAS3 from augmenting SUMO1 decoration of Kv4.2 (Figure 4-8A, B). SUMO2 decoration was unaltered as well (Figure 4-8 C, B). These data suggested that PKA-mediated phosphorylation at S552 blocks PIAS3-mediated K579 SUMOylation thereby reducing Rab11a-dependent slow recycling after endocytosis.

4.3.6 PIAS3 augments Kv4 SUMOylation in cardiomyocytes.

We extended our study to the rodent heart, where Kv4.2 and Kv4.3 channels form heterotetrametric I_{to} channels (Niwa & Nerbonne, 2010). We first asked if Kv4.2 and Kv4.3 channels were SUMOylated. IP and WB experiments demonstrated that Kv4.2 and Kv4.3 channels were decorated by SUMO1 and SUMO2 in mouse heart lysates (Figure 4-9A,B). Previous studies showed that PIAS3 co-IPs with Kv4 channels in rat heart lysate (Kuryshv et al., 2000). We replicated these experiments in mouse heart lysate and found that PIAS3 co-IP'd with Kv4.2 channels suggesting a preserved interaction regardless of species (Figure 4-9C). We then asked if PIAS3 can augment Kv4 channel SUMOylation. We used Proximity Ligation

Assay (PLA) to measure Kv4 SUMOylation in cultured neonatal rat ventricular cardiomyocytes (Lonza). Cardiomyocytes were treated with either PBS, TAT-PIAS3 (50nM) or the TAT-PIAS3-SIM1 (50nM) mutant for 30 minutes at 37°C and 5% CO₂ prior to experiments. In PLA experiments, a fluorescent punctum is produced when two antibodies bind to their respective targets within a 40 nm distance of each other. We used a rabbit Kv4.3 antibody in conjugation with antibodies against mouse SUMO1 and mouse SUMO2 to measure Kv4.3 SUMOylation. For PLA analysis, cardiomyocytes were outlined to obtain cell area and thresholded to remove background puncta. The raw integrated density of the puncta above background within a cell was divided by the cell area to obtain the Kv4 SUMOylation index (Figure 4-10A). The data indicated that TAT-PIAS3 treatment increased Kv4.3 SUMOylation by 50% compared to PBS control (Figure 4-10B). The TAT-PIAS3-SIM1 mutant had no significant effect on the Kv4.3 SUMOylation index compared to PBS control (Figure 4-10B). Next, we measured the Kv4.2 SUMOylation index using a rabbit Kv4.2 antibody and doubled concentrations of TAT-PIAS3 and the TAT-PIAS3-SIM1 mutant. TAT-PIAS3 significantly increased Kv4.2 SUMOylation by ~70% compared to PBS (Figure 4-10C). TAT-PIAS3-SIM1 mutant and PBS were not significantly different from each other (Figure 4-10C). These data suggest that PIAS3 increases Kv4 SUMOylation by acting as an E3 SUMO ligase for Kv4 channels in ventricular cardiomyocytes.

We then asked if the TAT-PIAS3-mediated increase in Kv4 SUMOylation could be blocked by PKA activation using 8-bromo cAMP (100 μM). Kv4.3 SUMOylation was not significantly different in cardiomyocytes treated with either PBS, 8-bromo cAMP, or 8-bromo cAMP and TAT-PIAS3, indicating that 8-bromo cAMP had no effect on baseline channel SUMOylation but could block the effects of TAT-PIAS3 on channel SUMOylation (Figure 4-

11A). Repeating these experiments with a Kv4.2 antibody produced a similar result (Figure 4-11B). These data indicate that the effects of PIAS3 on Kv4 SUMOylation can be blocked by PKA activation, most likely through phosphorylation of Kv4 channels in cardiomyocytes.

4.4 Discussion

In this work, we establish PIAS3 as a bona fide E3 SUMO ligase for ion channels, expand its repertoire of known targets and demonstrate a selective mechanism in PIAS3 target selection: substrate phosphorylation. We demonstrated that PIAS3 overexpression recapitulated the Rab11a-dependent effects of SUMO and Ubc9 on I_A and I_h in HEK cells. PIAS3 induced these effects regardless of overexpression or acute application as a TAT-PIAS3 protein. Further studies with Kv4.2, revealed that PIAS3 augmented channel SUMOylation at the established SUMO site K579. Both Ubc9 and the internal SIM1 of PIAS3 were necessary for its effects on I_A , strongly suggesting its role as an E3 SUMO ligase for Kv4. Further, the PIAS3-mediated increase in channel SUMOylation and I_A were blocked by PKA-mediated phosphorylation at S552 in HEK cells. The established effects in HEK cells were evident in ventricular rat cardiomyocytes, where TAT-PIAS3 increased Kv4.2 and Kv4.3 channel SUMOylation by 50%-70%, while the TAT-PIAS3-SIM1 mutant had no effect. The TAT-PIAS3 mediated increase in channel SUMOylation could be blocked by PKA activation with 8-bromo cAMP.

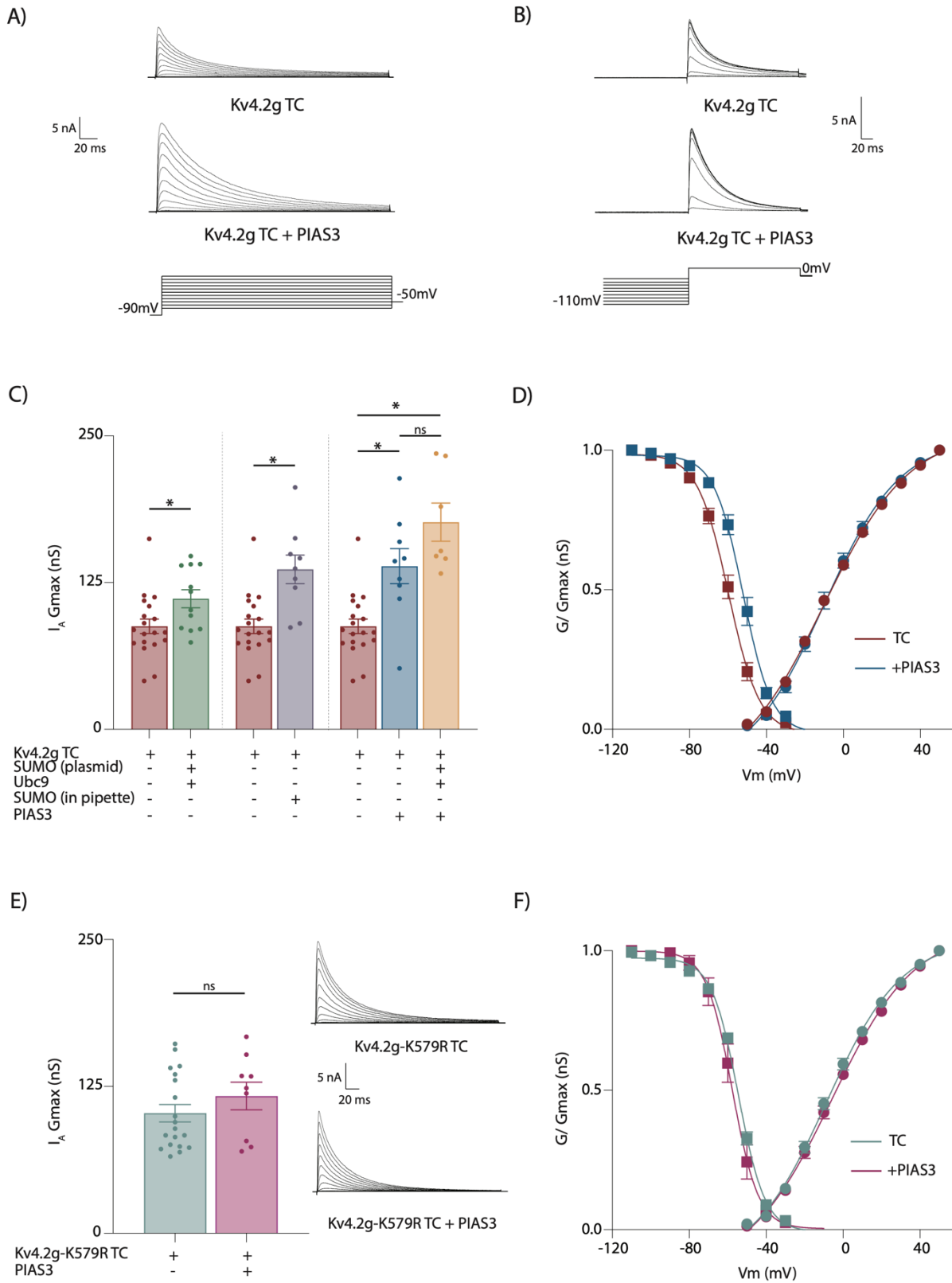


Figure 4-1 : PIAS3 increases I_A G_{max} at K579.

A) Representative current traces elicited using the protocol below to determine the voltage dependence of activation. B) Representative current traces obtained using the protocol below to determine the voltage dependence of steady state inactivation. C) Bar graphs show mean I_A G_{max} ± SEM. HEK cells were transiently transfected with the Kv4.2g TC. Enhanced SUMOylation was facilitated by either overexpressing SUMO2, Ubc9, and/or PIAS3 or including SUMO2/3 peptides in the recording pipette. SUMO2 and Ubc9 significantly increased I_A G_{max} by 30-50% in overexpression (111.20 ± 7.63 nS vs 87.72 ± 6.16 nS, *t*-test, $p=0.024$) and acute (136.30 ± 12.20 nS vs 87.72 ± 6.16 nS, *t*-test, $p=0.005$) studies (Welch et al., 2021). PIAS3 overexpression (139.0 ± 14.95 nS) significantly increased I_A G_{max} by 60% compared to the TC (87.72 ± 6.16 nS), while no further effect was observed when PIAS3, SUMO2, and Ubc9 were co-expressed (176.30 ± 16.27 nS). One-way ANOVA with Tukey's post hoc $F(2,32)=17.99$, $p=0.0001$. D) Activation (circle) and steady state-inactivation (square) curves for Kv4.2g TC +/- PIAS3. PIAS3 induced a significant 8mV shift in the V₅₀ of inactivation (-52.41 ± 1.32 mV vs. -59.92 ± 1.29 mV; *t*-test, $p=0.0015$), but had no effect on the V₅₀ of activation (-6.60 ± 2.170 mV vs. -5.27 ± 1.13 ; *t*-test, $p=0.554$). E) Bar graphs (right) show the mean I_A G_{max} ± SEM for Kv4.2g-K579R TC +/- PIAS3 HEK cells and representative current traces (left). Mutating K579 blocked the effect of PIAS3 on I_A G_{max} (116.8 ± 11.77 nS vs 102.2 ± 7.39 nS, *t*-test, $p=0.287$). F) Activation (circle) and steady state-inactivation (square) curves for Kv4.2g-K579R TC +/- PIAS3. PIAS3 had no effect on the V₅₀ of inactivation (-56.33 ± 1.64 mV vs. -54.38 ± 0.63 mV; *t*-test, $p=0.184$) or V₅₀ of activation (-3.085 ± 1.684 mV vs. -2.677 ± 1.005 ; *t*-test, $p=0.827$). Each dot represents 1 cell. Asterisks indicate significant difference.

A)

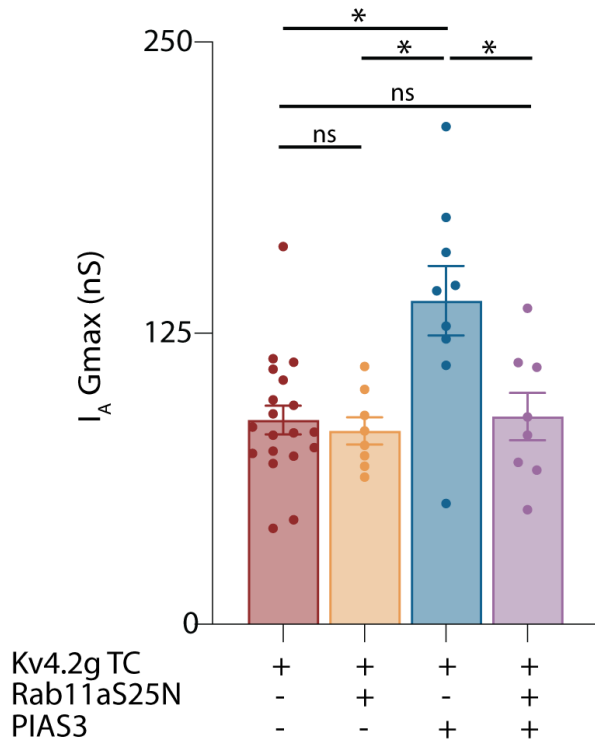
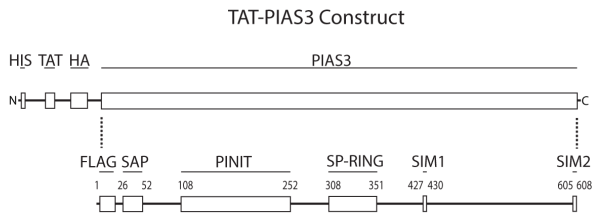


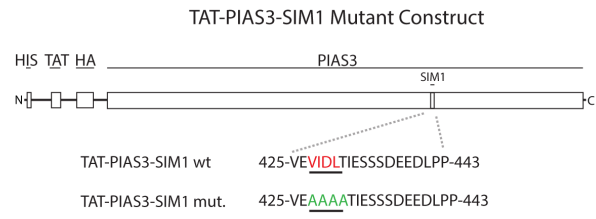
Figure 4-2 PIAS3 acts via slow recycling.

A) Bar graphs show the mean I_A Gmax \pm SEM for HEK cells transiently expressing the Kv4.2g TC +/- PIAS3 and +/- Rab11aS25N, a dominant negative form of Rab11a. Rab11aS25N (83.14 ± 5.82 nS) had no effect on the TC alone (87.17 ± 6.12 nS), but was able to block 90% of the PIAS3-mediated (139.0 ± 14.95 nS) increase in I_A gmax when co-expressed with PIAS3 (89.24 ± 10.11 nS). One-way ANOVA with Tukey's post hoc $F(3,40)=7.09$, $p=0.0006$. Each data point represents 1 cell. Asterisks indicate significant difference.

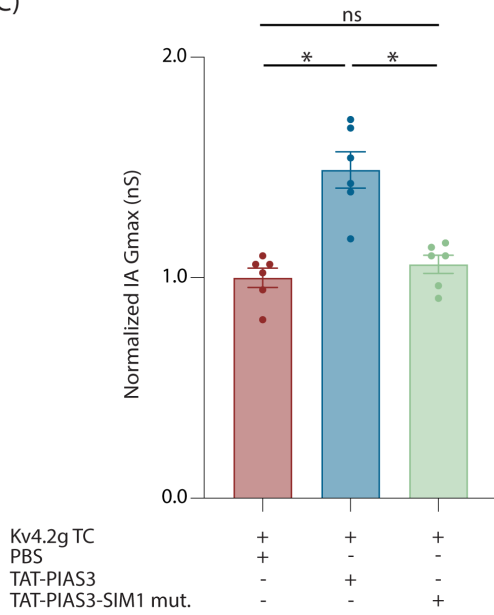
A)



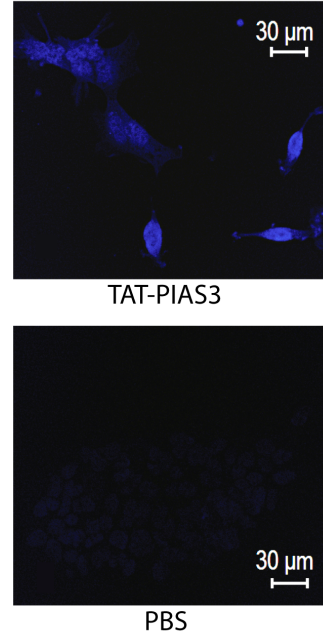
B)



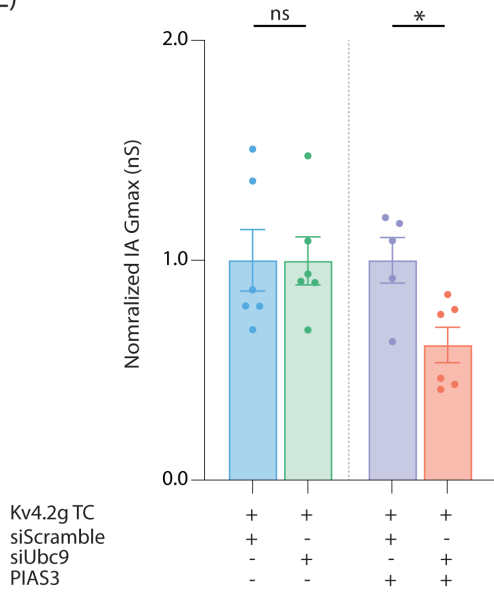
C)



D)



E)



F)

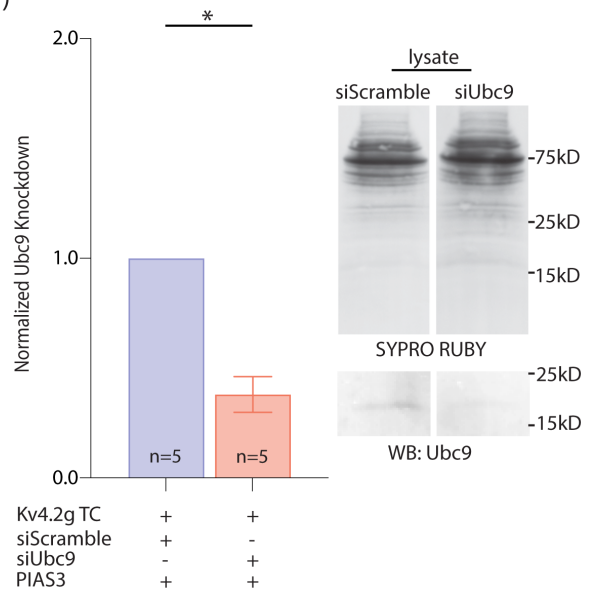


Figure 4-3 PIAS3 acts via SIM1 and requires Ubc9.

A) TAT-PIAS3 construct. A flag-PIAS3 plasmid was subcloned into a TAT-HA-HIS vector to produce an active PIAS3 protein when induced in BL21 cells. The conserved domains of PIAS3 include SAP, PINIT, SP-RING, SIM1, and SIM2. B) TAT-PIAS3-SIM1 mutant construct. The wildtype SIM1 (red) domain of TAT-PIAS3 was mutated (green) to prevent SUMO-SIM interactions. C) Bar graphs show mean I_A Gmax \pm SEM normalized to control. HEK Kv4.2g TC cells were incubated with PBS (control), TAT-PIAS3 (50mM), or TAT-PIAS3 SIM1 mutant (50mM) for 30 minutes at 37°C and 5% CO₂ prior to whole cell recording. TAT-PIAS3 (1.49 ± 0.08 nS) increased the normalized I_A Gmax by ~50%, while TAT-PIAS3 SIM1 mutant (1.06 ± 0.04 nS) had no effect compared to PBS alone (1.00 ± 0.04 nS). One way ANOVA with Tukey's post hoc $F(2, 15)=20.57, p<0.0001$. Each dot represents 1 cell. D) TAT-PIAS3 in HEK cells. HEK cells were incubated with TAT-PIAS3 (upper) or PBS (lower) for 30 minutes at 37°C and 5% CO₂. Cells were fixed and stained with an anti-HIV TAT antibody. Scale bars are 30 micron. E) Bar graphs show mean I_A Gmax \pm SEM normalized to control. HEK cells were transfected with the Kv4.2g TC +/- PIAS3 and +/- siUbc9 (25nM) or siScramble (25nM). The siUbc9 had no effect compared to siScramble (1.00 ± 0.11 nS vs 1.00 ± 0.14 nS; *t*test, $p=0.9902$), but blocked the effects of PIAS3 on the TC (0.61 ± 0.08 nS vs 1.00 ± 0.10 nS; *t*test, $p=0.0156$). Each dot represents 1 cell. F) Bar graph (left) and WB (right) of siUbc9 knockdown. Lysates were probed first with SYPRO RUBY and then probed with anti-Ubc9 (~17kD). The normalized mean knockdown (Ubc9 OD \div lysate OD) was 62% percent (0.38 ± 0.08 vs purple, 1.00 ± 0.00 , Mann-Whitney U, $p=0.0079$). Asterisks indicate significant difference.

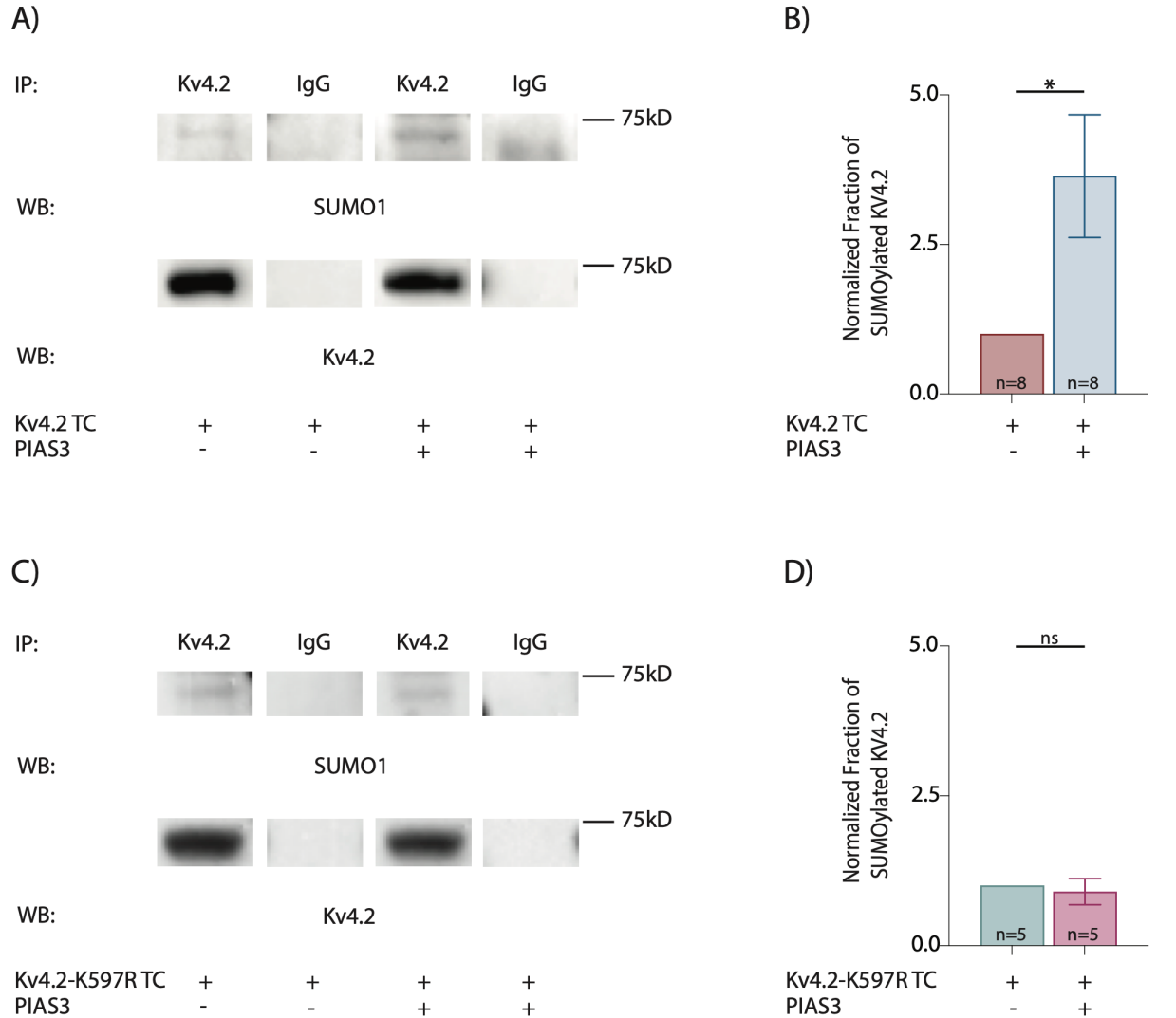


Figure 4-4 PIAS3 increases Kv4.2 SUMOylation.

A) WB Kv4.2 SUMOylation. Kv4.2 and IgG IP products from HEK Kv4.2 TC^{+/−} PIAS3 lysates were fractionated with SDS-PAGE and transferred to PVDF membrane. Blots were probed first with SUMO1 and then stripped and re-probed for Kv4.2 (~69kD). The SUMO1 OD was divided by the Kv4.2 OD to obtain the fraction of SUMOylated channel and normalized to control. B) Bar graphs show the mean ± SEM normalized fraction of SUMOylated Kv4.2. PIAS3

increased SUMO1 conjugation by 3.6x fold compared to the TC alone (3.6 ± 1.00 vs 1.00 ± 0.00 ; Mann-Whitney U, $p=0.0057$; $n=8$). C) WB of Kv4.2-K579R SUMOylation. D) Bar graphs show the mean \pm SEM normalized fraction of SUMO1 conjugated Kv4.2-K579R. PIAS3 did not alter Kv4 SUMOylation in the SUMO-deficient TC (0.90 ± 0.22 vs 1.0 ± 0.00 , Mann-Whitney U, $p=0.6825$; $n=5$). Asterisks indicate significant difference.

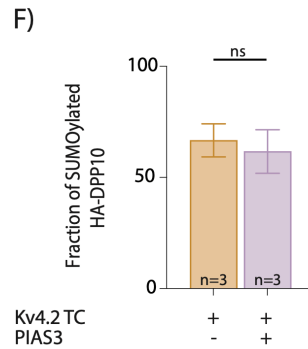
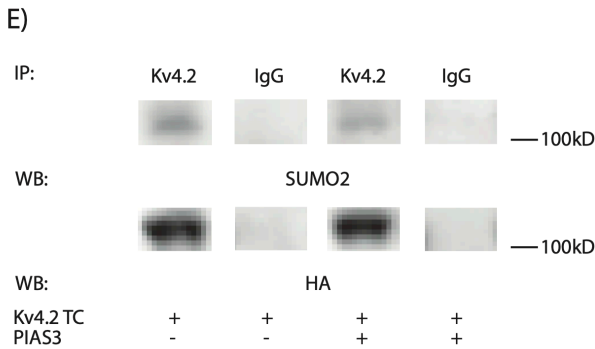
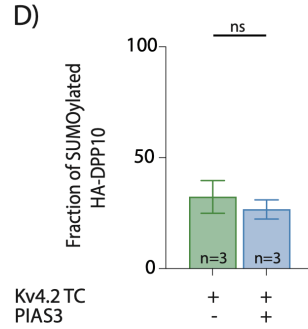
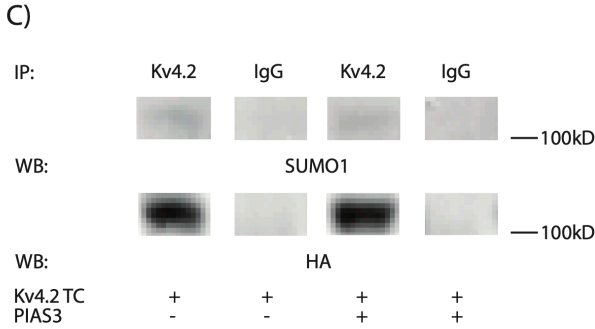
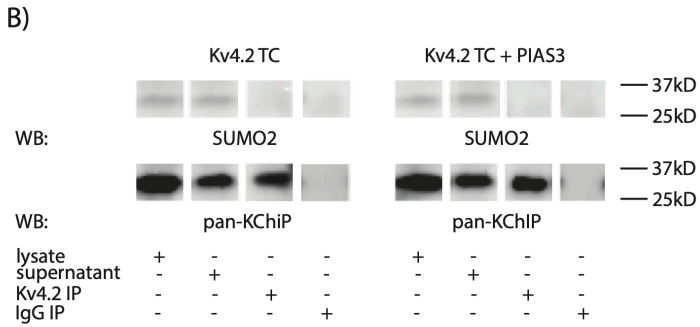
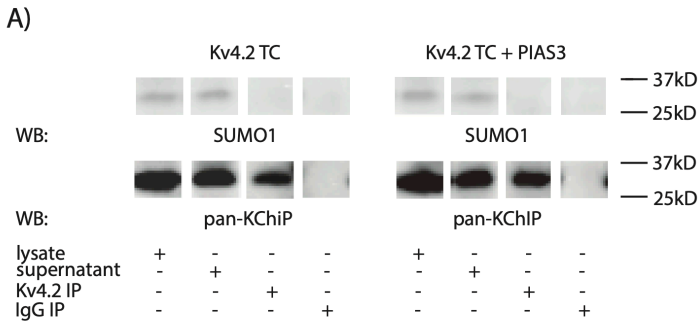


Figure 4-5 PIAS3 does not alter HA-KChIP2a and HA-DPP10 SUMOylation in the ternary complex.

A) WB of KChIP2a SUMO1 Conjugation. Lysates, Kv4.2 and IgG supernatants (unbound protein of IP), and IP products were fractionated with SDS-PAGE and transferred. Blots show that KChIP2a proteins interacting with Kv4.2 are not decorated with SUMO1 peptides, while KChIP2a proteins not interacting with the channel, i.e. those in the lysates and supernatants are decorated with SUMO1 peptides (n=4). B) WB of KChIP2a SUMO2 Conjugation. Blots show that KChIP2a is not decorated by SUMO2 in the co-IP fraction but is in lysates and supernatants (n=4). C) WB of HA-DPP10 SUMO1 decoration. Kv4.2 and IgG IPs were used in co-IP experiments. IP products were probed first for SUMO and then stripped and re-probed for anti-HA. Bands at ~100kD represent SUMOylated HA-DPP10. D) Bar graphs show the mean \pm SEM fraction of SUMO1 conjugated HA-DPP10 (SUMO1 OD \div HA OD). PIAS3 did not alter SUMO1 conjugation (32.33 ± 7.356 vs 26.77 ± 4.33 , ttest, $p=0.543$, n=3) to HA-DPP10. E) WB of HA-DPP10 SUMO2 decoration. PIAS3 did not alter SUMO2 conjugation to HA-DPP10 (66.67 ± 7.45 vs 61.61 ± 9.821 , ttest, $p=0.706$, n=3).

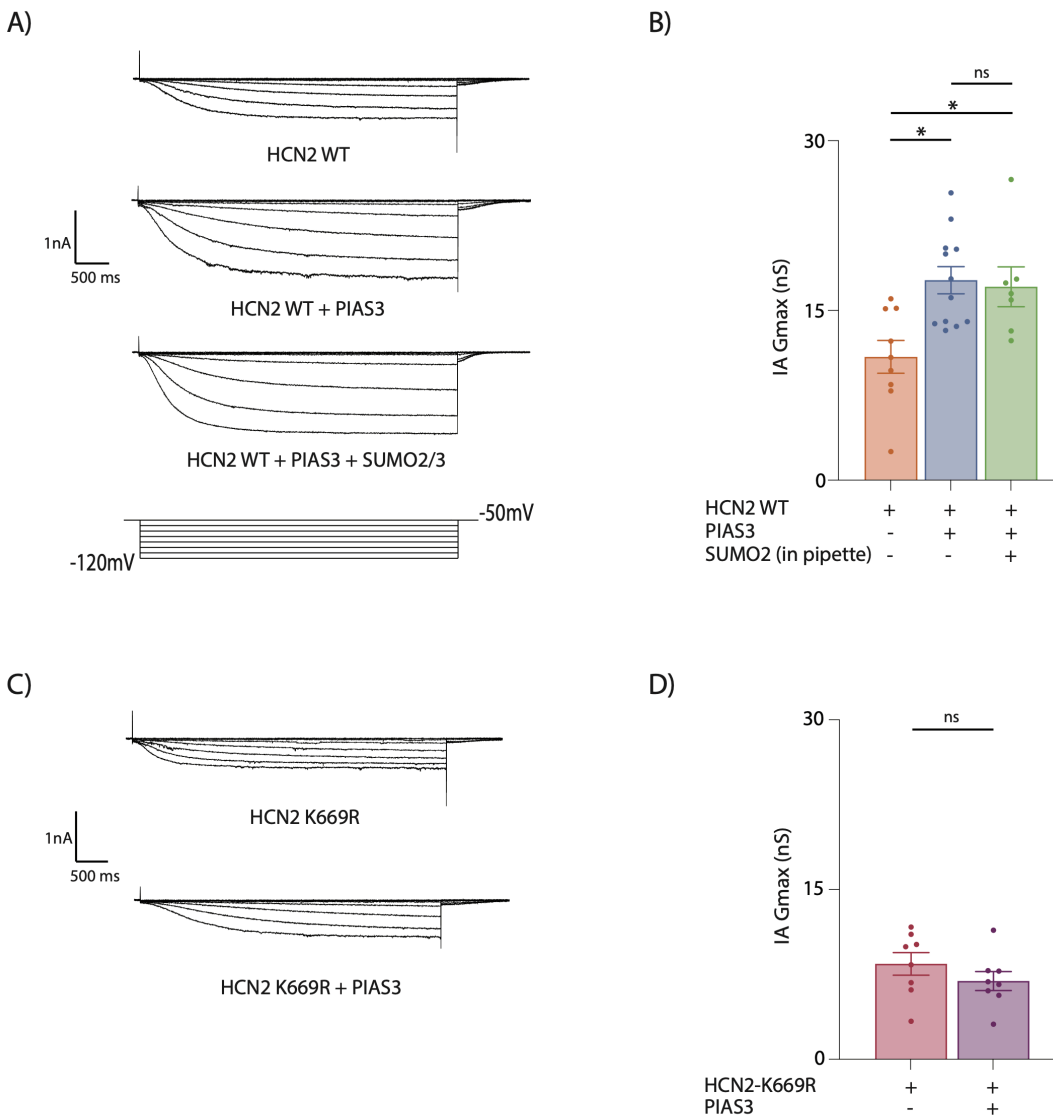


Figure 4-6 PIAS3 increases I_h at K669 of HCN2

A) Representative current traces elicited using the voltage protocol below in a wildtype HEK-HCN2 stable line. Enhanced SUMOylation was facilitated by transient transfection of PIAS3 and/or inclusion of SUMO2/3 peptides in the patch pipette. B) Bar graphs show mean I_h Gmax \pm SEM. PIAS3 (17.66 ± 1.20 nS) increased I_h by 62% compared to wildtype alone (10.89 ± 1.45 nS), and no further effect was observed when SUMO2/3 peptides were added in the patch pipette (17.09 ± 1.76 nS). One-way ANOVA with Tukey's post hoc $F(2,25)=7.01$, $p=0.0038$. C)

Representative current traces elicited using the same voltage protocol as in A) but in a SUMO-deficient stable line, HEK-HCN2-K669R. D) Bar graphs show mean I_h Gmax \pm SEM. The SUMO-deficient line blocked the PIAS3-mediated increase in I_h gmax (6.92 ± 0.83 nS vs 8.44 ± 1.00 nS, t-test, $p=0.263$). Each dot represents 1 cell. Asterisks indicate significant difference.

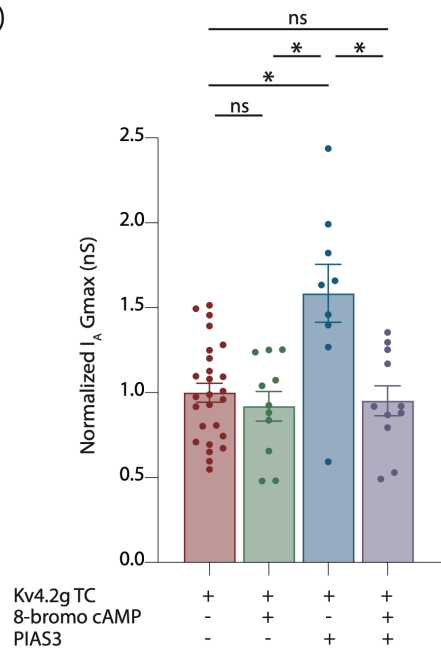
A)

m. Kv4.2 WT MAAGVAAWLPFARAAAIGWMPVASGPMPPRQERKRTQDALIVLNVSGTRFQWQDTLERYPDTLLGSSERDF 75
 YHPETQQYFFDRDPDFRHILNFYRTGKLYPRHECISAYDEELAFFGLIPEIIGDCCYEYKDRRRENAERLQDDADT 154
 DNTGESALPTMTARQRVWRAFENPHTSTMALVFYVYTGFFIAVSVIANVVETVPCGSSPGHIKELPCGERYAVAFCL 232
 DTACVMIFTVEYLLRLAAAPSRYRFVRSVMSIIDVVAILPYYIGLVMTDNEDVSGAFVTLRVFRVFRIFKFSRHSQGLRI 312
 LGYTLKSCASELGFLLFSLTMAIIIFATVMFYAEKGSASKFTSIPAAFYWTIVMTTLGYGDMVMPKTIAGKIFGSICLS 393
 GVLVIALPVPVIVSNFSRIYHQQRADKRRRAQKARLARIRAAKSGSANAYMQSKRNGLLSNQLQSSSEDEPAFISKS 470
 GSSFETQHHLLHCLEKTTNHEFVDEQVFEESCMEVATVNRPSHSPSLSSQOGVTSTCCSRRHKKTRIPNANVS 546
 GSHRGSVQELSTIQRCVERTPLNSRSSLNAKMEECVKLNCEQPVTTAISIPTPPVTTPEGDDRPEPEYSGGNIV 625
 RVSAL 630

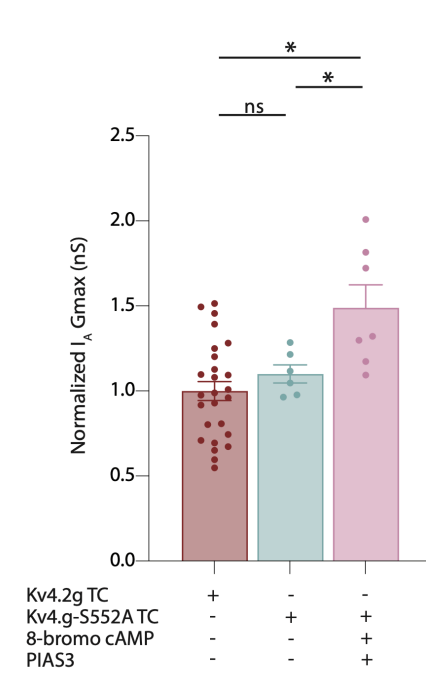
Kv4.2 S522A mutant 448 SHRGAVQEL 556 575 SLNAKMEEC 583

Kv4.2 S522E mutant 448 SHRGEVQEL 556 575 SLNAKMEEC 583

B)



C)



D)

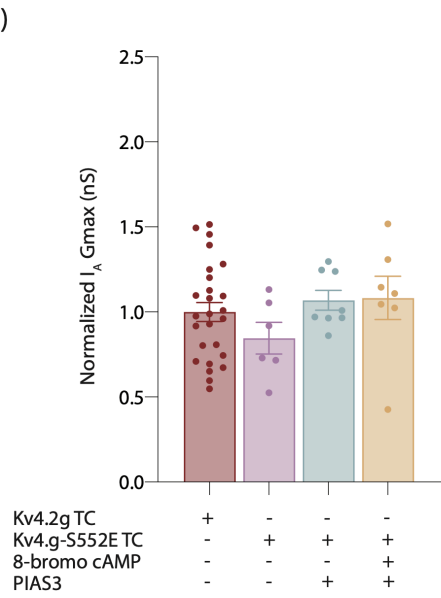


Figure 4-7 PKA-mediated phosphorylation of Kv4.2 at S552 blocks its PIAS3-mediated SUMOylation at K579.

A) Amino acid sequence of mouse Kv4.2. Site-directed mutagenesis was used to create a phosphodeficient (S552A) and a phosphomimetic (S552E) S552. The mutations are highlighted in blue, while the retained SUMO site, K579, is highlighted in pink. B) Bar graphs show normalized mean I_A gmax \pm SEM. HEK Kv4.g TC +/- PIAS3 cells were or were not superfused with 100 μ M 8-bromo cAMP, a cell permeable activator of PKA, during recordings. 8-bromo cAMP (0.95 ± 0.088 nS) blocked the PIAS3-mediated increase in I_A gmax (1.59 ± 0.17 nS). 8-bromo cAMP alone (0.91 ± 0.086 nS) had no effect on the TC (1.00 ± 0.056 nS). One-way ANOVA with Tukey's post hoc $F(3,44)=8.478$, $p=0.0001$. C) Bar graphs show mean normalized I_A gmax \pm SEM. The effects of 8-bromo cAMP were blocked by the S552A TC, as PIAS3 increased I_A gmax by $\sim 50\%$ (1.49 ± 0.134 nS) in these cells. The S552A mutation alone (1.10 ± 0.053 nS) had no effect compared to the TC (1.00 ± 0.056 nS). One-way ANOVA with Tukey's post hoc $F(2,35)=14.98$, $p \leq 0.0001$. S552E TC had no effect compared to the wildtype TC (1.00 ± 0.056 nS). The S552E TC (0.85 ± 0.09 nS) was able to mimic (1.07 ± 0.058 nS) and occlude the effects of 8-bromo cAMP (1.08 ± 0.13 nS). One-way ANOVA with Tukey's post hoc $F(3,42)=1.694$, $p=0.1829$. All data were normalized to TC control. Each data point represents 1 cell. Asterisks indicate significant difference.

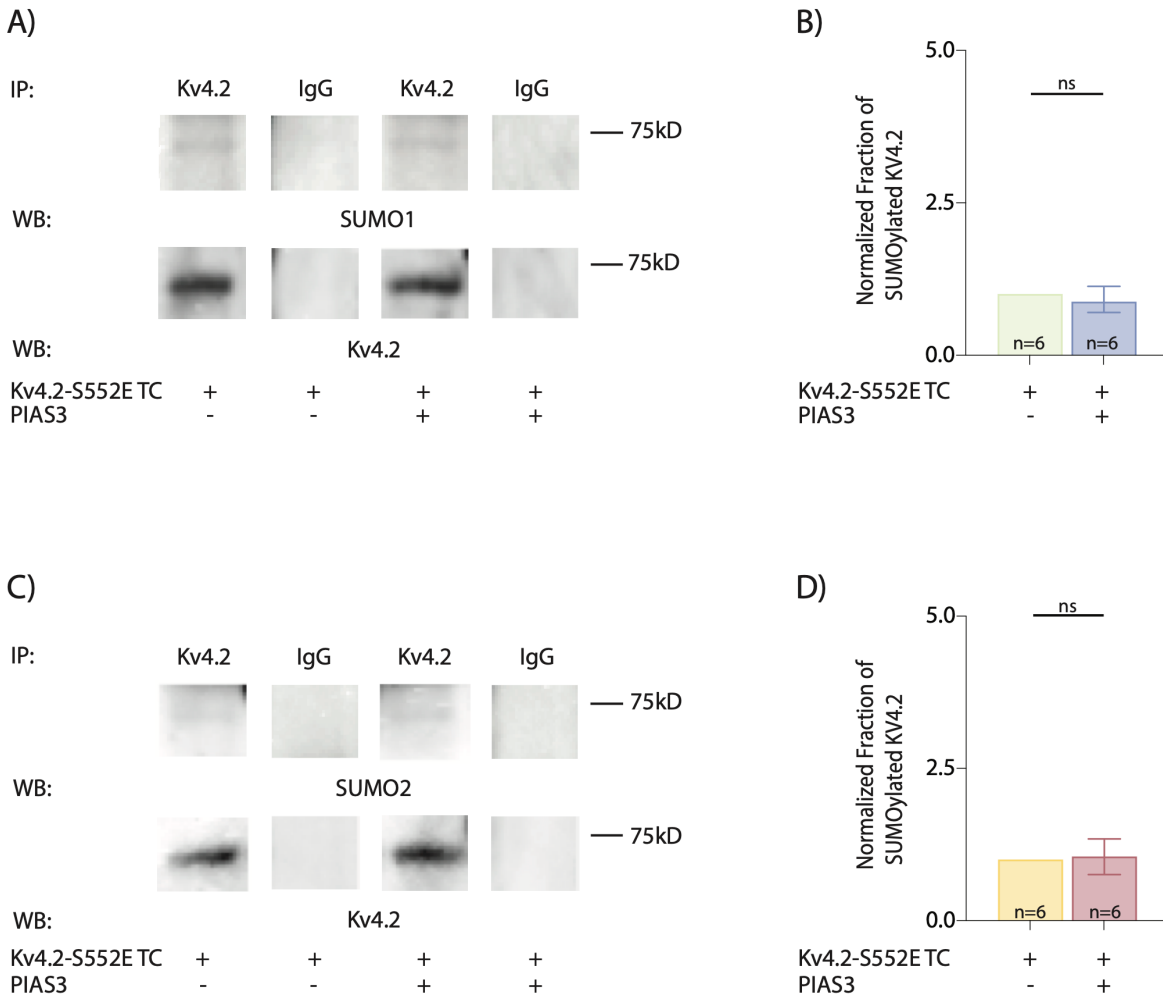


Figure 4-8 PKA-mediated phosphorylation of Kv4.2 at S552 blocks the PIAS3-mediated increase in Kv4.2 SUMOylation

A) WB of Kv4.2 SUMO1 conjugation. Kv4.2 and IgG IPs from S552E TC +/- PIAS3 HEK cell lysates were fractionated with SDS-PAGE. Blots were probed with SUMO1 and then stripped and re-probed for Kv4.2 (~69kD). The fraction of SUMOylated channel (SUMO OD÷Kv4 OD) was normalized to control. B) Bar graphs show the mean ± SEM normalized fraction of SUMOylated Kv4.2. The phosphomimetic mutation blocked the PIAS3-mediated increase in Kv4.2 SUMO1 conjugation (0.88 ± 0.22 vs 1.00 ± 0.00 , Mann-Whitney U, $p=0.364$).

C) WB of Kv4.2 SUMO2 conjugation. PIAS3 did not alter SUMO2 conjugation compared to the S552E TC alone (1.05 ± 0.22 vs 1.00 ± 0.00 , Mann-Whitney U, $p=0.364$).

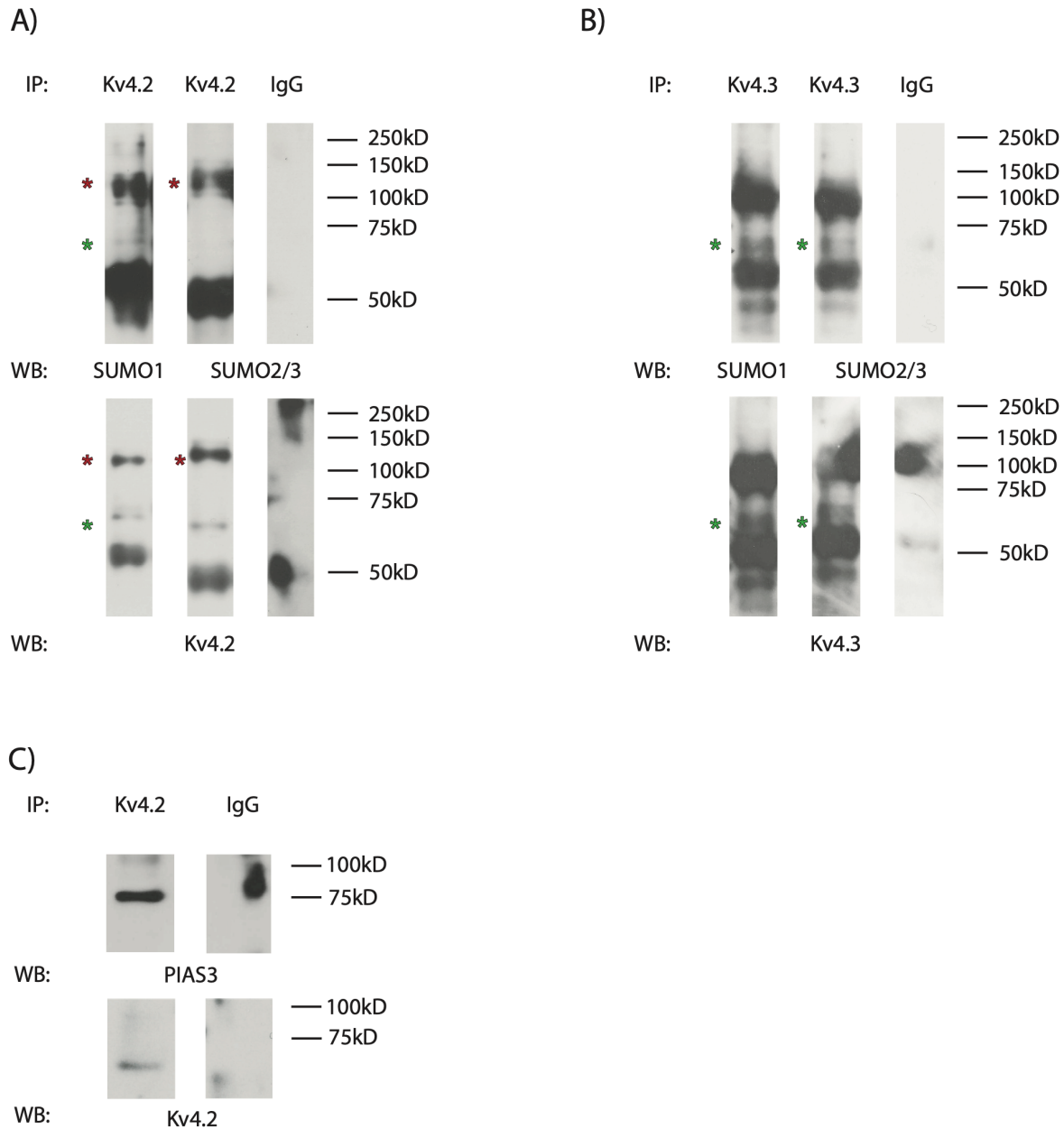


Figure 4-9 Kv4 channels are SUMOylated in the mouse heart and interact with PIAS3.

A) WB of Kv4.2 SUMOylation. Kv4.2 or IgG control antibodies were incubated with mouse heart lysates overnight at 4°C. IP products were fractionated with SDS-PAGE and transferred. Blots were probed for either SUMO1 (upper left) or SUMO2/3 (upper right) and then stripped and re-probed for Kv4.2 (lower); n=3. Green asterisks indicate SUMOylated Kv4.2 at ~69 kD; red asterisks indicate Kv4.2 with other post-translational modification including

SUMOylation (~130kD). B) WB of Kv4.3 SUMOylation. IP and WB experiments were repeated in mouse heart lysates using antibodies against Kv4.3 and IgG. C) PIAS3 co-IPs with Kv4.2 channels. Kv4.2 and IgG IPs from mouse heart lysates were probed first for PIAS3 (~65-75kD) and then stripped and re-probed for Kv4.2; n=3.

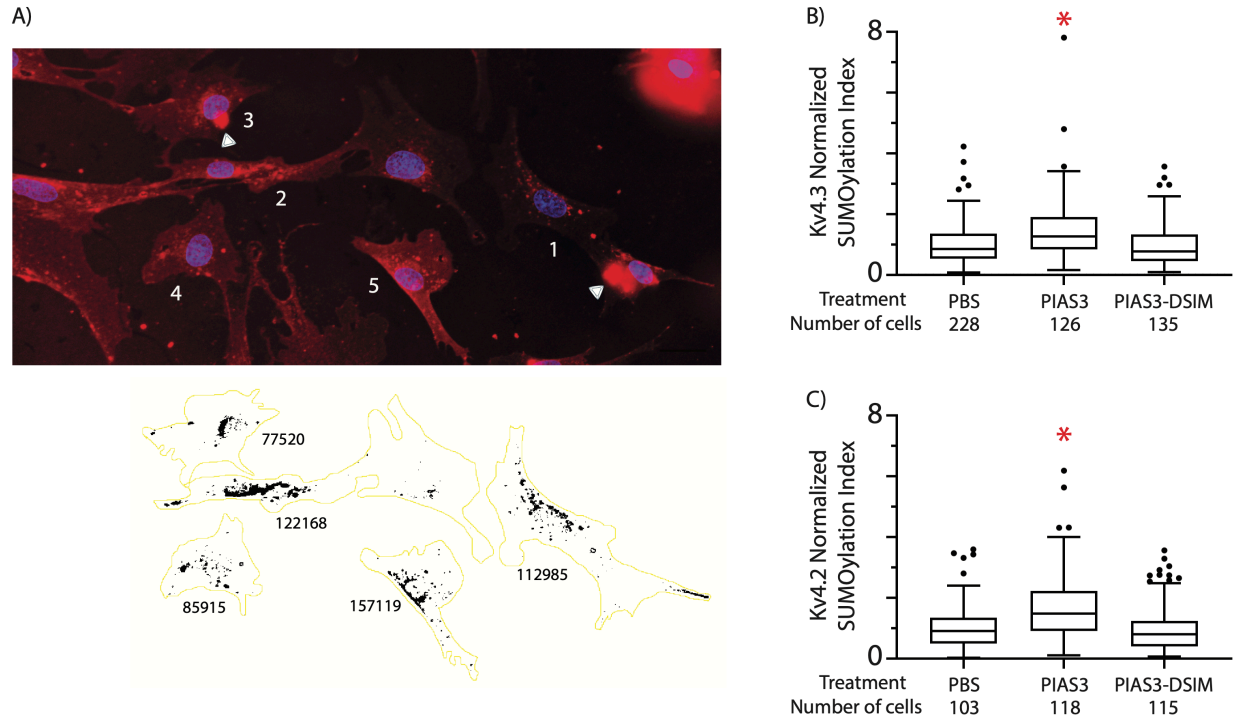


Figure 4-10 TAT-PIAS3 increases Kv4 SUMOylation in cardiomyocytes.

A) Representative PLA and analysis from TAT-PIAS3 treated cardiomyocytes.

Cardiomyocytes were outlined (yellow) to obtain cell area. Cells were thresholded using the Triangle method on ImageJ to remove background puncta and the raw integrated density of all puncta above background was divided by cell area to give the Kv4 SUMOylation Index. Data were normalized to the mean of the PBS group. B) Box and whiskers plots show quantification of Kv4.3 SUMOylation Index in PBS, TAT-PIAS3 (50nM), and TAT-PIAS3-SIM1 mutant (TAT-DSIM) (50nM) treated cardiomyocytes. TAT PIAS3 (1.50 ± 0.09) significantly increased Kv4.3 SUMOylation by 50% compared to PBS (1.00 ± 0.04) and TAT-DSIM (1.00 ± 0.06), which were not significantly different from each other. Kruskal-Wallis (3,489) = 37.59; $p < 0.0001$. C) Box and whiskers plots show quantification of Kv4.2 SUMOylation in PBS, TAT-PIAS3 (100nM), and TAT-DSIM (100nM) treated cells. TAT PIAS3 (1.68 ± 0.10) significantly increased Kv4.2 SUMOylation by ~70% compared to PBS (1.00 ± 0.07) and TAT-

DSIM (1.02 ± 0.07) treatments, which were not significantly different from each other. Kruskal-Wallis ($3,335$) = 38.90; $p < 0.0001$.

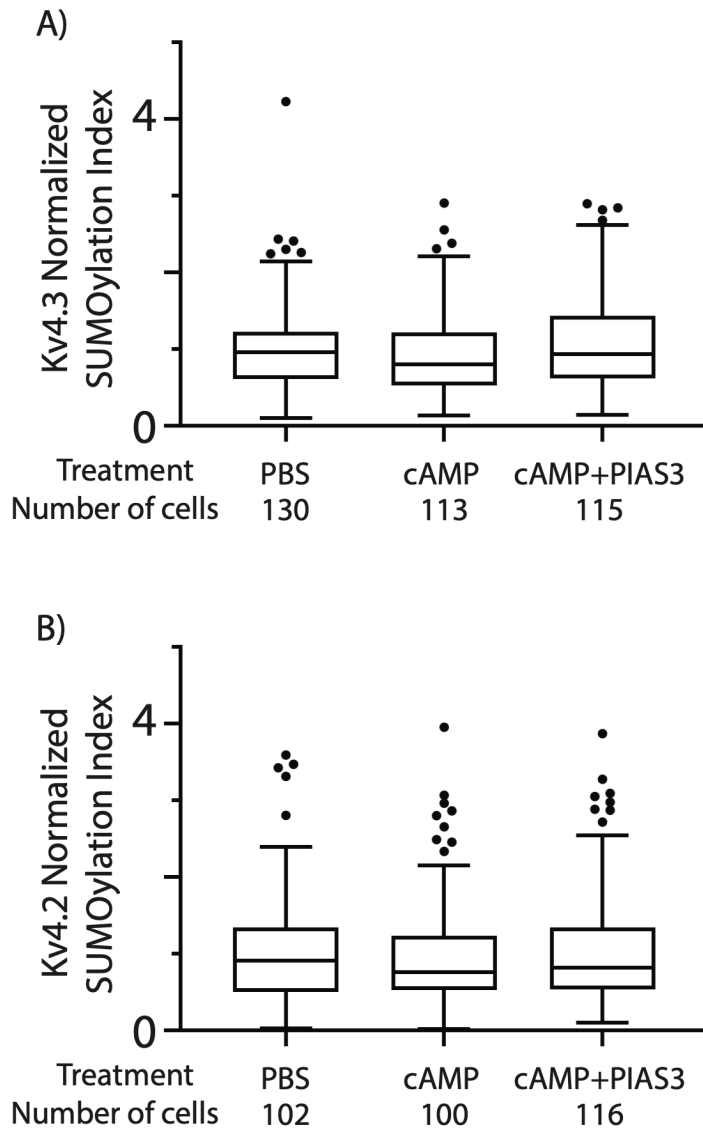


Figure 4-11- PKA Activation blocks the TAT-PIAS3-mediated increase in Kv4 SUMOylation

A) Box and whiskers plots show quantification of Kv4.3 SUMOylation Index in PBS, 8-bromo cAMP (100 μ M), and 8-bromo cAMP (100 μ M) + TAT-PIAS3 (50nM) treated cardiomyocytes. The Kv4.3 SUMOylation index was similar between PBS (1.00 ± 0.05), 8-bromo cAMP (0.96 ± 0.06), and 8-bromo cAMP + TAT-PIAS3 (1.09 ± 0.06) treated

cardiomyocytes. Kruskal-Wallis (3,358) = 2.658; $p=0.265$. B) Box and whiskers plots show quantification of the Kv4.2 SUMOylation Index in PBS, 8-bromo cAMP (100 μM), and 8-bromo cAMP (100 μM) + TAT-PIAS3 (100 nM) treated cardiomyocytes. There were no significant differences in the Kv4.2 SUMOylation index between PBS (1.00 ± 0.07), 8-bromo cAMP (1.01 ± 0.07), and 8-bromo cAMP + TAT-PIAS3 (1.04 ± 0.07) treated cardiomyocytes. Kruskal-Wallis (3,318) = 0.027; $p=0.9868$.

Table 4-Whole-patch clamp data for the Kv4.2g TC +/- PIAS3.

	Kv4.2g TC	Kv4.2g TC+PIAS3
Gmax (nS)	87.72 ± 6.16	139.0 ± 14.95 ⁺
V ₅₀ activation (mV)	-5.27 ± 1.13	-6.60 ± 2.17
V ₅₀ inactivation (mV)	-59.92 ± 1.30	-52.41 ± 1.32 ⁺
Tau slow (ms)	72.50 ± 4.54	80.61 ± 10.92
Tau fast (ms)	21.60 ± 1.79	29.05 ± 3.22

Mean ± SEM are shown for I_A Gmax, V₅₀ of activation, V₅₀ inactivation, and tau slow and fast.

⁺ Indicates significant difference from Kv4.2g TC

Table 5-Whole-patch clamp data for the Kv4.2g-K579R TC +/- PIAS3.

	Kv4.2g TC	Kv4.2g TC+PIAS3
Gmax (nS)	102.20 ± 7.39	116.80 ± 11.77
V ₅₀ activation (mV)	-2.68 ± 1.005	-3.089 ± 1.68
V ₅₀ inactivation (mV)	-54.38 ± 0.63	-56.33 ± 1.64
Tau slow (ms)	93.80 ± 13.32	82.34 ± 13.00
Tau fast (ms)	28.03 ± 3.00	22.74 ± 3.49

Mean ± SEM are shown for I_A Gmax, V₅₀ of activation, V₅₀ inactivation, and tau slow and fast.

5 CONCLUSION

5.1 Summary

This dissertation work has shown that HCN2 expression and HCN2 SUMOylation is altered in DRG neurons following CFA-induced inflammation in the rat hind paw. In Chapter 2, HCN2 intensity increased in small and medium diameter L5 DRG neurons at day 1 post-CFA injection but returned to normal at day 3. The increase in HCN2 intensity occurred in both contralateral and ipsilateral small diameter L5 DRG neurons, and only in ipsilateral medium diameter L5 DRG neurons. There was a significant bilateral increase in the number of small and medium diameter L5 DRG neurons expressing HCN2 at day 3 but not at day 1 post-injection. HCN2 channels were decorated by SUMO1 and SUMO2/3 peptides in the rat DRG, and SUMO2/3 conjugation was preferentially augmented at day 1, while only SUMO1 conjugation was increased at day 3 in ipsilateral small diameter L5 DRG neurons relative to contralateral neurons. In Chapter 3, HCN2 intensity was bilaterally increased in small diameter L4 and L6 DRG neurons at day 1 but not at day 3 post-CFA injection. HCN2 frequency was not altered in small diameter neurons but did increase bilaterally in medium and large diameter neurons at day 1. There was no change in HCN2 SUMOylation in any L4 and L6 DRG neurons at day 1. However, at day 3 post-CFA, HCN2 SUMOylation increased in medium and large diameter ipsilateral versus contralateral L6 DRG neurons. These findings raise an important question: does enhanced SUMOylation promote pain phenotypes?

This dissertation work has identified PIAS3 as an E3 SUMO ligase for Kv4 channels. In HEK cell experiments, PIAS3 recapitulated the effects of SUMO and Ubc9 on Kv4.2-mediated I_A and Kv4 channel SUMOylation. PIAS3 increased Kv4.2-mediated I_A by ~60% in HEK cells transiently transfected with ternary complex in Rab11a-dependent manner and no further effect

was seen when PIAS3 was co-expressed with SUMO and Ubc9, suggesting that PIAS3 acted in a SUMOylation-dependent pathway. Using a SUMO-deficient Kv4.2-K579R ternary complex blocked the PIAS3-mediated increase in I_A , indicating that PIAS3 acts at K579, the same target lysine as SUMO and Ubc9. The PIAS3-mediated effects on I_A were dependent on Ubc9 and an internal SIM1 of PIAS3, suggesting that PIAS3 interacted with Kv4 channels through its canonical E3 SUMO ligase properties. PIAS3 increased Kv4 channel SUMOylation at K579. Further, PIAS3 targets were preferentially alpha subunits as PIAS3 had no effect on the SUMOylation of Kv4 auxiliary subunits KChIP2a and DPP10 but could induce similar increases in HCN2-mediated I_h . The PIAS3-mediated increase in I_A and channel SUMOylation could be blocked by PKA-mediated phosphorylation at Kv4.2-S552. In cardiomyocytes, PIAS3 increased Kv4.3 and Kv4.2 SUMOylation by 50-70%, and this effect was eliminated by using either a PIAS3-SIM1 mutant or co-treatment with PIAS3 and 8-bromo cAMP, a PKA activator. The findings raise two important questions. The first, how is target SUMOylation antagonized? The second, is target dephosphorylation a conserved mechanism for selecting SUMO targets?

5.2 SUMOylation as a modulator of pain behaviors

HCN2 channels mediate mechanical hyperalgesia during CFA-induced inflammation. This pain behavior is only observed ipsilateral to the site of injection; however, our data shows that HCN2 channel expression is increased in both contralateral and ipsilateral putative nociceptors. Therefore, increased HCN2 expression alone is not sufficient for hyperalgesia. Post-translational modification of the HCN2 channels on the ipsilateral side may be necessary to facilitate pain behaviors. In heterologous systems, HCN2 SUMOylation at K669 increases I_h and surface expression by enhancing rab11a-slow recycling of the channel (L. A. Forster, Jansen L.R., Baro D.J; Parker et al., 2017). Therefore, the increase in HCN2 SUMOylation observed in

small DRG neurons at day 1 may promote pain behaviors by augmenting HCN2 surface expression and I_h in ipsilateral nociceptors. While the role of SUMOylation in pain is only emerging, the data so far suggests that SUMOylation promotes pain phenotypes. The collapsin response element 2 (CRMP2) is an auxiliary subunit of Nav1.7, a peripherally restricted ion channel that is enriched in nociceptive neurons and plays an important role amplifying generator potentials and impulse initiation (Bennett, Clark, Huang, Waxman, & Dib-Hajj, 2019).

SUMOylation of CRMP2 at K374 is necessary for Nav1.7 surface expression and function (Dustrude et al., 2013). Nav1.7 channel expression is augmented during pathological pain (Hameed, 2019), and selective targeting of Nav1.7 by antagonizing CRMP2 SUMOylation provides antinociceptive effects in models of neuropathic pain (S. Cai et al., 2021; Moutal, Dustrude, et al., 2017). SUMOylation is implicated in the development to thermal hyperalgesia during chronic pain. SUMOylation of PKC ϵ at K534 increases TRPV1 activation by increasing PKC ϵ -mediated phosphorylation of the channel during persistent inflammation (Zhao et al., 2020). Blocking PKC ϵ SUMOylation prevents the development of CFA-induced thermal hyperalgesia by reducing PKC ϵ kinase activity and binding to TRPV1 (Zhao et al., 2020).

SUMOylation of TRPV1 at K882 increases channel sensitization to thermal stimuli. Preventing SUMOylation at this site prevents thermal hyperalgesia during CFA-induced inflammation by reducing sensitization to thermal stimuli (Y. Wang et al., 2018b). Rats develop mechanical allodynia in spared nerve injury (SNI) model, due, in part, to decreased Kir7.1 channel expression (Lv et al., 2022). Kir7.1 channels show increased channel SUMOylation after SNI and blocking SUMOylation can rescue the loss of Kir7.1 surface expression in DRG neurons after SNI (Lv et al., 2022). Most targets show increased SUMOylation during chronic pain, however USP5 deubiquitinase, exhibits lower levels of SUMOylation (Garcia-Caballero et al.,

2014). In HEK cells, deSUMOylation of USP5 increases Cav3.2 interactions in HEK cells (Garcia-Caballero et al., 2019), and uncoupling this interaction in DRG neurons provides analgesic effects during chronic pain (Garcia-Caballero et al., 2014). These data indicate that enhanced SUMOylation is overwhelmingly pronociceptive during chronic pain. In these cases, enhanced SUMOylation either promotes protein-protein interactions or modulates the activity and/or expression of the target itself.

5.3 Target SUMOylation can be altered by disrupting PIAS3-Ubc9 interactions or PIAS3-target interactions.

As stated in Chapter 4, this dissertation work is the first to identify PIAS3 as an E3 SUMO ligase for ion channels. Prior to this, the targets for PIAS3 have been overwhelmingly nuclear. Only a few cytosolic targets have been reported for PIAS3. PIAS3 SUMOylation of the Rho-like GTPase Rac1 controls Rac1's GTP bound state and its ability to stimulate lamellipodia, cell migration and invasion responses (Castillo-Lluva et al., 2010). The ubiquitin-ligase Smurf2 is SUMOylated at K26 and K329 by Ubc9 and PIAS3, which enhances degradation of TGF β thereby suppressing the epithelial to mesenchymal transition in NMuMG cells (Chandhoke et al., 2016). Viral infection induces PIAS3 mediated poly-SUMOylation of the mitochondrial antiviral signaling protein, resulting in its phase-separation through internal SIMs and subsequent recruitment and activation of IRF3 to mediate an antiviral immune response (T. Dai et al., 2023). PIAS3-mediated SUMOylation of the scaffolding protein gephyrin at K148R and K724R is an essential determinant for scaffolding at GABAergic synapses (Ghosh et al., 2016). In neurons, activity induced PIAS3 SUMOylation of Akt1 at K24 and K276 increases its enzymatic activity and promotes downstream phosphorylation (Meng et al., 2021). In neurons, PIAS3 SUMOylates

nNOS at K725 and K739, which upregulates NO production and nNOS S1412 phosphorylation (C. P. Du et al., 2020).

Target SUMOylation is reduced or lost due to disruptions in Ubc9-PIAS3 interactions. In HEK239T cells, PIAS3-mediated SUMOylation of the Interferon regulatory factor-1 is blocked when a catalytic cysteine in the RING-domain is mutated to serine (Nakagawa & Yokosawa, 2002). PIAS3 suppresses cone development and promotes rod development in retinal cells by SUMOylating Nr2e3, a photoreceptor transcription factor, using two catalytic residues in its RING domain (Onishi, Peng, Chen, & Blackshaw, 2010). Mutating these residues prevents Nr2e3 SUMOylation. PIAS proteins bind to Ubc9 via the RING domain to stabilize the SUMO conjugation complex. In these examples, mutating the RING domain most likely alters PIAS3-Ubc9 interactions thereby reducing target SUMOylation. In other cases, blocking interactions between the target and PIAS3 appears to be consequential for substrate SUMOylation. A synthetic TAT-SAP domain blocked the activity induced PIAS3-mediated SUMOylation of Akt1 (Meng et al., 2021), and an Tat-tagged N-terminal segment of PIAS3 corresponding to amino acids 43–86 suppressed activity-induced nNOS SUMOylation by disrupting PIAS3-nNOS association (C. P. Du et al., 2020). In these examples, PIAS3 must interact simultaneously with the target and Ubc9 to facilitate SUMOylation. Our data shows that PIAS3-Ubc9 interactions are a determining factor in Kv4.2 SUMOylation, as mutating only the SIM1 domain of PIAS3 or knocking down Ubc9 resulted in current densities that were equivalent to control.

5.4 Target SUMOylation is gated by a target's phosphorylation status.

Proteins contain multiple post-translational modifications and crosstalk between target phosphorylation and target SUMOylation is well established. The phosphorylation dependent SUMOylation motif (PDSM) has been proposed as a regulatory site for substrate SUMOylation,

Here, a proline-directed serine adjacent to a SUMO consensus motif (V/L-K-X-E-X-X-SP) has been shown to facilitate the phosphorylation-directed SUMOylation of the Smad nuclear interacting protein 1, nuclear receptor ERR γ , and heat shock factor HSF4b (Hietakangas et al., 2006). The PDSM can also antagonize SUMOylation of c-Fos (Bossis et al., 2005). Kv4.2-S552 was identified as phosphorylated residue in hippocampal neurons using TAT-MS and in mouse brain and heart tissue using LC-MS/MS (Huttlin et al., 2010). S552 is not localized to a PDSM. Phosphorylation has been shown to gate SUMOylation independent of the PDSM.

Phosphorylation of CRMP2 at S522 is required for SUMOylation at K374 and subsequent trafficking of Nav1.7 channels to the surface (Dustrude et al., 2016). Phosphorylation of PKC α at non PDSM sites T497, T638, and S657 promotes its SUMOylation at K465 which in turn prevents its ubiquitination (Y. Wang et al., 2016). This relationship is mimicked in PKC δ , where phosphorylation at non-PDSM sites T05, S643, S663 facilitates SUMOylation at K473 (S. Gao et al., 2021). In both cases, dephosphorylation results in deSUMOylation and increased ubiquitination. Interestingly, mutating the phosphorylation sites on PKC δ to a phosphodeficient or phosphomimetic form had no effect on its interaction with SENP2. However, the phosphodeficient PKC δ possessed a reduced interaction with Ubc9 and PIAS2, while the phosphomimetic PKC δ had an enhanced or same interaction with Ubc9 and PIAS2 (S. Gao et al., 2021). A similar effect was seen with PKC ϵ , where phosphodeficient mutants showed reduced Ubc9 interactions compared to wild-type or phosphomimetic mutants (Zhao et al., 2020). These data suggest that the phosphorylation of the target controls the recruitment of the SUMOylation machinery thereby gating target SUMOylation. Therefore, PKA-mediated phosphorylation at S552 may recruit a SENP complex to K579 or simply lower the binding affinity of the PIAS3-

SUMO-Ubc9 complex through physical hinderance or by inducing a conformational change that effectively hides K579.

REFERENCES

- Acosta, C., McMullan, S., Djouhri, L., Gao, L., Watkins, R., Berry, C., . . . Lawson, S. N. (2012). HCN1 and HCN2 in Rat DRG neurons: levels in nociceptors and non-nociceptors, NT3-dependence and influence of CFA-induced skin inflammation on HCN2 and NT3 expression. *PLoS One*, *7*(12), e50442. doi:10.1371/journal.pone.0050442
- Alday, A., Urrutia, J., Gallego, M., & Casis, O. (2010). alpha1-adrenoceptors regulate only the caveolae-located subpopulation of cardiac K(V)4 channels. *Channels (Austin)*, *4*(3), 168-178. doi:10.4161/chan.4.3.11479
- Allgood, S. C., & Neunuebel, M. R. (2018). The recycling endosome and bacterial pathogens. *Cell Microbiol*, *20*(7), e12857. doi:10.1111/cmi.12857
- Amarillo, Y., De Santiago-Castillo, J. A., Dougherty, K., Maffie, J., Kwon, E., Covarrubias, M., & Rudy, B. (2008). Ternary Kv4.2 channels recapitulate voltage-dependent inactivation kinetics of A-type K⁺ channels in cerebellar granule neurons. *J Physiol*, *586*(8), 2093-2106. doi:10.1113/jphysiol.2007.150540
- An, W. F., Bowlby, M. R., Betty, M., Cao, J., Ling, H. P., Mendoza, G., . . . Rhodes, K. J. (2000). Modulation of A-type potassium channels by a family of calcium sensors. *Nature*, *403*(6769), 553-556. doi:10.1038/35000592
- Anderson, D. D., Eom, J. Y., & Stover, P. J. (2012). Competition between sumoylation and ubiquitination of serine hydroxymethyltransferase 1 determines its nuclear localization and its accumulation in the nucleus. *J Biol Chem*, *287*(7), 4790-4799. doi:10.1074/jbc.M111.302174
- Arendt, K. L., Royo, M., Fernandez-Monreal, M., Knafo, S., Petrok, C. N., Martens, J. R., & Esteban, J. A. (2010). PIP3 controls synaptic function by maintaining AMPA receptor clustering at the postsynaptic membrane. *Nat Neurosci*, *13*(1), 36-44. doi:10.1038/nn.2462
- Bae, S. H., Jeong, J. W., Park, J. A., Kim, S. H., Bae, M. K., Choi, S. J., & Kim, K. W. (2004). Sumoylation increases HIF-1alpha stability and its transcriptional activity. *Biochem Biophys Res Commun*, *324*(1), 394-400. doi:10.1016/j.bbrc.2004.09.068
- Bähring, R., Dannenberg, J., Peters, H. C., Leicher, T., Pongs, O., & Isbrandt, D. (2001). Conserved Kv4 N-terminal domain critical for effects of Kv channel-interacting protein 2.2 on channel expression and gating. *J Biol Chem*, *276*(26), 23888-23894. doi:10.1074/jbc.M101320200
- Barbuti, A., Scavone, A., Mazzocchi, N., Terragni, B., Baruscotti, M., & DiFrancesco, D. (2012). A caveolin-binding domain in the HCN4 channels mediates functional interaction with caveolin proteins. *J Mol Cell Cardiol*, *53*(2), 187-195. doi:10.1016/j.yjmcc.2012.05.013
- Basbaum, A. I., Bautista, D. M., Scherrer, G., & Julius, D. (2009). Cellular and molecular mechanisms of pain. *Cell*, *139*(2), 267-284. doi:10.1016/j.cell.2009.09.028
- Belau, F., Metzner, K., Christ, T., Ravens, U., Schaefer, M., Kunzel, S., . . . Kammerer, S. (2019). DPP10 is a new regulator of Nav1.5 channels in human heart. *Int J Cardiol*, *284*, 68-73. doi:10.1016/j.ijcard.2018.12.072
- Belkouch, M., Dansereau, M. A., Tetreault, P., Biet, M., Beaudet, N., Dumaine, R., . . . Sarret, P. (2014). Functional up-regulation of Nav1.8 sodium channel in Abeta afferent fibers subjected to chronic peripheral inflammation. *J Neuroinflammation*, *11*, 45. doi:10.1186/1742-2094-11-45

- Bennett, D. L., Clark, A. J., Huang, J., Waxman, S. G., & Dib-Hajj, S. D. (2019). The Role of Voltage-Gated Sodium Channels in Pain Signaling. *Physiol Rev*, *99*(2), 1079-1151. doi:10.1152/physrev.00052.2017
- Benson, M. D., Li, Q. J., Kieckhafer, K., Dudek, D., Whorton, M. R., Sunahara, R. K., . . . Martens, J. R. (2007). SUMO modification regulates inactivation of the voltage-gated potassium channel Kv1.5. *Proc Natl Acad Sci U S A*, *104*(6), 1805-1810. doi:10.1073/pnas.0606702104
- Berta, T., Qadri, Y., Tan, P. H., & Ji, R. R. (2017). Targeting dorsal root ganglia and primary sensory neurons for the treatment of chronic pain. *Expert Opin Ther Targets*, *21*(7), 695-703. doi:10.1080/14728222.2017.1328057
- Biel, M., Wahl-Schott, C., Michalakis, S., & Zong, X. (2009). Hyperpolarization-activated cation channels: from genes to function. *Physiol Rev*, *89*(3), 847-885. doi:10.1152/physrev.00029.2008
- Birnbaum, S. G., Varga, A. W., Yuan, L. L., Anderson, A. E., Sweatt, J. D., & Schrader, L. A. (2004). Structure and function of Kv4-family transient potassium channels. *Physiol Rev*, *84*(3), 803-833. doi:10.1152/physrev.00039.2003
- Boadas-Vaello, P., Homs, J., Reina, F., Carrera, A., & Verdu, E. (2017). Neuroplasticity of Supraspinal Structures Associated with Pathological Pain. *Anat Rec (Hoboken)*, *300*(8), 1481-1501. doi:10.1002/ar.23587
- Bossis, G., Malnou, C. E., Farras, R., Andermarcher, E., Hipskind, R., Rodriguez, M., . . . Piechaczyk, M. (2005). Down-regulation of c-Fos/c-Jun AP-1 dimer activity by sumoylation. *Mol Cell Biol*, *25*(16), 6964-6979. doi:10.1128/MCB.25.16.6964-6979.2005
- Brandt, M. C., Endres-Becker, J., Zagidullin, N., Motloch, L. J., Er, F., Rottlaender, D., . . . Hoppe, U. C. (2009). Effects of KCNE2 on HCN isoforms: distinct modulation of membrane expression and single channel properties. *Am J Physiol Heart Circ Physiol*, *297*(1), H355-363. doi:10.1152/ajpheart.00154.2009
- Braz, J., Solorzano, C., Wang, X., & Basbaum, A. I. (2014). Transmitting pain and itch messages: a contemporary view of the spinal cord circuits that generate gate control. *Neuron*, *82*(3), 522-536. doi:10.1016/j.neuron.2014.01.018
- Brazda, V., Klusakova, I., Svizenska, I., Veselkova, Z., & Dubovy, P. (2009). Bilateral changes in IL-6 protein, but not in its receptor gp130, in rat dorsal root ganglia following sciatic nerve ligature. *Cell Mol Neurobiol*, *29*(6-7), 1053-1062. doi:10.1007/s10571-009-9396-0
- Cai, Q., Verma, S. C., Kumar, P., Ma, M., & Robertson, E. S. (2010). Hypoxia inactivates the VHL tumor suppressor through PIASy-mediated SUMO modification. *PLoS One*, *5*(3), e9720. doi:10.1371/journal.pone.0009720
- Cai, S., Moutal, A., Yu, J., Chew, L. A., Isensee, J., Chawla, R., . . . Khanna, R. (2021). Selective targeting of NaV1.7 via inhibition of the CRMP2-Ubc9 interaction reduces pain in rodents. *Sci Transl Med*, *13*(619), eabh1314. doi:10.1126/scitranslmed.abh1314
- Cappadocia, L., & Lima, C. D. (2018). Ubiquitin-like Protein Conjugation: Structures, Chemistry, and Mechanism. *Chem Rev*, *118*(3), 889-918. doi:10.1021/acs.chemrev.6b00737
- Cappadocia, L., Pichler, A., & Lima, C. D. (2015). Structural basis for catalytic activation by the human ZNF451 SUMO E3 ligase. *Nat Struct Mol Biol*, *22*(12), 968-975. doi:10.1038/nsmb.3116

- Castillo-Lluva, S., Tatham, M. H., Jones, R. C., Jaffray, E. G., Edmondson, R. D., Hay, R. T., & Malliri, A. (2010). SUMOylation of the GTPase Rac1 is required for optimal cell migration. *Nat Cell Biol*, *12*(11), 1078-1085. doi:10.1038/ncb2112
- Celen, A. B., & Sahin, U. (2020). Sumoylation on its 25th anniversary: mechanisms, pathology, and emerging concepts. *FEBS J*, *287*(15), 3110-3140. doi:10.1111/febs.15319
- Chachami, G., Stankovic-Valentin, N., Karagiota, A., Basagianni, A., Plessmann, U., Urlaub, H., . . . Simos, G. (2019). Hypoxia-induced Changes in SUMO Conjugation Affect Transcriptional Regulation Under Low Oxygen. *Mol Cell Proteomics*, *18*(6), 1197-1209. doi:10.1074/mcp.RA119.001401
- Chamberlain, S. E., Gonzalez-Gonzalez, I. M., Wilkinson, K. A., Konopacki, F. A., Kantamneni, S., Henley, J. M., & Mellor, J. R. (2012). SUMOylation and phosphorylation of GluK2 regulate kainate receptor trafficking and synaptic plasticity. *Nat Neurosci*, *15*(6), 845-852. doi:10.1038/nn.3089
- Chandhoke, A. S., Karve, K., Dadakhujaev, S., Netherton, S., Deng, L., & Bonni, S. (2016). The ubiquitin ligase Smurf2 suppresses TGFbeta-induced epithelial-mesenchymal transition in a sumoylation-regulated manner. *Cell Death Differ*, *23*(5), 876-888. doi:10.1038/cdd.2015.152
- Chaplan, S. R., Guo, H. Q., Lee, D. H., Luo, L., Liu, C., Kuei, C., . . . Dubin, A. E. (2003). Neuronal hyperpolarization-activated pacemaker channels drive neuropathic pain. *J Neurosci*, *23*(4), 1169-1178. Retrieved from <https://www.ncbi.nlm.nih.gov/pubmed/12598605>
- Chen, J., Bian, X., Li, Y., Xiao, X., Yin, Y., Du, X., . . . Liu, X. (2020). Moderate hypothermia induces protection against hypoxia/reoxygenation injury by enhancing SUMOylation in cardiomyocytes. *Mol Med Rep*, *22*(4), 2617-2626. doi:10.3892/mmr.2020.11374
- Cheng, C. F., Wang, W. C., Huang, C. Y., Du, P. H., Yang, J. H., & Tsaur, M. L. (2016). Coexpression of auxiliary subunits KChIP and DPPL in potassium channel Kv4-positive nociceptors and pain-modulating spinal interneurons. *J Comp Neurol*, *524*(4), 846-873. doi:10.1002/cne.23876
- Cheng, J., Kang, X., Zhang, S., & Yeh, E. T. (2007). SUMO-specific protease 1 is essential for stabilization of HIF1alpha during hypoxia. *Cell*, *131*(3), 584-595. doi:10.1016/j.cell.2007.08.045
- Cheng, J. K., & Ji, R. R. (2008). Intracellular signaling in primary sensory neurons and persistent pain. *Neurochem Res*, *33*(10), 1970-1978. doi:10.1007/s11064-008-9711-z
- Cho, H. J., Staikopoulos, V., Furness, J. B., & Jennings, E. A. (2009). Inflammation-induced increase in hyperpolarization-activated, cyclic nucleotide-gated channel protein in trigeminal ganglion neurons and the effect of buprenorphine. *Neuroscience*, *162*(2), 453-461. doi:10.1016/j.neuroscience.2009.04.063
- Chung, C. D., Liao, J., Liu, B., Rao, X., Jay, P., Berta, P., & Shuai, K. (1997). Specific inhibition of Stat3 signal transduction by PIAS3. *Science*, *278*(5344), 1803-1805. doi:10.1126/science.278.5344.1803
- Cimarosti, H., Lindberg, C., Bomholt, S. F., Ronn, L. C., & Henley, J. M. (2008). Increased protein SUMOylation following focal cerebral ischemia. *Neuropharmacology*, *54*(2), 280-289. doi:10.1016/j.neuropharm.2007.09.010
- Clark, B. D., Kwon, E., Maffie, J., Jeong, H. Y., Nadal, M., Strop, P., & Rudy, B. (2008). DPP6 Localization in Brain Supports Function as a Kv4 Channel Associated Protein. *Front Mol Neurosci*, *1*, 8. doi:10.3389/neuro.02.008.2008

- Combe, C. L., & Gasparini, S. (2021). I(h) from synapses to networks: HCN channel functions and modulation in neurons. *Prog Biophys Mol Biol*, *166*, 119-132. doi:10.1016/j.pbiomolbio.2021.06.002
- Comerford, K. M., Leonard, M. O., Karhausen, J., Carey, R., Colgan, S. P., & Taylor, C. T. (2003). Small ubiquitin-related modifier-1 modification mediates resolution of CREB-dependent responses to hypoxia. *Proc Natl Acad Sci U S A*, *100*(3), 986-991. doi:10.1073/pnas.0337412100
- Craig, T. J., Jaafari, N., Petrovic, M. M., Jacobs, S. C., Rubin, P. P., Mellor, J. R., & Henley, J. M. (2012). Homeostatic synaptic scaling is regulated by protein SUMOylation. *J Biol Chem*, *287*(27), 22781-22788. doi:10.1074/jbc.M112.356337
- Cremona, C. A., Sarangi, P., Yang, Y., Hang, L. E., Rahman, S., & Zhao, X. (2012). Extensive DNA damage-induced sumoylation contributes to replication and repair and acts in addition to the mec1 checkpoint. *Mol Cell*, *45*(3), 422-432. doi:10.1016/j.molcel.2011.11.028
- Dai, T., Zhang, L., Ran, Y., Zhang, M., Yang, B., Lu, H., . . . Zhou, F. (2023). MAVS deSUMOylation by SENP1 inhibits its aggregation and antagonizes IRF3 activation. *Nat Struct Mol Biol*, *30*(6), 785-799. doi:10.1038/s41594-023-00988-8
- Dai, X. Q., Kolic, J., Marchi, P., Sipione, S., & Macdonald, P. E. (2009). SUMOylation regulates Kv2.1 and modulates pancreatic beta-cell excitability. *J Cell Sci*, *122*(Pt 6), 775-779. doi:10.1242/jcs.036632
- Dalle, C., & Eisenach, J. C. (2005). Peripheral block of the hyperpolarization-activated cation current (I_h) reduces mechanical allodynia in animal models of postoperative and neuropathic pain. *Reg Anesth Pain Med*, *30*(3), 243-248. doi:10.1016/j.rapm.2005.01.010
- DiFrancesco, J. C., & DiFrancesco, D. (2015). Dysfunctional HCN ion channels in neurological diseases. *Front Cell Neurosci*, *6*, 174. doi:10.3389/fncel.2015.00071
- Dini, L., Del Lungo, M., Resta, F., Melchiorre, M., Spinelli, V., Di Cesare Mannelli, L., . . . Romanelli, M. N. (2018). Selective Blockade of HCN1/HCN2 Channels as a Potential Pharmacological Strategy Against Pain. *Front Pharmacol*, *9*, 1252. doi:10.3389/fphar.2018.01252
- Djoughri, L., Al Otaibi, M., Kahlat, K., Smith, T., Sathish, J., & Weng, X. (2015). Persistent hindlimb inflammation induces changes in activation properties of hyperpolarization-activated current (I_h) in rat C-fiber nociceptors in vivo. *Neuroscience*, *301*, 121-133. doi:10.1016/j.neuroscience.2015.05.074
- Djoughri, L., Dawbarn, D., Robertson, A., Newton, R., & Lawson, S. N. (2001). Time course and nerve growth factor dependence of inflammation-induced alterations in electrophysiological membrane properties in nociceptive primary afferent neurons. *J Neurosci*, *21*(22), 8722-8733. Retrieved from <https://www.ncbi.nlm.nih.gov/pubmed/11698584>
- Djoughri, L., & Lawson, S. N. (2004). Abeta-fiber nociceptive primary afferent neurons: a review of incidence and properties in relation to other afferent A-fiber neurons in mammals. *Brain Res Brain Res Rev*, *46*(2), 131-145. doi:10.1016/j.brainresrev.2004.07.015
- Du, C. P., Wang, M., Geng, C., Hu, B., Meng, L., Xu, Y., . . . Hou, X. Y. (2020). Activity-Induced SUMOylation of Neuronal Nitric Oxide Synthase Is Associated with Plasticity of Synaptic Transmission and Extracellular Signal-Regulated Kinase 1/2 Signaling. *Antioxid Redox Signal*, *32*(1), 18-34. doi:10.1089/ars.2018.7669

- Du, L., Wang, S. J., Cui, J., He, W. J., & Ruan, H. Z. (2013a). Inhibition of HCN channels within the periaqueductal gray attenuates neuropathic pain in rats. *Behav Neurosci*, *127*(2), 325-329. doi:10.1037/a0031893
- Du, L., Wang, S. J., Cui, J., He, W. J., & Ruan, H. Z. (2013b). The role of HCN channels within the periaqueductal gray in neuropathic pain. *Brain Res*, *1500*, 36-44. doi:10.1016/j.brainres.2013.01.035
- Dubin, A. E., & Patapoutian, A. (2010). Nociceptors: the sensors of the pain pathway. *J Clin Invest*, *120*(11), 3760-3772. doi:10.1172/JCI42843
- Dubovy, P., Brazda, V., Klusakova, I., & Hradilova-Svizenska, I. (2013). Bilateral elevation of interleukin-6 protein and mRNA in both lumbar and cervical dorsal root ganglia following unilateral chronic compression injury of the sciatic nerve. *J Neuroinflammation*, *10*, 55. doi:10.1186/1742-2094-10-55
- Dustrude, E. T., Moutal, A., Yang, X., Wang, Y., Khanna, M., & Khanna, R. (2016). Hierarchical CRMP2 posttranslational modifications control NaV1.7 function. *Proc Natl Acad Sci U S A*, *113*(52), E8443-E8452. doi:10.1073/pnas.1610531113
- Dustrude, E. T., Wilson, S. M., Ju, W., Xiao, Y., & Khanna, R. (2013). CRMP2 protein SUMOylation modulates NaV1.7 channel trafficking. *J Biol Chem*, *288*(34), 24316-24331. doi:10.1074/jbc.M113.474924
- El-Haou, S., Balse, E., Neyroud, N., Dilanian, G., Gavillet, B., Abriel, H., . . . Hatem, S. N. (2009). Kv4 potassium channels form a tripartite complex with the anchoring protein SAP97 and CaMKII in cardiac myocytes. *Circ Res*, *104*(6), 758-769. doi:10.1161/CIRCRESAHA.108.191007
- Emery, E. C., Young, G. T., Berrocso, E. M., Chen, L., & McNaughton, P. A. (2011). HCN2 ion channels play a central role in inflammatory and neuropathic pain. *Science*, *333*(6048), 1462-1466. doi:10.1126/science.1206243
- Emery, E. C., Young, G. T., & McNaughton, P. A. (2012). HCN2 ion channels: an emerging role as the pacemakers of pain. *Trends Pharmacol Sci*, *33*(8), 456-463. doi:10.1016/j.tips.2012.04.004
- Feligioni, M., Nishimune, A., & Henley, J. M. (2009). Protein SUMOylation modulates calcium influx and glutamate release from presynaptic terminals. *Eur J Neurosci*, *29*(7), 1348-1356. doi:10.1111/j.1460-9568.2009.06692.x
- Fenske, S., Krause, S., Biel, M., & Wahl-Schott, C. (2011). The role of HCN channels in ventricular repolarization. *Trends Cardiovasc Med*, *21*(8), 216-220. doi:10.1016/j.tcm.2012.05.013
- Flotho, A., & Melchior, F. (2013). Sumoylation: a regulatory protein modification in health and disease. *Annu Rev Biochem*, *82*, 357-385. doi:10.1146/annurev-biochem-061909-093311
- Flotho, A., & Werner, A. (2012). The RanBP2/RanGAP1*SUMO1/Ubc9 complex: a multisubunit E3 ligase at the intersection of sumoylation and the RanGTPase cycle. *Nucleus*, *3*(5), 429-432. doi:10.4161/nucl.21980
- Flowerdew, S. E., & Burgoyne, R. D. (2009). A VAMP7/Vti1a SNARE complex distinguishes a non-conventional traffic route to the cell surface used by KChIP1 and Kv4 potassium channels. *Biochem J*, *418*(3), 529-540. doi:10.1042/BJ20081736
- Foeger, N. C., Norris, A. J., Wren, L. M., & Nerbonne, J. M. (2012). Augmentation of Kv4.2-encoded currents by accessory dipeptidyl peptidase 6 and 10 subunits reflects selective cell surface Kv4.2 protein stabilization. *J Biol Chem*, *287*(12), 9640-9650. doi:10.1074/jbc.M111.324574

- Foeger, N. C., Wang, W., Mellor, R. L., & Nerbonne, J. M. (2013). Stabilization of Kv4 protein by the accessory K(+) channel interacting protein 2 (KChIP2) subunit is required for the generation of native myocardial fast transient outward K(+) currents. *J Physiol*, *591*(17), 4149-4166. doi:10.1113/jphysiol.2013.255836
- Forster, L. A., Jansen L.R., Baro D.J. *C-terminal post-translational modification of ion channels by the small ubiquitin like modifier (SUMO) promotes rab11a mediated slow recycling of endocytosed channels*. Unpublished manuscript.
- Forster, L. A., Jansen, L. R., Rubaharan, M., Murphy, A. Z., & Baro, D. J. (2020). Alterations in SUMOylation of the hyperpolarization-activated cyclic nucleotide gated ion channel 2 during persistent inflammation. *Eur J Pain*. doi:10.1002/ejp.1606
- Francois-Moutal, L., Dustrude, E. T., Wang, Y., Brustovetsky, T., Dorame, A., Ju, W., . . . Khanna, R. (2018). Inhibition of the Ubc9 E2 SUMO-conjugating enzyme-CRMP2 interaction decreases Nav1.7 currents and reverses experimental neuropathic pain. *Pain*, *159*(10), 2115-2127. doi:10.1097/j.pain.0000000000001294
- Francois-Moutal, L., Scott, D. D., Perez-Miller, S., Gokhale, V., Khanna, M., & Khanna, R. (2018). Chemical shift perturbation mapping of the Ubc9-CRMP2 interface identifies a pocket in CRMP2 amenable for allosteric modulation of Nav1.7 channels. *Channels (Austin)*, *12*(1), 219-227. doi:10.1080/19336950.2018.1491244
- Gallego, M., Casis, E., Izquierdo, M. J., & Casis, O. (2000). Restoration of cardiac transient outward potassium current by norepinephrine in diabetic rats. *Pflugers Arch*, *441*(1), 102-107. doi:10.1007/s004240000374
- Gallego, M., Setien, R., Puebla, L., Boyano-Adanez Mdel, C., Arilla, E., & Casis, O. (2005). alpha1-Adrenoceptors stimulate a Galphas protein and reduce the transient outward K+ current via a cAMP/PKA-mediated pathway in the rat heart. *Am J Physiol Cell Physiol*, *288*(3), C577-585. doi:10.1152/ajpcell.00124.2004
- Gao, L. L., McMullan, S., Djouhri, L., Acosta, C., Harper, A. A., & Lawson, S. N. (2012). Expression and properties of hyperpolarization-activated current in rat dorsal root ganglion neurons with known sensory function. *J Physiol*, *590*(19), 4691-4705. doi:10.1113/jphysiol.2012.238485
- Gao, S., Zhao, X., Hou, L., Ma, R., Zhou, J., Zhu, M. X., . . . Li, Y. (2021). The interplay between SUMOylation and phosphorylation of PKCdelta facilitates oxidative stress-induced apoptosis. *FEBS J*, *288*(22), 6447-6464. doi:10.1111/febs.16050
- Garcia-Caballero, A., Gadotti, V. M., Stemkowski, P., Weiss, N., Souza, I. A., Hodgkinson, V., . . . Zamponi, G. W. (2014). The deubiquitinating enzyme USP5 modulates neuropathic and inflammatory pain by enhancing Cav3.2 channel activity. *Neuron*, *83*(5), 1144-1158. doi:10.1016/j.neuron.2014.07.036
- Garcia-Caballero, A., Zhang, F. X., Chen, L., M'Dahoma, S., Huang, J., & Zamponi, G. W. (2019). SUMOylation regulates USP5-Cav3.2 calcium channel interactions. *Mol Brain*, *12*(1), 73. doi:10.1186/s13041-019-0493-9
- Gardoni, F., Mauceri, D., Marcello, E., Sala, C., Di Luca, M., & Jeromin, A. (2007). SAP97 directs the localization of Kv4.2 to spines in hippocampal neurons: regulation by CaMKII. *J Biol Chem*, *282*(39), 28691-28699. doi:10.1074/jbc.M701899200
- Ghosh, H., Auguadri, L., Battaglia, S., Simone Thirouin, Z., Zemoura, K., Messner, S., . . . Tyagarajan, S. K. (2016). Several posttranslational modifications act in concert to regulate gephyrin scaffolding and GABAergic transmission. *Nat Commun*, *7*, 13365. doi:10.1038/ncomms13365

- Goff, J. R., Burkey, A. R., Goff, D. J., & Jasmin, L. (1998). Reorganization of the spinal dorsal horn in models of chronic pain: correlation with behaviour. *Neuroscience*, *82*(2), 559-574. Retrieved from <https://www.ncbi.nlm.nih.gov/pubmed/9466461>
<https://www.sciencedirect.com/science/article/pii/S0306452297002984?via%3Dihub>
- Gold, M. S., & Gebhart, G. F. (2010). Nociceptor sensitization in pain pathogenesis. *Nat Med*, *16*(11), 1248-1257. doi:10.1038/nm.2235
- Golebiowski, F., Matic, I., Tatham, M. H., Cole, C., Yin, Y., Nakamura, A., . . . Hay, R. T. (2009). System-wide changes to SUMO modifications in response to heat shock. *Sci Signal*, *2*(72), ra24. doi:10.1126/scisignal.2000282
- Gonzalez-Prieto, R., Eifler-Olivi, K., Claessens, L. A., Willemstein, E., Xiao, Z., Talavera Ormeno, C. M. P., . . . Vertegaal, A. C. O. (2021). Global non-covalent SUMO interaction networks reveal SUMO-dependent stabilization of the non-homologous end joining complex. *Cell Rep*, *34*(4), 108691. doi:10.1016/j.celrep.2021.108691
- Good, C. H., Hoffman, A. F., Hoffer, B. J., Chefer, V. I., Shippenberg, T. S., Backman, C. M., . . . Lupica, C. R. (2011). Impaired nigrostriatal function precedes behavioral deficits in a genetic mitochondrial model of Parkinson's disease. *FASEB J*, *25*(4), 1333-1344. doi:10.1096/fj.10-173625
- Guo, D., & Hu, J. (2014). Spinal presynaptic inhibition in pain control. *Neuroscience*, *283*, 95-106. doi:10.1016/j.neuroscience.2014.09.032
- Guo, W., Kamiya, K., & Toyama, J. (1995). Effect of chronic hypoxia on ion channel development in cultured cardiac cells. *Environ Med*, *39*(1), 57-60. Retrieved from <https://www.ncbi.nlm.nih.gov/pubmed/11540542>
- Hameed, S. (2019). Na(v)1.7 and Na(v)1.8: Role in the pathophysiology of pain. *Mol Pain*, *15*, 1744806919858801. doi:10.1177/1744806919858801
- Hammond, G. R. V., & Burke, J. E. (2020). Novel roles of phosphoinositides in signaling, lipid transport, and disease. *Curr Opin Cell Biol*, *63*, 57-67. doi:10.1016/j.ceb.2019.12.007
- Hammond, R. S., Lin, L., Sidorov, M. S., Wikenheiser, A. M., & Hoffman, D. A. (2008). Protein kinase a mediates activity-dependent Kv4.2 channel trafficking. *J Neurosci*, *28*(30), 7513-7519. doi:10.1523/JNEUROSCI.1951-08.2008
- Hasdemir, B., Fitzgerald, D. J., Prior, I. A., Tepikin, A. V., & Burgoyne, R. D. (2005). Traffic of Kv4 K⁺ channels mediated by KChIP1 is via a novel post-ER vesicular pathway. *J Cell Biol*, *171*(3), 459-469. doi:10.1083/jcb.200506005
- He, C., Chen, F., Li, B., & Hu, Z. (2014). Neurophysiology of HCN channels: from cellular functions to multiple regulations. *Prog Neurobiol*, *112*, 1-23. doi:10.1016/j.pneurobio.2013.10.001
- He, Q., Feng, Y., & Wang, Y. (2015). Transient outward potassium channel: a heart failure mediator. *Heart Fail Rev*, *20*(3), 349-362. doi:10.1007/s10741-015-9474-y
- Hendriks, I. A., D'Souza, R. C., Chang, J. G., Mann, M., & Vertegaal, A. C. (2015). System-wide identification of wild-type SUMO-2 conjugation sites. *Nat Commun*, *6*, 7289. doi:10.1038/ncomms8289
- Hendriks, I. A., Treffers, L. W., Verlaan-de Vries, M., Olsen, J. V., & Vertegaal, A. C. O. (2015). SUMO-2 Orchestrates Chromatin Modifiers in Response to DNA Damage. *Cell Rep*, *10*(10), 1778-1791. doi:10.1016/j.celrep.2015.02.033
- Herrity, A. N., Rau, K. K., Petruska, J. C., Stirling, D. P., & Hubscher, C. H. (2014). Identification of bladder and colon afferents in the nodose ganglia of male rats. *J Comp Neurol*, *522*(16), 3667-3682. doi:10.1002/cne.23629

- Herrmann, S., Layh, B., & Ludwig, A. (2011). Novel insights into the distribution of cardiac HCN channels: an expression study in the mouse heart. *J Mol Cell Cardiol*, *51*(6), 997-1006. doi:10.1016/j.yjmcc.2011.09.005
- Herrmann, S., Rajab, H., Christ, I., Schirdewahn, C., Hofler, D., Fischer, M. J. M., . . . Ludwig, A. (2017). Protein kinase A regulates inflammatory pain sensitization by modulating HCN2 channel activity in nociceptive sensory neurons. *Pain*, *158*(10), 2012-2024. doi:10.1097/j.pain.0000000000001005
- Herrmann, S., Schnorr, S., & Ludwig, A. (2015). HCN channels--modulators of cardiac and neuronal excitability. *Int J Mol Sci*, *16*(1), 1429-1447. doi:10.3390/ijms16011429
- Hietakangas, V., Anckar, J., Blomster, H. A., Fujimoto, M., Palvimo, J. J., Nakai, A., & Sistonen, L. (2006). PDSM, a motif for phosphorylation-dependent SUMO modification. *Proc Natl Acad Sci U S A*, *103*(1), 45-50. doi:10.1073/pnas.0503698102
- Hoffman, D. A., Magee, J. C., Colbert, C. M., & Johnston, D. (1997). K⁺ channel regulation of signal propagation in dendrites of hippocampal pyramidal neurons. *Nature*, *387*(6636), 869-875. doi:10.1038/43119
- Hofmann, F., Fabritz, L., Stieber, J., Schmitt, J., Kirchhof, P., Ludwig, A., & Herrmann, S. (2012). Ventricular HCN channels decrease the repolarization reserve in the hypertrophic heart. *Cardiovasc Res*, *95*(3), 317-326. doi:10.1093/cvr/cvs184
- Hotz, P. W., Wiesnet, M., Tascher, G., Braun, T., Muller, S., & Mendler, L. (2020). Profiling the Murine SUMO Proteome in Response to Cardiac Ischemia and Reperfusion Injury. *Molecules*, *25*(23). doi:10.3390/molecules25235571
- Hu, J. H., Liu, Y., & Hoffman, D. A. (2022). Identification of Kv4.2 protein complex and modifications by tandem affinity purification-mass spectrometry in primary neurons. *Front Cell Neurosci*, *16*, 1070305. doi:10.3389/fncel.2022.1070305
- Hu, J. H., Malloy, C., Tabor, G. T., Gutzmann, J. J., Liu, Y., Abebe, D., . . . Hoffman, D. A. (2020). Activity-dependent isomerization of Kv4.2 by Pin1 regulates cognitive flexibility. *Nat Commun*, *11*(1), 1567. doi:10.1038/s41467-020-15390-x
- Huang, B., Qin, D., & El-Sherif, N. (2001). Spatial alterations of Kv channels expression and K(+) currents in post-MI remodeled rat heart. *Cardiovasc Res*, *52*(2), 246-254. doi:10.1016/s0008-6363(01)00378-9
- Huang, H., Zhang, Z., & Huang, D. (2019). Decreased HCN2 channel expression attenuates neuropathic pain by inhibiting pro-inflammatory reactions and NF-kappaB activation in mice. *Int J Clin Exp Pathol*, *12*(1), 154-163. Retrieved from <https://www.ncbi.nlm.nih.gov/pubmed/31933729>
- Hucho, T., & Levine, J. D. (2007). Signaling pathways in sensitization: toward a nociceptor cell biology. *Neuron*, *55*(3), 365-376. doi:10.1016/j.neuron.2007.07.008
- Hurley, R. W., & Hammond, D. L. (2000). The analgesic effects of supraspinal mu and delta opioid receptor agonists are potentiated during persistent inflammation. *J Neurosci*, *20*(3), 1249-1259. Retrieved from <https://www.ncbi.nlm.nih.gov/pubmed/10648729>
- Hutcheon, B., & Yarom, Y. (2000). Resonance, oscillation and the intrinsic frequency preferences of neurons. *Trends Neurosci*, *23*(5), 216-222. doi:10.1016/s0166-2236(00)01547-2
- Huttlin, E. L., Jedrychowski, M. P., Elias, J. E., Goswami, T., Rad, R., Beausoleil, S. A., . . . Gygi, S. P. (2010). A tissue-specific atlas of mouse protein phosphorylation and expression. *Cell*, *143*(7), 1174-1189. doi:10.1016/j.cell.2010.12.001

- Jaafari, N., Konopacki, F. A., Owen, T. F., Kantamneni, S., Rubin, P., Craig, T. J., . . . Henley, J. M. (2013). SUMOylation is required for glycine-induced increases in AMPA receptor surface expression (ChemLTP) in hippocampal neurons. *PLoS One*, *8*(1), e52345. doi:10.1371/journal.pone.0052345
- Jancalek, R., Dubovy, P., Svizenska, I., & Klusakova, I. (2010). Bilateral changes of TNF-alpha and IL-10 protein in the lumbar and cervical dorsal root ganglia following a unilateral chronic constriction injury of the sciatic nerve. *J Neuroinflammation*, *7*, 11. doi:10.1186/1742-2094-7-11
- Jancalek, R., Svizenska, I., Klusakova, I., & Dubovy, P. (2011). Bilateral changes of IL-10 protein in lumbar and cervical dorsal root ganglia following proximal and distal chronic constriction injury of peripheral nerve. *Neurosci Lett*, *501*(2), 86-91. doi:10.1016/j.neulet.2011.06.052
- Jentsch, S., & Psakhye, I. (2013). Control of nuclear activities by substrate-selective and protein-group SUMOylation. *Annu Rev Genet*, *47*, 167-186. doi:10.1146/annurev-genet-111212-133453
- Jerng, H. H., Kunjilwar, K., & Pfaffinger, P. J. (2005). Multiprotein assembly of Kv4.2, KChIP3 and DPP10 produces ternary channel complexes with ISA-like properties. *J Physiol*, *568*(Pt 3), 767-788. doi:10.1113/jphysiol.2005.087858
- Jerng, H. H., Lauver, A. D., & Pfaffinger, P. J. (2007). DPP10 splice variants are localized in distinct neuronal populations and act to differentially regulate the inactivation properties of Kv4-based ion channels. *Mol Cell Neurosci*, *35*(4), 604-624. doi:10.1016/j.mcn.2007.03.008
- Jerng, H. H., & Pfaffinger, P. J. (2008). Multiple Kv channel-interacting proteins contain an N-terminal transmembrane domain that regulates Kv4 channel trafficking and gating. *J Biol Chem*, *283*(51), 36046-36059. doi:10.1074/jbc.M806852200
- Jerng, H. H., & Pfaffinger, P. J. (2014). Modulatory mechanisms and multiple functions of somatodendritic A-type K (+) channel auxiliary subunits. *Front Cell Neurosci*, *8*, 82. doi:10.3389/fncel.2014.00082
- Jerng, H. H., Pfaffinger, P. J., & Covarrubias, M. (2004). Molecular physiology and modulation of somatodendritic A-type potassium channels. *Mol Cell Neurosci*, *27*(4), 343-369. doi:10.1016/j.mcn.2004.06.011
- Jerng, H. H., Qian, Y., & Pfaffinger, P. J. (2004). Modulation of Kv4.2 channel expression and gating by dipeptidyl peptidase 10 (DPP10). *Biophys J*, *87*(4), 2380-2396. doi:10.1529/biophysj.104.042358
- Jiang, Y. Q., Xing, G. G., Wang, S. L., Tu, H. Y., Chi, Y. N., Li, J., . . . Wan, Y. (2008). Axonal accumulation of hyperpolarization-activated cyclic nucleotide-gated cation channels contributes to mechanical allodynia after peripheral nerve injury in rat. *Pain*, *137*(3), 495-506. doi:10.1016/j.pain.2007.10.011
- Johnson, E. K., Springer, S. J., Wang, W., Dranoff, E. J., Zhang, Y., Kanter, E. M., . . . Nerbonne, J. M. (2018). Differential Expression and Remodeling of Transient Outward Potassium Currents in Human Left Ventricles. *Circ Arrhythm Electrophysiol*, *11*(1), e005914. doi:10.1161/CIRCEP.117.005914
- Johnson, E. S., & Gupta, A. A. (2001). An E3-like factor that promotes SUMO conjugation to the yeast septins. *Cell*, *106*(6), 735-744. doi:10.1016/s0092-8674(01)00491-3

- Jung, S. C., Kim, J., & Hoffman, D. A. (2008). Rapid, bidirectional remodeling of synaptic NMDA receptor subunit composition by A-type K⁺ channel activity in hippocampal CA1 pyramidal neurons. *Neuron*, *60*(4), 657-671. doi:10.1016/j.neuron.2008.08.029
- Kahyo, T., Nishida, T., & Yasuda, H. (2001). Involvement of PIAS1 in the sumoylation of tumor suppressor p53. *Mol Cell*, *8*(3), 713-718. doi:10.1016/s1097-2765(01)00349-5
- Kaku, R., Matsuoka, Y., & Yang, J. (2019). Incorporation of one N-glycosylation-deficient subunit within a tetramer of HCN2 channel is tolerated. *Neuroreport*, *30*(15), 998-1003. doi:10.1097/WNR.0000000000001310
- Kaprielian, R., Wickenden, A. D., Kassiri, Z., Parker, T. G., Liu, P. P., & Backx, P. H. (1999). Relationship between K⁺ channel down-regulation and [Ca²⁺]_i in rat ventricular myocytes following myocardial infarction. *J Physiol*, *517* (Pt 1)(Pt 1), 229-245. doi:10.1111/j.1469-7793.1999.0229z.x
- Keskanokwong, T., Lim, H. J., Zhang, P., Cheng, J., Xu, L., Lai, D., & Wang, Y. (2011). Dynamic Kv4.3-CaMKII unit in heart: an intrinsic negative regulator for CaMKII activation. *Eur Heart J*, *32*(3), 305-315. doi:10.1093/eurheartj/ehq469
- Kim, E. Y., Zhang, Y., Ye, B., Segura, A. M., Beketaev, I., Xi, Y., . . . Wang, J. (2015). Involvement of activated SUMO-2 conjugation in cardiomyopathy. *Biochim Biophys Acta*, *1852*(7), 1388-1399. doi:10.1016/j.bbadis.2015.03.013
- Kim, J., Jung, S. C., Clemens, A. M., Petralia, R. S., & Hoffman, D. A. (2007). Regulation of dendritic excitability by activity-dependent trafficking of the A-type K⁺ channel subunit Kv4.2 in hippocampal neurons. *Neuron*, *54*(6), 933-947. doi:10.1016/j.neuron.2007.05.026
- Kim, J., Wei, D. S., & Hoffman, D. A. (2005). Kv4 potassium channel subunits control action potential repolarization and frequency-dependent broadening in rat hippocampal CA1 pyramidal neurones. *J Physiol*, *569*(Pt 1), 41-57. doi:10.1113/jphysiol.2005.095042
- Kimura, K., Kitano, J., Nakajima, Y., & Nakanishi, S. (2004). Hyperpolarization-activated, cyclic nucleotide-gated HCN2 cation channel forms a protein assembly with multiple neuronal scaffold proteins in distinct modes of protein-protein interaction. *Genes Cells*, *9*(7), 631-640. doi:10.1111/j.1356-9597.2004.00752.x
- Kitazawa, M., Kubo, Y., & Nakajo, K. (2015). Kv4.2 and accessory dipeptidyl peptidase-like protein 10 (DPP10) subunit preferentially form a 4:2 (Kv4.2:DPP10) channel complex. *J Biol Chem*, *290*(37), 22724-22733. doi:10.1074/jbc.M115.646794
- Knipscheer, P., van Dijk, W. J., Olsen, J. V., Mann, M., & Sixma, T. K. (2007). Noncovalent interaction between Ubc9 and SUMO promotes SUMO chain formation. *EMBO J*, *26*(11), 2797-2807. doi:10.1038/sj.emboj.7601711
- Koidl, S., Eisenhardt, N., Fatouros, C., Droscher, M., Chaugule, V. K., & Pichler, A. (2016). The SUMO2/3 specific E3 ligase ZNF451-1 regulates PML stability. *Int J Biochem Cell Biol*, *79*, 478-487. doi:10.1016/j.biocel.2016.06.011
- Koltzenburg, M., Wall, P. D., & McMahon, S. B. (1999). Does the right side know what the left is doing? *Trends Neurosci*, *22*(3), 122-127. doi:10.1016/s0166-2236(98)01302-2
- Kotaja, N., Karvonen, U., Janne, O. A., & Palvimo, J. J. (2002). PIAS proteins modulate transcription factors by functioning as SUMO-1 ligases. *Mol Cell Biol*, *22*(14), 5222-5234. doi:10.1128/MCB.22.14.5222-5234.2002
- Kouranova, E. V., Strassle, B. W., Ring, R. H., Bowlby, M. R., & Vasilyev, D. V. (2008). Hyperpolarization-activated cyclic nucleotide-gated channel mRNA and protein expression in large versus small diameter dorsal root ganglion neurons: correlation with

- hyperpolarization-activated current gating. *Neuroscience*, 153(4), 1008-1019.
doi:10.1016/j.neuroscience.2008.03.032
- Kunadt, M., Eckermann, K., Stuendl, A., Gong, J., Russo, B., Strauss, K., . . . Schneider, A. (2015). Extracellular vesicle sorting of alpha-Synuclein is regulated by sumoylation. *Acta Neuropathol*, 129(5), 695-713. doi:10.1007/s00401-015-1408-1
- Kuner, R., & Flor, H. (2016). Structural plasticity and reorganisation in chronic pain. *Nat Rev Neurosci*, 18(1), 20-30. doi:10.1038/nrn.2016.162
- Kunz, K., Piller, T., & Muller, S. (2018). SUMO-specific proteases and isopeptidases of the SENP family at a glance. *J Cell Sci*, 131(6). doi:10.1242/jcs.211904
- Kunz, K., Wagner, K., Mendler, L., Holper, S., Dehne, N., & Muller, S. (2016). SUMO Signaling by Hypoxic Inactivation of SUMO-Specific Isopeptidases. *Cell Rep*, 16(11), 3075-3086. doi:10.1016/j.celrep.2016.08.031
- Kuo, H. C., Cheng, C. F., Clark, R. B., Lin, J. J., Lin, J. L., Hoshijima, M., . . . Chien, K. R. (2001). A defect in the Kv channel-interacting protein 2 (KChIP2) gene leads to a complete loss of I(to) and confers susceptibility to ventricular tachycardia. *Cell*, 107(6), 801-813. doi:10.1016/s0092-8674(01)00588-8
- Kuo, Y. L., Cheng, J. K., Hou, W. H., Chang, Y. C., Du, P. H., Jian, J. J., . . . Tsauro, M. L. (2017). K(+) Channel Modulatory Subunits KChIP and DPP Participate in Kv4-Mediated Mechanical Pain Control. *J Neurosci*, 37(16), 4391-4404.
doi:10.1523/JNEUROSCI.1619-16.2017
- Kuryshv, Y. A., Guduz, T. I., Brown, A. M., & Wible, B. A. (2000). KChAP as a chaperone for specific K(+) channels. *Am J Physiol Cell Physiol*, 278(5), C931-941.
doi:10.1152/ajpcell.2000.278.5.C931
- Kuryshv, Y. A., Wible, B. A., Guduz, T. I., Ramirez, A. N., & Brown, A. M. (2001). KChAP/Kvbeta1.2 interactions and their effects on cardiac Kv channel expression. *Am J Physiol Cell Physiol*, 281(1), C290-299. doi:10.1152/ajpcell.2001.281.1.C290
- Lainez, S., Tsantoulas, C., Biel, M., & McNaughton, P. A. (2019). HCN3 ion channels: roles in sensory neuronal excitability and pain. *J Physiol*, 597(17), 4661-4675.
doi:10.1113/JP278211
- Lameris, T. W., de Zeeuw, S., Alberts, G., Boomsma, F., Duncker, D. J., Verdouw, P. D., . . . van Den Meiracker, A. H. (2000). Time course and mechanism of myocardial catecholamine release during transient ischemia in vivo. *Circulation*, 101(22), 2645-2650. doi:10.1161/01.cir.101.22.2645
- Lascorz, J., Codina-Fabra, J., Reverter, D., & Torres-Rosell, J. (2022). SUMO-SIM interactions: From structure to biological functions. *Semin Cell Dev Biol*, 132, 193-202.
doi:10.1016/j.semdb.2021.11.007
- Lee, A., Jeong, D., Mitsuyama, S., Oh, J. G., Liang, L., Ikeda, Y., . . . Kho, C. (2014). The role of SUMO-1 in cardiac oxidative stress and hypertrophy. *Antioxid Redox Signal*, 21(14), 1986-2001. doi:10.1089/ars.2014.5983
- Lee, D. H., Chang, L., Sorokin, L. S., & Chaplan, S. R. (2005). Hyperpolarization-activated, cation-nonspecific, cyclic nucleotide-modulated channel blockade alleviates mechanical allodynia and suppresses ectopic discharge in spinal nerve ligated rats. *J Pain*, 6(7), 417-424. doi:10.1016/j.jpain.2005.02.002
- Li, C. L., Li, K. C., Wu, D., Chen, Y., Luo, H., Zhao, J. R., . . . Zhang, X. (2016). Somatosensory neuron types identified by high-coverage single-cell RNA-sequencing and functional heterogeneity. *Cell Res*, 26(1), 83-102. doi:10.1038/cr.2015.149

- Li, M., Tonggu, L., Tang, L., & Wang, L. (2015). Effects of N-glycosylation on hyperpolarization-activated cyclic nucleotide-gated (HCN) channels. *Biochem J*, 466(1), 77-84. doi:10.1042/BJ20140692
- Li, W. M., Cui, K. M., Li, N., Gu, Q. B., Schwarz, W., Ding, G. H., & Wu, G. C. (2005). Analgesic effect of electroacupuncture on complete Freund's adjuvant-induced inflammatory pain in mice: a model of antipain treatment by acupuncture in mice. *Jpn J Physiol*, 55(6), 339-344. doi:10.2170/jjphysiol.RP001505
- Li, Y., Duan, H., Yi, J., Wang, G., Cheng, W., Feng, L., & Liu, J. (2022). Kv4.2 phosphorylation by PKA drives Kv4.2-KChIP2 dissociation, leading to Kv4.2 out of lipid rafts and internalization. *Am J Physiol Cell Physiol*, 323(1), C190-C201. doi:10.1152/ajpcell.00307.2021
- Liang, Y. C., Lee, C. C., Yao, Y. L., Lai, C. C., Schmitz, M. L., & Yang, W. M. (2016). SUMO5, a Novel Poly-SUMO Isoform, Regulates PML Nuclear Bodies. *Sci Rep*, 6, 26509. doi:10.1038/srep26509
- Liebelt, F., Sebastian, R. M., Moore, C. L., Mulder, M. P. C., Ovaa, H., Shoulders, M. D., & Vertegaal, A. C. O. (2019). SUMOylation and the HSF1-Regulated Chaperone Network Converge to Promote Proteostasis in Response to Heat Shock. *Cell Rep*, 26(1), 236-249 e234. doi:10.1016/j.celrep.2018.12.027
- Lin, L., Long, L. K., Hatch, M. M., & Hoffman, D. A. (2014). DPP6 domains responsible for its localization and function. *J Biol Chem*, 289(46), 32153-32165. doi:10.1074/jbc.M114.578070
- Lin, L., Sun, W., Kung, F., Dell'Acqua, M. L., & Hoffman, D. A. (2011). AKAP79/150 impacts intrinsic excitability of hippocampal neurons through phospho-regulation of A-type K⁺ channel trafficking. *J Neurosci*, 31(4), 1323-1332. doi:10.1523/JNEUROSCI.5383-10.2011
- Liu, B., Liao, J., Rao, X., Kushner, S. A., Chung, C. D., Chang, D. D., & Shuai, K. (1998). Inhibition of Stat1-mediated gene activation by PIAS1. *Proc Natl Acad Sci U S A*, 95(18), 10626-10631. doi:10.1073/pnas.95.18.10626
- Liu, Y., Feng, Y., & Zhang, T. (2015). Pulsed Radiofrequency Treatment Enhances Dorsal Root Ganglion Expression of Hyperpolarization-Activated Cyclic Nucleotide-Gated Channels in a Rat Model of Neuropathic Pain. *J Mol Neurosci*, 57(1), 97-105. doi:10.1007/s12031-015-0582-x
- Loriol, C., Khayachi, A., Poupon, G., Gwizdek, C., & Martin, S. (2013). Activity-dependent regulation of the sumoylation machinery in rat hippocampal neurons. *Biol Cell*, 105(1), 30-45. doi:10.1111/boc.201200016
- Ludwig, A., Budde, T., Stieber, J., Moosmang, S., Wahl, C., Holthoff, K., . . . Hofmann, F. (2003). Absence epilepsy and sinus dysrhythmia in mice lacking the pacemaker channel HCN2. *EMBO J*, 22(2), 216-224. doi:10.1093/emboj/cdg032
- Luo, L., Chang, L., Brown, S. M., Ao, H., Lee, D. H., Higuera, E. S., . . . Chaplan, S. R. (2007). Role of peripheral hyperpolarization-activated cyclic nucleotide-modulated channel pacemaker channels in acute and chronic pain models in the rat. *Neuroscience*, 144(4), 1477-1485. doi:10.1016/j.neuroscience.2006.10.048
- Lussier-Price, M., Mascle, X. H., Cappadocia, L., Kamada, R., Sakaguchi, K., Wahba, H. M., & Omichinski, J. G. (2020). Characterization of a C-Terminal SUMO-Interacting Motif Present in Select PIAS-Family Proteins. *Structure*, 28(5), 573-585 e575. doi:10.1016/j.str.2020.04.002

- Lv, Y. Y., Wang, H., Fan, H. T., Xu, T., Xin, W. J., & Guo, R. X. (2022). SUMOylation of Kir7.1 participates in neuropathic pain through regulating its membrane expression in spinal cord neurons. *CNS Neurosci Ther*, 28(8), 1259-1267. doi:10.1111/cns.13871
- Malmberg, A. B., Brandon, E. P., Idzerda, R. L., Liu, H., McKnight, G. S., & Basbaum, A. I. (1997). Diminished inflammation and nociceptive pain with preservation of neuropathic pain in mice with a targeted mutation of the type I regulatory subunit of cAMP-dependent protein kinase. *J Neurosci*, 17(19), 7462-7470. Retrieved from <https://www.ncbi.nlm.nih.gov/pubmed/9295392>
- Martin, S., Nishimune, A., Mellor, J. R., & Henley, J. M. (2007). SUMOylation regulates kainate-receptor-mediated synaptic transmission. *Nature*, 447(7142), 321-325. doi:10.1038/nature05736
- Masclé, X. H., Lussier-Price, M., Cappadocia, L., Estéphan, P., Raiola, L., Omichinski, J. G., & Aubry, M. (2013). Identification of a non-covalent ternary complex formed by PIAS1, SUMO1, and UBC9 proteins involved in transcriptional regulation. *J Biol Chem*, 288(51), 36312-36327. doi:10.1074/jbc.M113.486845
- Mendell, L. M. (2014). Constructing and deconstructing the gate theory of pain. *Pain*, 155(2), 210-216. doi:10.1016/j.pain.2013.12.010
- Meng, L., Du, C. P., Lu, C. Y., Zhang, K., Li, L., Yan, J. Z., & Hou, X. Y. (2021). Neuronal activity-induced SUMOylation of Akt1 by PIAS3 is required for long-term potentiation of synaptic transmission. *FASEB J*, 35(8), e21769. doi:10.1096/fj.202002728R
- Michels, G., Er, F., Khan, I. F., Endres-Becker, J., Brandt, M. C., Gassanov, N., . . . Hoppe, U. C. (2008). K⁺ channel regulator KCR1 suppresses heart rhythm by modulating the pacemaker current I_f. *PLoS One*, 3(1), e1511. doi:10.1371/journal.pone.0001511
- Millan, M. J., Czlonkowski, A., Morris, B., Stein, C., Arendt, R., Huber, A., . . . Herz, A. (1988). Inflammation of the hind limb as a model of unilateral, localized pain: influence on multiple opioid systems in the spinal cord of the rat. *Pain*, 35(3), 299-312. Retrieved from <https://www.ncbi.nlm.nih.gov/pubmed/2906425>
- Momin, A., Cadiou, H., Mason, A., & McNaughton, P. A. (2008). Role of the hyperpolarization-activated current I_h in somatosensory neurons. *J Physiol*, 586(24), 5911-5929. doi:10.1113/jphysiol.2008.163154
- Moutal, A., Dustrude, E. T., Largent-Milnes, T. M., Vanderah, T. W., Khanna, M., & Khanna, R. (2017). Blocking CRMP2 SUMOylation reverses neuropathic pain. *Mol Psychiatry*. doi:10.1038/mp.2017.117
- Moutal, A., Yang, X., Li, W., Gilbraith, K. B., Luo, S., Cai, S., . . . Khanna, R. (2017). CRISPR/Cas9 editing of Nf1 gene identifies CRMP2 as a therapeutic target in neurofibromatosis type 1-related pain that is reversed by (S)-Lacosamide. *Pain*, 158(12), 2301-2319. doi:10.1097/j.pain.0000000000001002
- Much, B., Wahl-Schott, C., Zong, X., Schneider, A., Baumann, L., Moosmang, S., . . . Biel, M. (2003). Role of subunit heteromerization and N-linked glycosylation in the formation of functional hyperpolarization-activated cyclic nucleotide-gated channels. *J Biol Chem*, 278(44), 43781-43786. doi:10.1074/jbc.M306958200
- Murphy, J. G., & Hoffman, D. A. (2019). A polybasic motif in alternatively spliced KChIP2 isoforms prevents Ca²⁺ regulation of Kv4 channels. *J Biol Chem*, 294(10), 3683-3695. doi:10.1074/jbc.RA118.006549

- Nadal, M. S., Amarillo, Y., Vega-Saenz de Miera, E., & Rudy, B. (2006). Differential characterization of three alternative spliced isoforms of DPPX. *Brain Res*, *1094*(1), 1-12. doi:10.1016/j.brainres.2006.03.106
- Nadal, M. S., Ozaita, A., Amarillo, Y., Vega-Saenz de Miera, E., Ma, Y., Mo, W., . . . Rudy, B. (2003). The CD26-related dipeptidyl aminopeptidase-like protein DPPX is a critical component of neuronal A-type K⁺ channels. *Neuron*, *37*(3), 449-461. doi:10.1016/s0896-6273(02)01185-6
- Nagi, S. S., Marshall, A. G., Makdani, A., Jarocka, E., Liljencrantz, J., Ridderstrom, M., . . . Olausson, H. (2019). An ultrafast system for signaling mechanical pain in human skin. *Sci Adv*, *5*(7), eaaw1297. doi:10.1126/sciadv.aaw1297
- Nakagawa, K., & Yokosawa, H. (2002). PIAS3 induces SUMO-1 modification and transcriptional repression of IRF-1. *FEBS Lett*, *530*(1-3), 204-208. doi:10.1016/s0014-5793(02)03486-5
- Nakajima, T., Ohtori, S., Inoue, G., Koshi, T., Yamamoto, S., Nakamura, J., . . . Harada, Y. (2008). The characteristics of dorsal-root ganglia and sensory innervation of the hip in rats. *J Bone Joint Surg Br*, *90*(2), 254-257. doi:10.1302/0301-620X.90B2.19808
- Namanja, A. T., Li, Y. J., Su, Y., Wong, S., Lu, J., Colson, L. T., . . . Chen, Y. (2012). Insights into high affinity small ubiquitin-like modifier (SUMO) recognition by SUMO-interacting motifs (SIMs) revealed by a combination of NMR and peptide array analysis. *J Biol Chem*, *287*(5), 3231-3240. doi:10.1074/jbc.M111.293118
- Nawathe, P. A., Kryukova, Y., Oren, R. V., Milanese, R., Clancy, C. E., Lu, J. T., . . . Robinson, R. B. (2013). An LQTS6 MiRP1 mutation suppresses pacemaker current and is associated with sinus bradycardia. *J Cardiovasc Electrophysiol*, *24*(9), 1021-1027. doi:10.1111/jce.12163
- Nestor, M. W., & Hoffman, D. A. (2012). Differential cycling rates of Kv4.2 channels in proximal and distal dendrites of hippocampal CA1 pyramidal neurons. *Hippocampus*, *22*(5), 969-980. doi:10.1002/hipo.20899
- Niskanen, E. A., Malinen, M., Sutinen, P., Toropainen, S., Paakinaho, V., Vihervaara, A., . . . Palvimo, J. J. (2015). Global SUMOylation on active chromatin is an acute heat stress response restricting transcription. *Genome Biol*, *16*(1), 153. doi:10.1186/s13059-015-0717-y
- Niwa, N., & Nerbonne, J. M. (2010). Molecular determinants of cardiac transient outward potassium current (I_{to}) expression and regulation. *J Mol Cell Cardiol*, *48*(1), 12-25. doi:10.1016/j.yjmcc.2009.07.013
- Onishi, A., Peng, G. H., Chen, S., & Blackshaw, S. (2010). Pias3-dependent SUMOylation controls mammalian cone photoreceptor differentiation. *Nat Neurosci*, *13*(9), 1059-1065. doi:10.1038/nn.2618
- Pace, M. C., Passavanti, M. B., De Nardis, L., Bosco, F., Sansone, P., Pota, V., . . . Aurilio, C. (2018). Nociceptor plasticity: A closer look. *J Cell Physiol*, *233*(4), 2824-2838. doi:10.1002/jcp.25993
- Papp, I., Hollo, K., & Antal, M. (2010). Plasticity of hyperpolarization-activated and cyclic nucleotid-gated cation channel subunit 2 expression in the spinal dorsal horn in inflammatory pain. *Eur J Neurosci*, *32*(7), 1193-1201. doi:10.1111/j.1460-9568.2010.07370.x
- Parker, A. R., Forster, L. A., & Baro, D. J. (2019). Modulator-Gated, SUMOylation-Mediated, Activity-Dependent Regulation of Ionic Current Densities Contributes to Short-Term

- Activity Homeostasis. *J Neurosci*, 39(4), 596-611. doi:10.1523/JNEUROSCI.1379-18.2018
- Parker, A. R., Welch, M. A., Forster, L. A., Tasneem, S. M., Dubhashi, J. A., & Baro, D. J. (2017). SUMOylation of the Hyperpolarization-Activated Cyclic Nucleotide-Gated Channel 2 Increases Surface Expression and the Maximal Conductance of the Hyperpolarization-Activated Current. *Front Mol Neurosci*, 9, 168. doi:10.3389/fnmol.2016.00168
- Peters, C. H., Singh, R. K., Bankston, J. R., & Proenza, C. (2022). Regulation of HCN Channels by Protein Interactions. *Front Physiol*, 13, 928507. doi:10.3389/fphys.2022.928507
- Pichler, A., Fatouros, C., Lee, H., & Eisenhardt, N. (2017). SUMO conjugation - a mechanistic view. *Biomol Concepts*, 8(1), 13-36. doi:10.1515/bmc-2016-0030
- Pinho-Ribeiro, F. A., Verri, W. A., Jr., & Chiu, I. M. (2017). Nociceptor Sensory Neuron-Immune Interactions in Pain and Inflammation. *Trends Immunol*, 38(1), 5-19. doi:10.1016/j.it.2016.10.001
- Pioletti, M., Findeisen, F., Hura, G. L., & Minor, D. L., Jr. (2006). Three-dimensional structure of the KChIP1-Kv4.3 T1 complex reveals a cross-shaped octamer. *Nat Struct Mol Biol*, 13(11), 987-995. doi:10.1038/nsmb1164
- Piskorowski, R., Santoro, B., & Siegelbaum, S. A. (2011). TRIP8b splice forms act in concert to regulate the localization and expression of HCN1 channels in CA1 pyramidal neurons. *Neuron*, 70(3), 495-509. doi:10.1016/j.neuron.2011.03.023
- Plant, L. D., Dementieva, I. S., Kollewe, A., Olikara, S., Marks, J. D., & Goldstein, S. A. (2010). One SUMO is sufficient to silence the dimeric potassium channel K2P1. *Proc Natl Acad Sci U S A*, 107(23), 10743-10748. doi:10.1073/pnas.1004712107
- Plant, L. D., Dowdell, E. J., Dementieva, I. S., Marks, J. D., & Goldstein, S. A. (2011). SUMO modification of cell surface Kv2.1 potassium channels regulates the activity of rat hippocampal neurons. *J Gen Physiol*, 137(5), 441-454. doi:10.1085/jgp.201110604
- Plant, L. D., Marks, J. D., & Goldstein, S. A. (2016). SUMOylation of NaV1.2 channels mediates the early response to acute hypoxia in central neurons. *Elife*, 5. doi:10.7554/eLife.20054
- Plant, L. D., Xiong, D., Romero, J., Dai, H., & Goldstein, S. A. N. (2020). Hypoxia Produces Pro-arrhythmic Late Sodium Current in Cardiac Myocytes by SUMOylation of NaV1.5 Channels. *Cell Rep*, 30(7), 2225-2236 e2224. doi:10.1016/j.celrep.2020.01.025
- Plant, L. D., Zuniga, L., Araki, D., Marks, J. D., & Goldstein, S. A. (2012). SUMOylation silences heterodimeric TASK potassium channels containing K2P1 subunits in cerebellar granule neurons. *Sci Signal*, 5(251), ra84. doi:10.1126/scisignal.2003431
- Proenza, C., Tran, N., Angoli, D., Zahynacz, K., Balcar, P., & Accili, E. A. (2002). Different roles for the cyclic nucleotide binding domain and amino terminus in assembly and expression of hyperpolarization-activated, cyclic nucleotide-gated channels. *J Biol Chem*, 277(33), 29634-29642. doi:10.1074/jbc.M200504200
- Pruunsild, P., & Timmusk, T. (2005). Structure, alternative splicing, and expression of the human and mouse KCNIP gene family. *Genomics*, 86(5), 581-593. doi:10.1016/j.ygeno.2005.07.001
- Psakhye, I., & Jentsch, S. (2012). Protein group modification and synergy in the SUMO pathway as exemplified in DNA repair. *Cell*, 151(4), 807-820. doi:10.1016/j.cell.2012.10.021

- Qi, S. Y., Riviere, P. J., Trojnar, J., Junien, J. L., & Akinsanya, K. O. (2003). Cloning and characterization of dipeptidyl peptidase 10, a new member of an emerging subgroup of serine proteases. *Biochem J*, 373(Pt 1), 179-189. doi:10.1042/BJ20021914
- Qi, Y., Wang, J., Bomben, V. C., Li, D. P., Chen, S. R., Sun, H., . . . Yeh, E. T. (2014). Hyper-SUMOylation of the Kv7 potassium channel diminishes the M-current leading to seizures and sudden death. *Neuron*, 83(5), 1159-1171. doi:10.1016/j.neuron.2014.07.042
- Qu, J., Kryukova, Y., Potapova, I. A., Doronin, S. V., Larsen, M., Krishnamurthy, G., . . . Robinson, R. B. (2004). MiRP1 modulates HCN2 channel expression and gating in cardiac myocytes. *J Biol Chem*, 279(42), 43497-43502. doi:10.1074/jbc.M405018200
- Rajan, S., Plant, L. D., Rabin, M. L., Butler, M. H., & Goldstein, S. A. (2005). Sumoylation silences the plasma membrane leak K⁺ channel K2P1. *Cell*, 121(1), 37-47. doi:10.1016/j.cell.2005.01.019
- Reichling, D. B., & Levine, J. D. (2009). Critical role of nociceptor plasticity in chronic pain. *Trends Neurosci*, 32(12), 611-618. doi:10.1016/j.tins.2009.07.007
- Ren, K., & Dubner, R. (1999). Inflammatory Models of Pain and Hyperalgesia. *ILAR J*, 40(3), 111-118. doi:10.1093/ilar.40.3.111
- Ren, X., Hayashi, Y., Yoshimura, N., & Takimoto, K. (2005). Transmembrane interaction mediates complex formation between peptidase homologues and Kv4 channels. *Mol Cell Neurosci*, 29(2), 320-332. doi:10.1016/j.mcn.2005.02.003
- Resta, F., Masi, A., Sili, M., Laurino, A., Moroni, F., & Mannaioni, G. (2016). Kynurenic acid and zaprinast induce analgesia by modulating HCN channels through GPR35 activation. *Neuropharmacology*, 108, 136-143. doi:10.1016/j.neuropharm.2016.04.038
- Resta, F., Micheli, L., Laurino, A., Spinelli, V., Mello, T., Sartiani, L., . . . Masi, A. (2018). Selective HCN1 block as a strategy to control oxaliplatin-induced neuropathy. *Neuropharmacology*, 131, 403-413. doi:10.1016/j.neuropharm.2018.01.014
- Richards, N., & Dilley, A. (2015). Contribution of hyperpolarization-activated channels to heat hypersensitivity and ongoing activity in the neuritis model. *Neuroscience*, 284, 87-98. doi:10.1016/j.neuroscience.2014.08.058
- Rigaud, M., Gemes, G., Barabas, M. E., Chernoff, D. I., Abram, S. E., Stucky, C. L., & Hogan, Q. H. (2008). Species and strain differences in rodent sciatic nerve anatomy: implications for studies of neuropathic pain. *Pain*, 136(1-2), 188-201. doi:10.1016/j.pain.2008.01.016
- Rivolta, I., Binda, A., Masi, A., & DiFrancesco, J. C. (2020). Cardiac and neuronal HCN channelopathies. *Pflugers Arch*, 472(7), 931-951. doi:10.1007/s00424-020-02384-3
- Robinson, R. B., & Siegelbaum, S. A. (2003). Hyperpolarization-activated cation currents: from molecules to physiological function. *Annu Rev Physiol*, 65, 453-480. doi:10.1146/annurev.physiol.65.092101.142734
- Rosati, B., Pan, Z., Lypen, S., Wang, H. S., Cohen, I., Dixon, J. E., & McKinnon, D. (2001). Regulation of KChIP2 potassium channel beta subunit gene expression underlies the gradient of transient outward current in canine and human ventricle. *J Physiol*, 533(Pt 1), 119-125. doi:10.1111/j.1469-7793.2001.0119b.x
- Rose, J., Armoundas, A. A., Tian, Y., DiSilvestre, D., Burysek, M., Halperin, V., . . . Tomaselli, G. F. (2005). Molecular correlates of altered expression of potassium currents in failing rabbit myocardium. *Am J Physiol Heart Circ Physiol*, 288(5), H2077-2087. doi:10.1152/ajpheart.00526.2003

- Rossow, C. F., Dilly, K. W., & Santana, L. F. (2006). Differential calcineurin/NFATc3 activity contributes to the Ito transmural gradient in the mouse heart. *Circ Res*, *98*(10), 1306-1313. doi:10.1161/01.RES.0000222028.92993.10
- Rossow, C. F., Dilly, K. W., Yuan, C., Nieves-Cintrón, M., Cabarrus, J. L., & Santana, L. F. (2009). NFATc3-dependent loss of I(to) gradient across the left ventricular wall during chronic beta adrenergic stimulation. *J Mol Cell Cardiol*, *46*(2), 249-256. doi:10.1016/j.yjmcc.2008.10.016
- Rossow, C. F., Minami, E., Chase, E. G., Murry, C. E., & Santana, L. F. (2004). NFATc3-induced reductions in voltage-gated K⁺ currents after myocardial infarction. *Circ Res*, *94*(10), 1340-1350. doi:10.1161/01.RES.0000128406.08418.34
- Rudakova, E., Wagner, M., Frank, M., & Volk, T. (2015). Localization of Kv4.2 and KChIP2 in lipid rafts and modulation of outward K⁺ currents by membrane cholesterol content in rat left ventricular myocytes. *Pflugers Arch*, *467*(2), 299-309. doi:10.1007/s00424-014-1521-3
- Rytinki, M. M., Kaikkonen, S., Pehkonen, P., Jaaskelainen, T., & Palvimo, J. J. (2009). PIAS proteins: pleiotropic interactors associated with SUMO. *Cell Mol Life Sci*, *66*(18), 3029-3041. doi:10.1007/s00018-009-0061-z
- Sahin, U., de The, H., & Lallemand-Breitenbach, V. (2022). Sumoylation in Physiology, Pathology and Therapy. *Cells*, *11*(5). doi:10.3390/cells11050814
- Saitoh, H., & Hinchev, J. (2000). Functional heterogeneity of small ubiquitin-related protein modifiers SUMO-1 versus SUMO-2/3. *J Biol Chem*, *275*(9), 6252-6258. doi:10.1074/jbc.275.9.6252
- Salo, P. T., & Theriault, E. (1997). Number, distribution and neuropeptide content of rat knee joint afferents. *J Anat*, *190* (Pt 4), 515-522. doi:10.1046/j.1469-7580.1997.19040515.x
- Santoro, B., Hu, L., Liu, H., Saponaro, A., Pian, P., Piskorowski, R. A., . . . Siegelbaum, S. A. (2011). TRIP8b regulates HCN1 channel trafficking and gating through two distinct C-terminal interaction sites. *J Neurosci*, *31*(11), 4074-4086. doi:10.1523/JNEUROSCI.5707-10.2011
- Santoro, B., Piskorowski, R. A., Pian, P., Hu, L., Liu, H., & Siegelbaum, S. A. (2009). TRIP8b splice variants form a family of auxiliary subunits that regulate gating and trafficking of HCN channels in the brain. *Neuron*, *62*(6), 802-813. doi:10.1016/j.neuron.2009.05.009
- Santoro, B., Wainger, B. J., & Siegelbaum, S. A. (2004). Regulation of HCN channel surface expression by a novel C-terminal protein-protein interaction. *J Neurosci*, *24*(47), 10750-10762. doi:24/47/10750 [pii] 10.1523/JNEUROSCI.3300-04.2004
- Saponaro, A., Pauleta, S. R., Cantini, F., Matzapetakis, M., Hammann, C., Donadoni, C., . . . Moroni, A. (2014). Structural basis for the mutual antagonism of cAMP and TRIP8b in regulating HCN channel function. *Proc Natl Acad Sci U S A*, *111*(40), 14577-14582. doi:10.1073/pnas.1410389111
- Sartiani, L., Mannaioni, G., Masi, A., Novella Romanelli, M., & Cerbai, E. (2017). The Hyperpolarization-Activated Cyclic Nucleotide-Gated Channels: from Biophysics to Pharmacology of a Unique Family of Ion Channels. *Pharmacol Rev*, *69*(4), 354-395. doi:10.1124/pr.117.014035
- Schmidt, D., & Muller, S. (2002). Members of the PIAS family act as SUMO ligases for c-Jun and p53 and repress p53 activity. *Proc Natl Acad Sci U S A*, *99*(5), 2872-2877. doi:10.1073/pnas.052559499

- Schnorr, S., Eberhardt, M., Kistner, K., Rajab, H., Kaer, J., Hess, A., . . . Herrmann, S. (2014). HCN2 channels account for mechanical (but not heat) hyperalgesia during long-standing inflammation. *Pain*, *155*(6), 1079-1090. doi:10.1016/j.pain.2014.02.006
- Schnorr, S., Eberhardt, M., Kistner, K., Rajab, H., Kasser, J., Hess, A., . . . Herrmann, S. (2014). HCN2 channels account for mechanical (but not heat) hyperalgesia during long-standing inflammation. *Pain*, *155*(6), 1079-1090. doi:10.1016/j.pain.2014.02.006
- Schrader, L. A., Anderson, A. E., Mayne, A., Pfaffinger, P. J., & Sweatt, J. D. (2002). PKA modulation of Kv4.2-encoded A-type potassium channels requires formation of a supramolecular complex. *J Neurosci*, *22*(23), 10123-10133. Retrieved from <https://www.ncbi.nlm.nih.gov/pubmed/12451113>
- Seifert, A., Schofield, P., Barton, G. J., & Hay, R. T. (2015). Proteotoxic stress reprograms the chromatin landscape of SUMO modification. *Sci Signal*, *8*(384), rs7. doi:10.1126/scisignal.aaa2213
- Shah, M. M. (2014). Cortical HCN channels: function, trafficking and plasticity. *J Physiol*, *592*(13), 2711-2719. doi:10.1113/jphysiol.2013.270058
- Shao, R., Zhang, F. P., Tian, F., Anders Friberg, P., Wang, X., Sjolund, H., & Billig, H. (2004). Increase of SUMO-1 expression in response to hypoxia: direct interaction with HIF-1alpha in adult mouse brain and heart in vivo. *FEBS Lett*, *569*(1-3), 293-300. doi:10.1016/j.febslet.2004.05.079
- Shibata, R., Misonou, H., Campomanes, C. R., Anderson, A. E., Schrader, L. A., Doliveira, L. C., . . . Trimmer, J. S. (2003). A fundamental role for KChIPs in determining the molecular properties and trafficking of Kv4.2 potassium channels. *J Biol Chem*, *278*(38), 36445-36454. doi:10.1074/jbc.M306142200
- Smith, T., Al Otaibi, M., Sathish, J., & Djouhri, L. (2015). Increased expression of HCN2 channel protein in L4 dorsal root ganglion neurons following axotomy of L5- and inflammation of L4-spinal nerves in rats. *Neuroscience*, *295*, 90-102. doi:10.1016/j.neuroscience.2015.03.041
- Soh, H., & Goldstein, S. A. (2008). I SA channel complexes include four subunits each of DPP6 and Kv4.2. *J Biol Chem*, *283*(22), 15072-15077. doi:10.1074/jbc.M706964200
- Steffensen, A. B., Andersen, M. N., Mutsaers, N., Mujezinovic, A., & Schmitt, N. (2018). SUMO co-expression modifies KV 11.1 channel activity. *Acta Physiol (Oxf)*, *222*(3). doi:10.1111/apha.12974
- Stein, C., Millan, M. J., & Herz, A. (1988). Unilateral inflammation of the hindpaw in rats as a model of prolonged noxious stimulation: alterations in behavior and nociceptive thresholds. *Pharmacol Biochem Behav*, *31*(2), 445-451.
- Su, H. L., & Li, S. S. (2002). Molecular features of human ubiquitin-like SUMO genes and their encoded proteins. *Gene*, *296*(1-2), 65-73. doi:10.1016/s0378-1119(02)00843-0
- Sun, Q., Xing, G. G., Tu, H. Y., Han, J. S., & Wan, Y. (2005). Inhibition of hyperpolarization-activated current by ZD7288 suppresses ectopic discharges of injured dorsal root ganglion neurons in a rat model of neuropathic pain. *Brain Res*, *1032*(1-2), 63-69. doi:10.1016/j.brainres.2004.10.033
- Swett, J. E., Torigoe, Y., Elie, V. R., Bourassa, C. M., & Miller, P. G. (1991). Sensory neurons of the rat sciatic nerve. *Exp Neurol*, *114*(1), 82-103. doi:10.1016/0014-4886(91)90087-s
- Taiwo, Y. O., & Levine, J. D. (1991). Further confirmation of the role of adenylyl cyclase and of cAMP-dependent protein kinase in primary afferent hyperalgesia. *Neuroscience*, *44*(1), 131-135. doi:10.1016/0306-4522(91)90255-m

- Takahashi, Y., Kahyo, T., Toh, E. A., Yasuda, H., & Kikuchi, Y. (2001). Yeast Ull1/Siz1 is a novel SUMO1/Smt3 ligase for septin components and functions as an adaptor between conjugating enzyme and substrates. *J Biol Chem*, *276*(52), 48973-48977. doi:10.1074/jbc.M109295200
- Takasu, K., Ono, H., & Tanabe, M. (2010). Spinal hyperpolarization-activated cyclic nucleotide-gated cation channels at primary afferent terminals contribute to chronic pain. *Pain*, *151*(1), 87-96. doi:10.1016/j.pain.2010.06.020
- Takeda, M., Takahashi, M., & Matsumoto, S. (2014). Inflammation enhanced brain-derived neurotrophic factor-induced suppression of the voltage-gated potassium currents in small-diameter trigeminal ganglion neurons projecting to the trigeminal nucleus interpolaris/caudalis transition zone. *Neuroscience*, *261*, 223-231. doi:10.1016/j.neuroscience.2013.12.048
- Tatham, M. H., Kim, S., Jaffray, E., Song, J., Chen, Y., & Hay, R. T. (2005). Unique binding interactions among Ubc9, SUMO and RanBP2 reveal a mechanism for SUMO paralog selection. *Nat Struct Mol Biol*, *12*(1), 67-74. doi:10.1038/nsmb878
- Tibbs, G. R., Posson, D. J., & Goldstein, P. A. (2016). Voltage-Gated Ion Channels in the PNS: Novel Therapies for Neuropathic Pain? *Trends Pharmacol Sci*, *37*(7), 522-542. doi:10.1016/j.tips.2016.05.002
- Tran, N., Proenza, C., Macri, V., Petigara, F., Sloan, E., Samler, S., & Accili, E. A. (2002). A conserved domain in the NH2 terminus important for assembly and functional expression of pacemaker channels. *J Biol Chem*, *277*(46), 43588-43592. doi:10.1074/jbc.M208477200
- Tsantoulas, C., Lainez, S., Wong, S., Mehta, I., Vilar, B., & McNaughton, P. A. (2017). Hyperpolarization-activated cyclic nucleotide-gated 2 (HCN2) ion channels drive pain in mouse models of diabetic neuropathy. *Sci Transl Med*, *9*(409), eaam6072. doi:10.1126/scitranslmed.aam6072
- Tsantoulas, C., Mooney, E. R., & McNaughton, P. A. (2016). HCN2 ion channels: basic science opens up possibilities for therapeutic intervention in neuropathic pain. *Biochem J*, *473*(18), 2717-2736. doi:10.1042/BCJ20160287
- Usoskin, D., Furlan, A., Islam, S., Abdo, H., Lonnerberg, P., Lou, D., . . . Ernfors, P. (2015). Unbiased classification of sensory neuron types by large-scale single-cell RNA sequencing. *Nat Neurosci*, *18*(1), 145-153. doi:10.1038/nn.3881
- Vertegaal, A. C. O. (2022). Signalling mechanisms and cellular functions of SUMO. *Nat Rev Mol Cell Biol*, *23*(11), 715-731. doi:10.1038/s41580-022-00500-y
- Wahl-Schott, C., & Biel, M. (2009). HCN channels: structure, cellular regulation and physiological function. *Cell Mol Life Sci*, *66*(3), 470-494. doi:10.1007/s00018-008-8525-0
- Walrant, A., Cardon, S., Burlina, F., & Sagan, S. (2017). Membrane Crossing and Membranotropic Activity of Cell-Penetrating Peptides: Dangerous Liaisons? *Acc Chem Res*, *50*(12), 2968-2975. doi:10.1021/acs.accounts.7b00455
- Wang, H., Yan, Y., Liu, Q., Huang, Y., Shen, Y., Chen, L., . . . Chai, J. (2007). Structural basis for modulation of Kv4 K⁺ channels by auxiliary KChIP subunits. *Nat Neurosci*, *10*(1), 32-39. doi:10.1038/nn1822
- Wang, W. C., Cheng, C. F., & Tsaur, M. L. (2015). Immunohistochemical localization of DPP10 in rat brain supports the existence of a Kv4/KChIP/DPPL ternary complex in neurons. *J Comp Neurol*, *523*(4), 608-628. doi:10.1002/cne.23698

- Wang, X., Wang, S., Wang, W., Duan, J., Zhang, M., Lv, X., . . . Xing, J. (2016). A novel intrinsic analgesic mechanism: the enhancement of the conduction failure along polymodal nociceptive C-fibers. *Pain*, *157*(10), 2235-2247. doi:10.1097/j.pain.0000000000000632
- Wang, Y., Gao, Y., Tian, Q., Deng, Q., Wang, Y., Zhou, T., . . . Li, Y. (2018a). Author Correction: TRPV1 SUMOylation regulates nociceptive signaling in models of inflammatory pain. *Nat Commun*, *9*(1), 2593. doi:10.1038/s41467-018-05022-w
- Wang, Y., Gao, Y., Tian, Q., Deng, Q., Wang, Y., Zhou, T., . . . Li, Y. (2018b). TRPV1 SUMOylation regulates nociceptive signaling in models of inflammatory pain. *Nat Commun*, *9*(1), 1529. doi:10.1038/s41467-018-03974-7
- Wang, Y., Wang, Y., Zhang, H., Gao, Y., Huang, C., Zhou, A., . . . Li, Y. (2016). Sequential posttranslational modifications regulate PKC degradation. *Mol Biol Cell*, *27*(2), 410-420. doi:10.1091/mbc.E15-09-0624
- Watts, F. Z. (2013). Starting and stopping SUMOylation. What regulates the regulator? *Chromosoma*, *122*(6), 451-463. doi:10.1007/s00412-013-0422-0
- Welch, M. A., Forster, L. A., Atlas, S. I., & Baro, D. J. (2019). SUMOylating Two Distinct Sites on the A-type Potassium Channel, Kv4.2, Increases Surface Expression and Decreases Current Amplitude. *Frontiers in Molecular Neuroscience*, *12*(144). doi:10.3389/fnmol.2019.00144
- Welch, M. A., Forster, L. A., Atlas, S. I., & Baro, D. J. (2019). SUMOylating Two Distinct Sites on the A-type Potassium Channel, Kv4.2, Increases Surface Expression and Decreases Current Amplitude. *Front Mol Neurosci*, *12*, 144. doi:10.3389/fnmol.2019.00144
- Welch, M. A., Jansen, L. R., & Baro, D. J. (2021). SUMOylation of the Kv4.2 Ternary Complex Increases Surface Expression and Current Amplitude by Reducing Internalization in HEK 293 Cells. *Front Mol Neurosci*, *14*, 757278. doi:10.3389/fnmol.2021.757278
- Welch MA, J. L., Baro DJ. (2021). SUMOylation of the Kv4.2 ternary complex increases surface expression and current amplitude by reducing internalization in HEK 293 cells. *Frontiers in Molecular Neuroscience*.
- Weng, X., Smith, T., Sathish, J., & Djouhri, L. (2012). Chronic inflammatory pain is associated with increased excitability and hyperpolarization-activated current (I_h) in C- but not Adelta-nociceptors. *Pain*, *153*(4), 900-914. doi:10.1016/j.pain.2012.01.019
- Werner, A., Flotho, A., & Melchior, F. (2012). The RanBP2/RanGAP1*SUMO1/Ubc9 complex is a multisubunit SUMO E3 ligase. *Mol Cell*, *46*(3), 287-298. doi:10.1016/j.molcel.2012.02.017
- Whitaker, G. M., Angoli, D., Nazzari, H., Shigemoto, R., & Accili, E. A. (2007). HCN2 and HCN4 isoforms self-assemble and co-assemble with equal preference to form functional pacemaker channels. *J Biol Chem*, *282*(31), 22900-22909. doi:10.1074/jbc.M610978200
- Wible, B. A., Yang, Q., Kuryshv, Y. A., Accili, E. A., & Brown, A. M. (1998). Cloning and expression of a novel K⁺ channel regulatory protein, KChAP. *J Biol Chem*, *273*(19), 11745-11751. doi:10.1074/jbc.273.19.11745
- Xiao, L., Koopmann, T. T., Ordog, B., Postema, P. G., Verkerk, A. O., Iyer, V., . . . Nattel, S. (2013). Unique cardiac Purkinje fiber transient outward current beta-subunit composition: a potential molecular link to idiopathic ventricular fibrillation. *Circ Res*, *112*(10), 1310-1322. doi:10.1161/CIRCRESAHA.112.300227

- Xiong, D., Li, T., Dai, H., Arena, A. F., Plant, L. D., & Goldstein, S. A. N. (2017). SUMOylation determines the voltage required to activate cardiac IKs channels. *Proc Natl Acad Sci U S A*, *114*(32), E6686-E6694. doi:10.1073/pnas.1706267114
- Xu, H., Li, H., & Nerbonne, J. M. (1999). Elimination of the transient outward current and action potential prolongation in mouse atrial myocytes expressing a dominant negative Kv4 alpha subunit. *J Physiol*, *519 Pt 1*(Pt 1), 11-21. doi:10.1111/j.1469-7793.1999.00110.x
- Xu, Q., & Yaksh, T. L. (2011). A brief comparison of the pathophysiology of inflammatory versus neuropathic pain. *Curr Opin Anaesthesiol*, *24*(4), 400-407. doi:10.1097/ACO.0b013e32834871df
- Xu, Y., Yang, Y., Chandrashekar, A., Gada, K. D., Masotti, M., Baggetta, A. M., . . . Plant, L. D. (2022). Hypoxia inhibits the cardiac I (K1) current through SUMO targeting Kir2.1 activation by PIP(2). *iScience*, *25*(9), 104969. doi:10.1016/j.isci.2022.104969
- Yagi, J., & Sumino, R. (1998). Inhibition of a hyperpolarization-activated current by clonidine in rat dorsal root ganglion neurons. *J Neurophysiol*, *80*(3), 1094-1104. doi:10.1152/jn.1998.80.3.1094
- Yao, H., Donnelly, D. F., Ma, C., & LaMotte, R. H. (2003). Upregulation of the hyperpolarization-activated cation current after chronic compression of the dorsal root ganglion. *J Neurosci*, *23*(6), 2069-2074. Retrieved from <https://www.ncbi.nlm.nih.gov/pubmed/12657665>
- Ye, B., Balijepalli, R. C., Foell, J. D., Kroboth, S., Ye, Q., Luo, Y. H., & Shi, N. Q. (2008). Caveolin-3 associates with and affects the function of hyperpolarization-activated cyclic nucleotide-gated channel 4. *Biochemistry*, *47*(47), 12312-12318. Retrieved from <https://www.ncbi.nlm.nih.gov/pubmed/19238754>
- Ye, B., & Nerbonne, J. M. (2009). Proteolytic processing of HCN2 and co-assembly with HCN4 in the generation of cardiac pacemaker channels. *J Biol Chem*, *284*(38), 25553-25559. doi:10.1074/jbc.M109.007583
- Zagha, E., Ozaita, A., Chang, S. Y., Nadal, M. S., Lin, U., Saganich, M. J., . . . Rudy, B. (2005). DPP10 modulates Kv4-mediated A-type potassium channels. *J Biol Chem*, *280*(19), 18853-18861. doi:10.1074/jbc.M410613200
- Zemel, B. M., Ritter, D. M., Covarrubias, M., & Mueqem, T. (2018). A-Type KV Channels in Dorsal Root Ganglion Neurons: Diversity, Function, and Dysfunction. *Front Mol Neurosci*, *11*, 253. doi:10.3389/fnmol.2018.00253
- Zhang, Q., Huang, A., Lin, Y. C., & Yu, H. G. (2009). Associated changes in HCN2 and HCN4 transcripts and I(f) pacemaker current in myocytes. *Biochim Biophys Acta*, *1788*(5), 1138-1147. doi:10.1016/j.bbamem.2009.02.011
- Zhao, X., Xia, B., Cheng, J., Zhu, M. X., & Li, Y. (2020). PKCepsilon SUMOylation Is Required for Mediating the Nociceptive Signaling of Inflammatory Pain. *Cell Rep*, *33*(1), 108191. doi:10.1016/j.celrep.2020.108191
- Zheng, Y., Liu, P., Bai, L., Trimmer, J. S., Bean, B. P., & Ginty, D. D. (2019). Deep Sequencing of Somatosensory Neurons Reveals Molecular Determinants of Intrinsic Physiological Properties. *Neuron*, *103*(4), 598-616 e597. doi:10.1016/j.neuron.2019.05.039
- Zhou, W., Qian, Y., Kunjilwar, K., Pfaffinger, P. J., & Choe, S. (2004). Structural insights into the functional interaction of KChIP1 with Shal-type K(+) channels. *Neuron*, *41*(4), 573-586. doi:10.1016/s0896-6273(04)00045-5